UNIVERSITÀ DEGLI STUDI DI TRIESTE

XXX CICLO DEL DOTTORATO DI RICERCA IN NANOTECNOLOGIE

DESIGN OF AN ENVIRONMENT-INDIPENDENT, TUNABLE 3D DNA-ORIGAMI PLASMONIC SENSOR

Settore scientifico-disciplinare: **FIS/03**

DOTTORANDA
VALENTINA MASCIOTTI

COORDINATORE
PROF. LUCIA PASQUATO

SUPERVISORE DI TESI
DR. MARCO LAZZARINO

ANNO ACCADEMICO 2016/2017

Contents

Abstract

DNA origami nanotechnology engineers DNA as the building blocks of newly conceived self-assembled materials and devices. Due to its high degree of customization and its precise spatial addressability, DNA origami provides an unmatched platform for nanoscale structures and devices design.

Gold nanoparticles (AuNP) have been largely investigated because of their peculiar optical properties and in particular their localized surface plasmon resonance (LSPR) that modifies significantly the electromagnetic environment in a thin shell around them, and provides a tool with unrivalled potential to tune the local optical properties.

The combination of DNA origami frameworks and AuNP into DNA based-plasmonic nanostructures offers a concrete approach for optical properties engineering. It has been successfully applied to design biosensor and to enhance Raman scattering or fluorescence emission. Moreover, it has been exploited to design molecular ruler in which the inter-particle gap is controlled with nanometric precision through the transduction of the conformational changes into univocally detectable optical signals.

In this thesis I present my PhD work which aims at the design of an environment-independent AuNP decorated-DNA origami. A tetrahedral DNA shape structure has been selected for its three dimensional robustness and thus a DNA origami prototype has been assembled, characterized with SEM, TEM and AFM to verify the proper folding of the structure. The origami has been equipped with an actuator probe which recognizes a specific target oligonucleotide inducing a structural reconfiguration of the tetrahedron. To detect the conformational change triggered by the hybridization event, I functionalized the origami with two gold nanoparticles placed in two opposite facets at a known distance of 10 nm: the change of the interparticle gap is effectively transduced in a LSPR shift. This working principle has been verified with optical extinction measurements and the interparticle distance reduction has been confirmed by SEM imaging and SAXS analysis performed in the SAXS beamline of Elettra Synchrotron, thus confirming that the operation of the device and its transduction mechanism are the same no matter of the external conditions, being them dry, liquid or solid.

In the first part of this thesis I will introduce you to DNA origami technology and AuNPs decoration using a rectangular shape nanostructure used for the working conditions optimization. The peculiar and robust shape of the DNA origami rectangle can be exploited as a platform to evaluate AuNP-DNA origami linkage and purification.

Successively, I will walk you through the core of my PhD project: how the synthesis, the purification, and the AuNP decoration of the tetrahedral DNA origami have been optimized, all the characterization performed on the structure and the results obtained with the different analysis.

Finally, I will present a collateral activity performed in collaboration with the University of Melbourne, in which we encapsulate DNA origami in a Metal Organic Framework (MOF). The protection offered by the crystal growth around biomolecule, in this case DNA origami, would enhance the half-life of the DNA origami structure addressing a topic, DNA-origami conservation, not yet considered in literature.

1 Introduction

1.1 DNA Nanotechnology: origin and applications

1.1.1 The molecule of life

The deoxyribonucleic acid or DNA is the polymer responsible of the genetic information storage. The molecule is composed by fundamental blocks called nucleotides characterized by three specific units: a sugar, a phosphate group and a base. The pentose sugar in the form of ß-D-2-deoxyribose is connected through carbon 5′ to tri-phosphate group and through carbon 1′ to the base. The bases are nitrogen-containing ring molecules classified as the derivatives of two parent compounds: pyrimidine and purine. While pyrimidines are composed by an aromatic heterocyclic compound and are uracil (U), cytosine (C) and thymine (T), purines consist of a pyrimidine ring fused to an imidazole ring and are adenine (A) and guanine (G). Phosphodiester bond between nucleotides induces the loss of two of the three phosphate groups, providing the energy content necessary for the reaction which forms the linear filament of DNA.

Nitrogenous bases hydrogen bind opposite DNA filaments to form the rungs of the "twisted ladder" or double helix of DNA following rigid base-paring rules, in particular adenine is always paired with thymine through two hydrogen bonds while guanine is always paired with cytosine through a stronger connection due to the third hydrogen bond (Figure 1.1a).

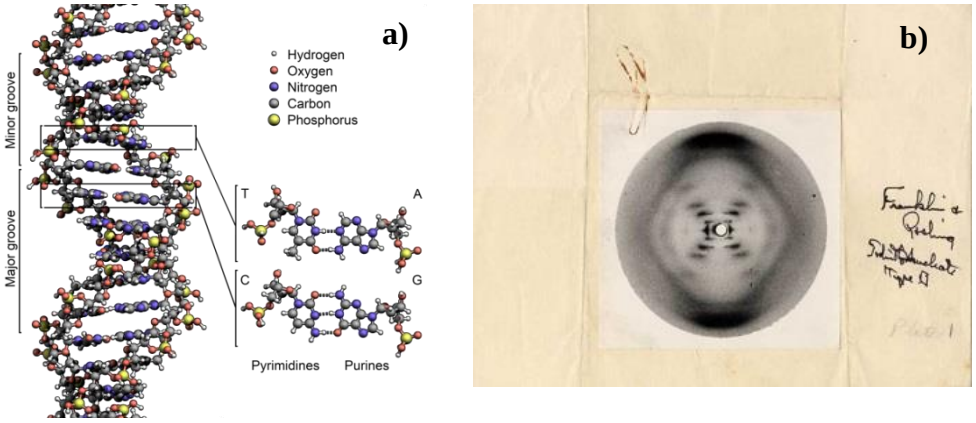

Figure 1.1 a) Atomic model of DNA molecule; **b)** Photograph 51, first X-ray diffraction image of DNA taken by a PhD student of Rosalind Franklin in 1952**.**

Single strand DNA is a reactive molecule, but the possibility to share hydrogen bonds between filaments stabilizes the polymer through the formation of a double helix structure.

The interaction and the spatial organization of the DNA is further strengthen by the hydrophobicity of the bases which are arranged within the structure and by the hydrophilicity of the phosphoric-sugar backbone which is placed outside. The 3D configuration of DNA was figured out by Rosalind Franklin in 1952 through X-ray diffraction analysis (Figure 1.1b); one year later Watson and Crick published a paper on Nature describing the most widespread B form of double-helix **[1]**. They observed a periodicity of about 0.34 nm among residues, with a rotation between adjacent nucleotides of ~ 34°, completing one turn around its axis every 10.4 - 10.5 base pairs with an helical diameter of 2.0 - 2.2 nm. In this repetitive 3D geometry it is possible to recognize minor groove and major groove, the latter is wider and represents the anchor point for many DNA-binding proteins. The hetero-polymer is directional because of the asymmetry of the sugar which has four carbon inside the cyclic structure and the fifth is outside and also because of the phosphate group position, involved in the link with carbon 5′. This directionality is maintained in the replication of the molecule, in the content and in the reading of genetic information.

The molecule of DNA is the designed material for the information storage and propagation, representing the genome of sub-living virus, one-cell prokaryotic organism up to more complex and evolved eukaryotic live organisms as human being.

In the eukaryotic cells, DNA is stored inside the nucleus and despite it is well protected by a strong barrier called nucleus membrane, it can receive external stimuli, rework them together through the help of dedicated proteins and chemo-physical input, in order to formulate the response and depending on the requirement the whole cell expression can be modified.

The double-helix has a stable configuration which allows a calculated half-life of 521 years; the pairing of the helices through base-stacking interactions is energetically favored, promoting a long-term stabilization of the molecule.

The recognition affinity, the programmability and the mechanical properties of the DNA triggered researchers to employ it not only as a biological target but also as an effective material opening a completely new prospective in the nanotechnology field.

1.1.2 DNA Nanotechnology

DNA molecule can assume different spontaneous geometries enabled by the extraordinary bending and rearranging properties: B form, the most common in nature, A form, typical of

dehydrated conditions and Z form promoted by alternating purine-pyrimidine sequence (especially poly(dGC)), negative DNA supercoiling or high salt concentration.

The versatility of DNA is fundamental for the evolution process because it allows the genetic information exchange. In 1964 Robin Holliday described a key intermediate in many types of genetic recombination composed by four DNA single strand junctions reassumed in a X structure where all the duplex pairing are in the classical B form. This particular configuration allows symmetric arrangement of sequences around the junction through the sliding of two double helix. At the beginning of 80's Ned Seeman demonstrated that immobile nucleic acid junctions could be artificially created by properly design the strand sequences to remove symmetry in the assembled molecule **[2]**, and that these immobile junctions could in principle be combined into rigid crystalline lattices.

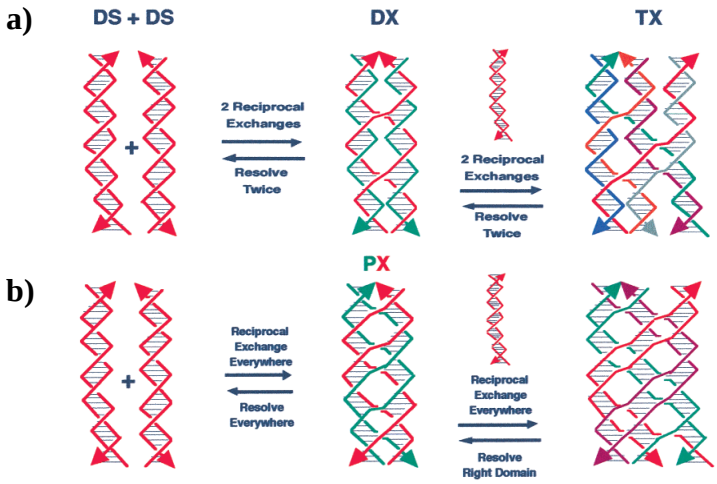

Figure 1.2 a) Formation of: (i) DX from double the reciprocal exchange of two dsDNA, (ii) TX from the 2 reciprocal exchange between DX and a third dsDNA; **b)** Formation of PX by the strands exchange of two double helices at every possible point where the filaments come into proximity (figure taken from [3]).

By using these stable branched DNA motifs, a range of DNA tiles such as double-crossover (DX), triple crossover (TX) **[4]** and paranemic (PX) **[3]** were designed and fabricated: double crossover contains two helical domains connected twice, triple crossover molecule is generated by two reciprocal exchanges between a helix of the DX molecule and another double helix (Figure 1.2a) **[5]**, and paranemic are described by the strands exchange of two double helices at every possible point where the filaments come into proximity (Figure 1.2b). The resolution of these structures can be effected either by joining the filaments of the same polarity either by joining strands of different polarity.

The rigidity of the DNA tiles allows to build up more complex and large nanostructure like cubic architecture composed by eight 3-arm junctions **[6]** a truncated octahedron (Figure 1.3a,b) **[7]** and Borromean DNA rings **[8]**.

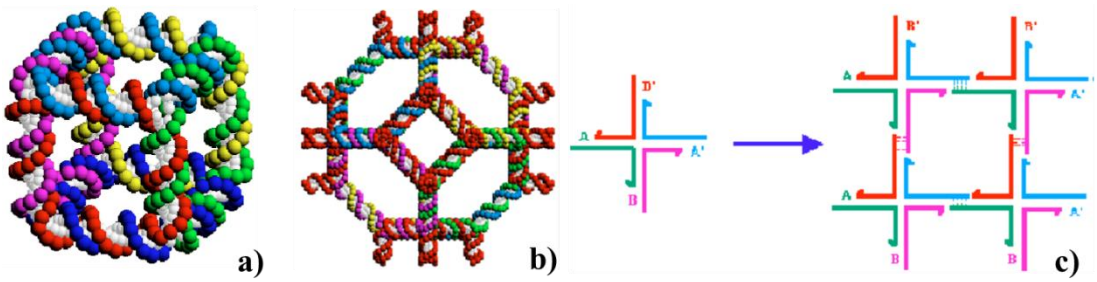

Figure 1.3 a) DNA cube shows that it contains six different cyclic strands. Each nucleotide is represented by a single-colored dot for the backbone and a single white dot representing the base (figure taken from [6]). **b)** A truncated octahedron contains six squares and eight hexagons. This is a view down the fourfold axis of one of the squares. Each edge of the truncated octahedron contains two double helical turns of DNA (figure taken from [7]). **c)** Formation of a two-dimensional lattice from an immobile junction with sticky ends (figure taken from [9]).

The ability to produce different kind of structures ranging from 1D to 3D, stimulates both the arrangements of different objects together and the development of DNA dynamic devices fundamentally based on the molecular transition triggered by various stimuli. The building up of composed structures starting from an elemental block was performed through the formation of periodic patterns (Figure 1.3c) fabricated exploiting the sticky-end cohesion and the rigidity of DX which is considered higher than dsDNA and Holliday junction (Figure 1.3c) **[9]**.

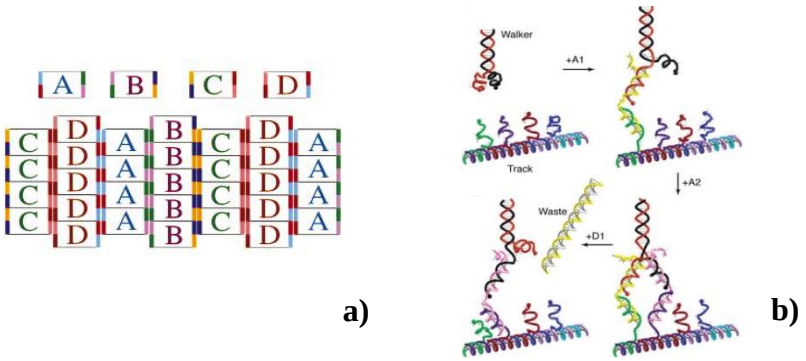

Figure 1.4 a) Design of DX molecular structure and arrangement into 2-D lattices consisting of four logic units (figure taken from [10]; **b)** Schematic of walker locomotion. Colored spheres represent dyes (HEX, green; Cy5, purple; FAM, red; Texas Red, blue) and quenchers (BHQ1, orange; IBRQ, black) for detecting walker movement: the sequentially addition/ removal of target strands produces the progressive attachment to the branches along the path (figure taken from [11]).

Winfree and colleagues, for example, tiled a plane alternating DX module and a second DX module that projects out of the plane of the helix axis (Figure 1.4a) **[10]**. DNA dynamic nano-machine have attracted large interest both because they are responsive to chemical or biochemical stimuli, and because they can be fueled with metal ions, enzymes, protons or complementary strands. One popular example is the DNA walker, powered by DNA strands hybridization (Figure 1.4b). In 2004 Pierce and coworkers developed a bipedal DNA motor which was able to walk in a predescribed path step-by-step through the addiction and the removal of specific targets and monitoring it through multiplex fluorescence quenching **[11]**. Recently Idili et al, designed efficient pH nanoswitches based on intramolecular triplex of DNA structures containing pH-sensitive parallel Hoogsteen interactions, and demonstrated the possibility to tune the pH of about 5 pH units by changing the relative content of TAT/CGC triplets **[12]**.

Thanks to its versatility, in the last decades DNA nanotechnology attracted an increased interest from multiple scientific fields reaching an high know-how level and even more awareness of the potentialities it offers.

1.2 DNA origami technology

1.2.1 The initial design

Tile-based DNA nanostructures is a promising method for building lattices, crystal or 3D structures, but there are some drawbacks: first it needs the design and the check of the sequence at each assembling steps and second the production of high order nanostructure with a precise control over the shape and size is very challenging. To overcome these technical limitations, a new self-assemble strategy has been developed in 2006 by Paul Rothemund and it is named DNA origami technology. The term origami refers to the old Japanese art of paper folding into a complex shape but instead of papers it uses only DNA **[13]**.

Employing hundreds of synthetic short single-strand DNA it is possible to induce the folding of a long circular viral scaffold strand (M13mp18; 7,249 bases) through the arrangements of periodic crossovers. The complexity of the achievable structures breaks the limit in length of the tile assembly and lead to the formation of more intricate architectures. In his famous paper published on Nature, Rothemund describes the main

steps for the design of DNA origami: the planning of the shape of interest, the folding of circular scaffold strand, the design of a set of oligonucleotides strands, called staples, the minimization of the strain, and the domain expansion of the DNA strands with the scaffold in order to achieve higher specificity and higher binding energy.

The scaffold strand is allocated to run back and forth as if the whole area of our shape should be painted without detaching the brush from the paper. The presence of a "seam" allows the folding of the circular scaffold strand and it is placed, usually, in the center of the structure to keep high stability but could be shifted in accord to the shape complexity. The structural design, as introduced by Rothemund, is based on slightly stretched DNA parameters: rather than assuming 10.5 base pairs (bp) per turn (which corresponds to standard B-DNA twist), it uses an integer number of bases between periodic crossovers (for example, 16 bp for 1.5 turns). Once the shape is designed, it can be completely filled from top to bottom with pair of parallel cylinders, idealizing DNA helix, with a diameter of 2 nm and a length of 3.6 nm (10.67 nts), which approximately represents one turn of the helix (Figure 1.5a). To hold the cylinder together, a periodic array of crossover is added; crossovers can occur every 1.5 turn but, in general, any odd number of half-turns helix can be used (Figure 1.5b). The fundamental constraint on a folding path is that the scaffold can form a crossover only at those locations where the DNA twist places it at a tangent point between helices. Thus for the scaffold to raster progressively from one helix to another and onto a third, the distance between successive scaffold crossovers must be an odd number of half turns. Conversely, where the raster reverses direction vertically and returns to a previously visited helix, the distance between scaffold crossovers must be an even number of half-turns.

The parallel helices organized in a lattice and joined by crossover are not closed-packed probably because of electrostatic repulsion: the calculated inter-helix gap is around 1 nm for 1.5-turn spacing and 1.5 nm for 2.5-turn spacing. This model approximates the desired shape with a nanometer *xy* resolution as shown in Figure 1.5a. The minimization and balancing of twist strain between crossovers is complicated by the non-integer number of base pairs per half-turn (5.25 in standard B-DNA). To reduce the strain, the twist of scaffold crossovers is calculated and their position is changed (typically by a single bp).

To fold the scaffold into a specific conformation, a set of helper strands called staples is added, providing Watson-Crick complements with the scaffold through crossovers between adjacent helices (Figure 1.5c).

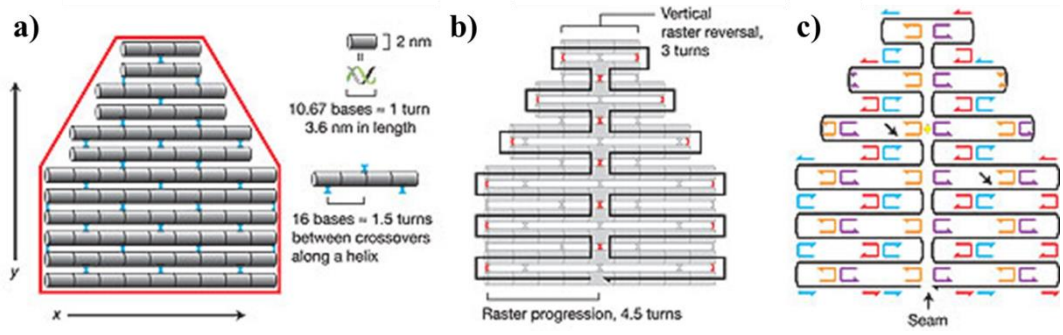

Figure 1.5 Design of DNA origami (figures taken from [13]). **a)** shape (red) approximated by parallel double helices joined by periodic crossovers (blue). **b)** A scaffold (black) runs through every helix and forms more crossovers (red). **c)** As first designed, most staples bind two helices and are 16-mers.

To give the staples strands larger domain with scaffold, it is possible to merge pair of consecutive strands together, in order to increase the stability of the entire structure. The length of a staple strand should be a multiple of 16 when crossover spacing is 1.5 turn. Shorter oligonucleotides are affected by less hybridization stability while longer sequence can modify their diffusion and assembling rate. The optimal length can varies from 20 to 50 nm. Moreover the presence of a seam can generate a weaker line in the structure and if no helper is crossing the seam, the two half of the architecture could be just weakly linked. To strengthen it, an additional pattern of merges and breaks can be used, imposing to an helper the crossing of the seam. Other tips regarding how to avoid accidental stacking of the structures have been supplied by the author. DNA origami shapes with straight edges have high probability to stick together at the edges since the DNA base-pairs exposed at the edge are highly hydrophobic and tend to stack to each other. To prevent this phenomenon the staples strands placed on the edges of the scaffold could be modified with 4 thymines sequence (4-T loop) that forms a non-interacting loop. The M13mp18 loop structure (usually not included in the assembling pattern) can be exploited also to insert some points as dots for patterning the structure that are detectable by the height difference with atomic force microscopy. The latter modification firstly opens the possibility to decorate the DNA substrate.

Each design needs around 200 oligos to fold the scaffold strand in the desired shape. The assembly consists in one-pot reaction in which the temperature has a fundamental role: in the first step high temperature degrees help to dehybridizes secondary structures and aspecific binding then it gradually decreases to induce the assembling of all the reagents in the most stable configuration, the one with higher free energy. Rothemund in his first

work, designed and successfully synthetized many 2D DNA origami (Figure 1.6), working also on the optimization of the folding protocol.

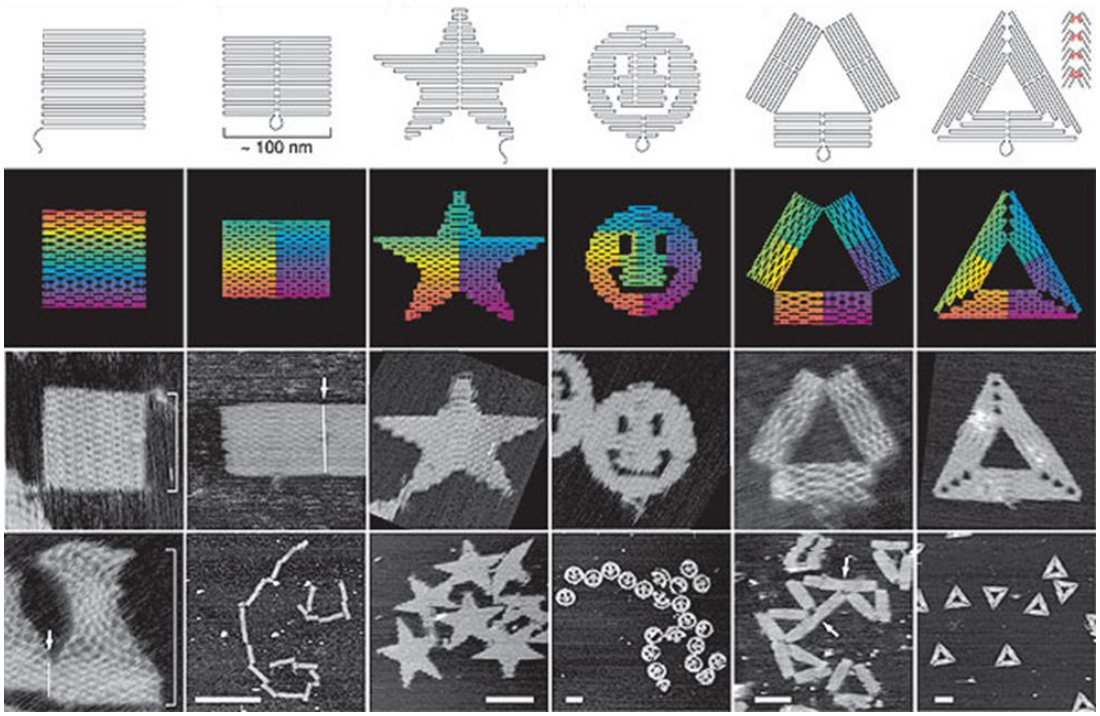

Figure 1.6 DNA origami structures of different shape in Rothemund's work. Graphical representation of the scaffold strand position (first line), simulation of the final helices arrangements (second line) and AFM images (third and fourth lines) (figures taken from [13]).

Even if DNA origami represents a revolutionary technology, it shows some tricky points: first the difficulty keeping track of thousands of sequences and second the unavoidable helical nature of DNA. In particular, it is fundamental to determine the crossover positions which should be as close as possible to the tangent between parallel helices. B form of DNA in nature, has a an angular twist each 10.5 bases while if constrained it can assume a slightly overtwisted or understwisted configuration. Moreover we should also consider the asymmetry of DNA double helix, which gives the characteristic major and minor grooves. In order to handle all these information, Rothemund used a clunky Matlab program for the design of DNA origami structure which presupposed hand-generated functions both for the drawing of the scaffold and for the design of crossovers and staples sequences.

1.2.2 DNA origami software-assisted design

During the last decade, the design of DNA origami structures has been automated by using suitable software that calculates the spacing of the double helix and the place where it is

possible to form DX crossovers. Usually, they also provide a graphical overview of the 3D structural assembly. The most used are SARSE-DNA origami, NanoEngineer-1, CaDNAno **[14]** and its evolution DEADALUS **[15]**. SARSE has been developed by Ebbe Andersen and colleagues in Aarhus, it is a free download software and it presents an user friendly interface and a 3D generator. The editing and the automatic folding with staple strands present some complexity and problems **[16]**. NanoEngineer-1 is an open source software to construct DNA folding designs, it is not user friendly and quite time consuming because the crossovers require to be added manually one by one. Shih and colleagues developed CaDNAno that is an open source design software based on the finite elements analysis performed by CanDo (Computer-Aided eNgineering for Dna Origami) previous developed by Mark Bathe from MIT **[17]**. The latter is the most used software to create DNA origami because its interface is simple and the process of folding is complete and automatic; there are two different lattices: "honeycomb" (Figure 1.7a) and "squared" (Figure 1.7b) depending on the desired structure. The second version of CaDNAno is based on the Autodesk Maya© platform and can create clear 3D graphical helices representations (Figure 1.7d).

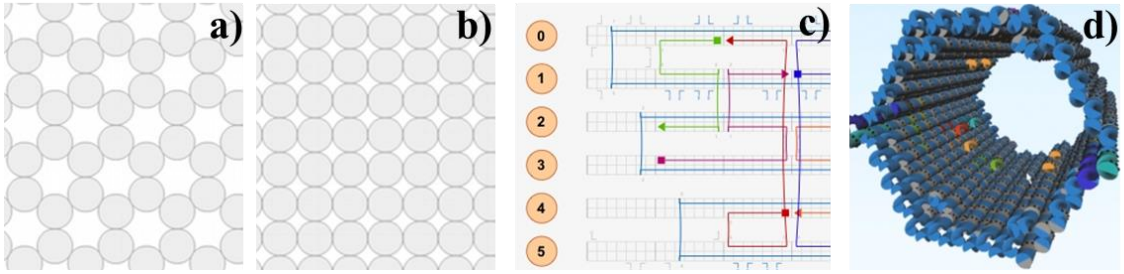

Figure 1.7 CaDNAno software interface: **a)** honeycomb lattice and **b)** square lattice **c)** design window representing scaffold strand (light blue lines) and staples strands (colored lines); **d)** simulation performed by Autodesk Maya of the DNA helices arrangements in a DNA origami structure (colors are consistent with the ones on caDNAno files).

DAEDALUS (DNA Origami Sequence Design Algorithm for User-defined Structures) named as the Greek craftsman and artist who designed labyrinths that resemble origami's complex scaffold structures, can build any type of 3D shape, provided it has a closed surface. With the new technique, the target geometric structure is firstly described in terms of a wire mesh made up of polyhedra, with a network of nodes and edges. A DNA scaffold using strands of custom length and sequence is generated, automatically guiding the routing of the DNA scaffold strand through the entire origami structure, touching each vertex in the geometric form once. Complementary staple strands are then assigned and the

final DNA structural model or nanoparticle self-assembles, and is then validated using 3D cryo-EM reconstruction.

1.2.3 From 2D to 3D

A direct extension of 2D DNA origami to 3D solid structures would involve the stacking of flat sheets of helices arranged in a square lattice. The multisquare lattice conceives that each helix has four neighbor in a fourfold symmetry (Figure 1.8a). DNA B form considers a complete rotation along helix axis each 10.5 bp, this implies that one helix can share a crossover with the same helix each 21 bp. It follows that crossover to the remaining three neighbors in the square lattice should be distributed with an average spacing of 21/4= 5.25 bp. And this can be obtained using non-periodic crossover. A smart way to achieve a constant crossover periodicity is to assume that B-form DNA has an average helicity of 10.67 bp/turn. Crossover may be placed in interval of 8 bp, sharing crossover with one of the four neighbor each 32 bp. The constant 8 bp cross-over spacing underwinds the DNA resulting in a twisting torque and causing a global twist deformation of the entire object **[18]**. To minimize this effect Dietz and coworkers observed that it is important to achieve a double-helix densities closer to 10.5 bp/turn or to create an object with high torsional stiffness which varies inversely with the length of the nanoparticle. Shih and Yan **[19]** analyzed the global twisting of DNA origami cuboids formed by multiple layers of parallel helices characterized by a different length (Figure 1.8 b-d).

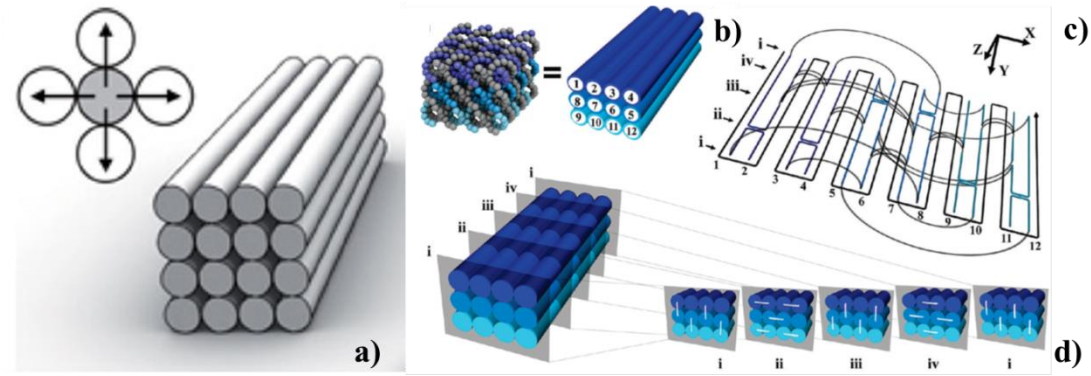

Figure 1.8 Multilattice DNA origami cuboid: **a)** in square lattice scheme each DNA helix has four neighbors displayed in fourfold symmetry (figure taken from [18]); **b)** helical model of the cuboid (scaffold in gray and staples in three shades of blue); **c)** layout and connection of scaffold strand and staples; **d)** the square-lattice arrangement of parallel helices is revealed in cross-sectional slices (i–iv) that are parallel to the xy-plane spaced at 8-bp intervals and repeating every 32 bp. Staple crossovers are shown as white lines linking two adjacent helices at each cross section (figures b,c,d taken from [19]).

Cuboids composed by shorter helices are subject to a smaller internal torque and greater torsional stiffness, which means a little noticeable global twisting.

Another way to design 3D DNA origami, as nanotubes and 3D wireframe polyhedral consists in the constraining of helices in a honeycomb lattice resulting in a bundle of double-helices **[20]**. This implementation in the design has led to the expansion of the possible shape with designed twist and curvatures. In the honeycomb array the helix has three nearest neighbors (Figure 1.9a). Every 7 bp, the strand rotates by 240°, assuming B-form twist density of 10.5 bp/turn. After 14 bp and 21 bp, the rotation achieved is respectively 120° (+ 360°) and 0° (2 x 360°). Antiparallel crossover in the honeycomb symmetry can be engineered each 7 bp. The addressable curvature or twist in the shape are programmed through the introduction or the deletion of single base pair. The deletion of a bp, will introduce an overwinding of that fragment which will torque and pull its neighbors (Figure 1.9b).

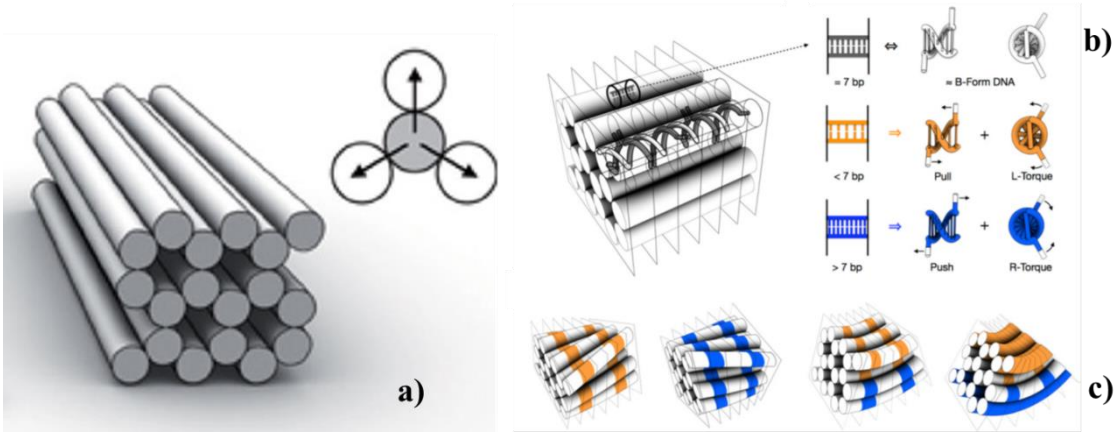

Figure 1.9 3D curved and bended DNA origami: **a)** in honeycomb lattice scheme each helix has 3 neighbors; **b)** helices constrained in a honeycomb lattice: in semi-transparence staple strands crossovers with 3 neighbor helices are spaced by 7 bp rotating the plane each time by 240°; on the right, array cell with default content of 7 bp, which exerts no stress on its neighbors; above, array cell with content of 5 bp, which is under strain and therefore exerts a left-handed torque and a pull on its neighbors; below, array cell with content of 9 bp, which is under strain and therefore exerts a right-handed torque and a push on its neighbors. **c)** from the left: 2 helix-bundles in which deletion or insertion of bp in the array cell (orange and blue parts) induce a global left-handed / right-handed twisting with cancellation of compensatory global bend contributions; 2 helix-bundles left in which in curvature and bending are accurately produced through gradient of bp deletion and insertion (figures taken from [20]).

This effect is then relieved by compensatory global left-hand twist of the bundle. In the same way insertion of a base pair can induce a local underwinding balanced out by a global

right-handed twist of the bundle. By the formation of a gradient between deletion and insertion Dietz and Shih reached different degrees of curvature (Figure 1.9c).

In addition of bended bundles or twisted lattices Dietz and colleagues created circular objects; using hierarchical assembly of small parts, a complete gear were developed as well as a toothed gear, six parts spiral, and a spherical wireframe. The spiral is essentially a continuum gradient with increasing radius of curvature of circle sections assembled **[20]** (Figure 1.10a). In 2011 Yan and coworkers completed the architectural possibilities of the curved 3D DNA origami creating a real spherical surface **[21]**.

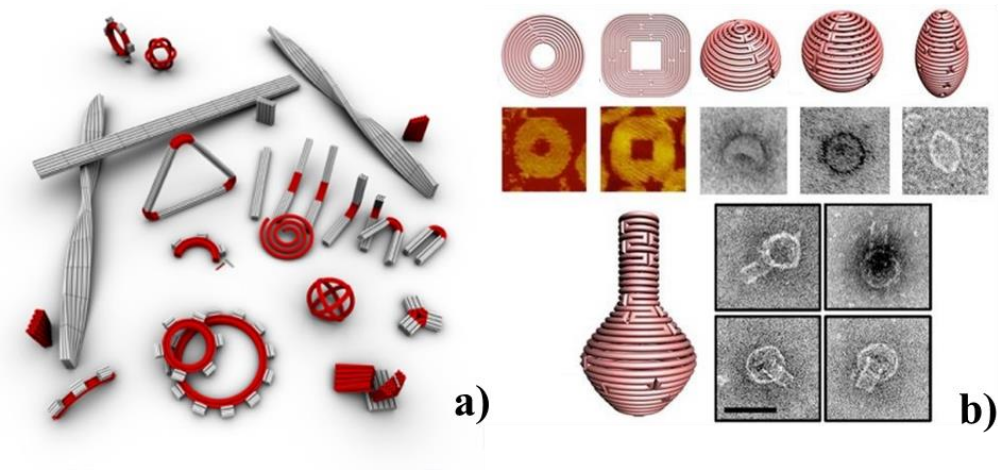

Figure 1.10 a) Curved and twisted nano-objects as gears, toothed gears, triangles, spirals (figure taken from [20]); **b)** 2D nanoforms with accompanying AFM images, and 3D structures of hemisphere, sphere, ellipsoid and narrowed nanoflask visualized at TEM (figure taken from [21]).

Concentric rings of DNA were used to generate in-plane curvature while, out-of-plane curvature was introduced by adjusting the particular position and pattern of crossovers between adjacent DNA double helices, whose conformation often deviates from the natural B-form twist density, and increasing the base pairs number. Adjusting the piling of these concentric rings incredible structures were developed such as spherical shells, ellipsoidal shells and narrowed nanoflask (Figure 1.10b).

1.2.4 Wireframe structures and polyhedra

The 2D and 3D DNA origami structures are most commonly designed through the alignment of parallel helices. The introduction of new motifs as DNA multiarm junctions allows the folding of wireframe architectures expanding the achievable configurations. Han et al. created wireframe DNA origami structure with a gridiron pattern **[22]**. The latter

was made by 4 arms-junction producing a square frame. Connecting more units together, they successfully produced a series of 2D lattices. Through the generation of tension/bending on the structure (described in the previous paragraph), they created curvatures to fold S structure and wireframe sphere (Figure 1.11a). The evolution of the method, was done by Zhang and colleagues by controlling the length of a T-loop inserted into the staple strands which surrounds the vertices to tune the angles amplitude and to create intricate structures such a flower-and-bird image (Figure 1.11b). In this design each edge contains two helices, so the scaffold strand should pass through the edges twice to connect all arms of the final object **[23]**.

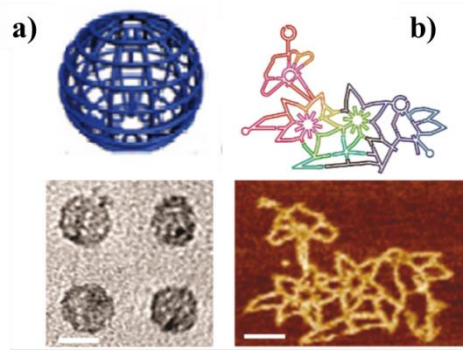

Figure 1.11 a) (figure taken from [22]) and **b)**: wireframe DNA structures made of 4 multiarm junctions. Scale bar 50 nm (figure taken from [23]).

The nanostructures produced were characterized by a rigid control over the angles degree, obtained through the hierarchical assembly of DNA origami tripods specifically arranged to form polyhedral architectures (Figure 1.12a).

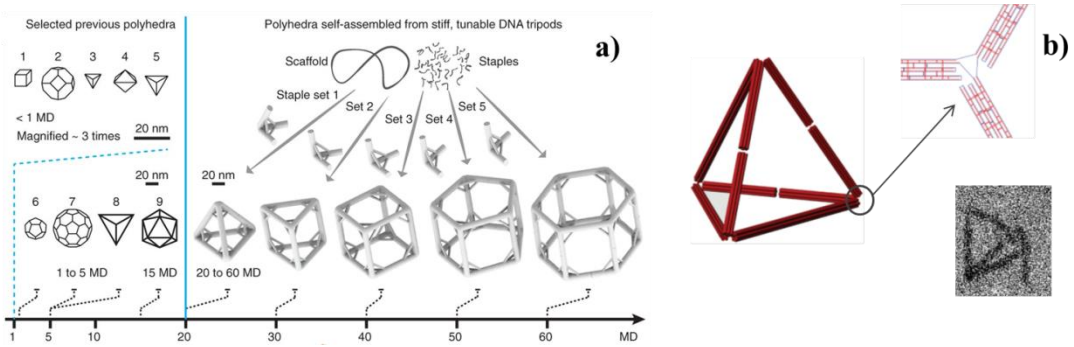

Figure 1.12 Design of wireframe polyhedral: **a)** hierarchical assembly of DNA origami tripods (polyhedral from 20 to 60 MD) through sticky-ends cohesion, the different set of staples shaped tripods with different angles (figure taken from [24]); **b)** tetrahedron-shape DNA origami with flexible joints at the vertices and TEM visualization (figure taken from [25]).

Iinuma et al, proposed an efficient method to assemble differently angled tripod monomers to obtain structures ranging from tetrahedron (composed by 4 monomers) to hexagonal prism (composed by 12 monomers).

The method is based on association sites consisting of sticky ends extensions protruding from the rigid bundles to form 3D polyhedron, whose inter-arm angles are tuned by supporting struts and strengthened by vertical helices. They were able to produce poly-structures with a maximum molecular weight of 60 MDa **[24]**.

A different approach to design wireframe 3D polyhedron was used by Smith and coworkers for the synthesis of a tetrahedral DNA origami structure (Figure 1.12b). The latter is composed by 6 six-helix-bundles connected at each of the four hinged vertices to the two neighboring bundles by a four-base single-stranded section of the circular scaffold extending between their termini. The tetrahedron benefits of great flexibility, can be produced with high yield of correctly assembly nanoparticle representing one class of structures which holds a broad relevance in applied nanoscience as potential container systems **[25]**.

A new method to design arbitrary polyhedron and wireframe structures is based on the use of a new DNA origami design-assisted software called DEADALUS. Top-down geometric specification of the target shape is followed by fully automatic sequence design and 3D atomic-level structure prediction (Figure 1.13).

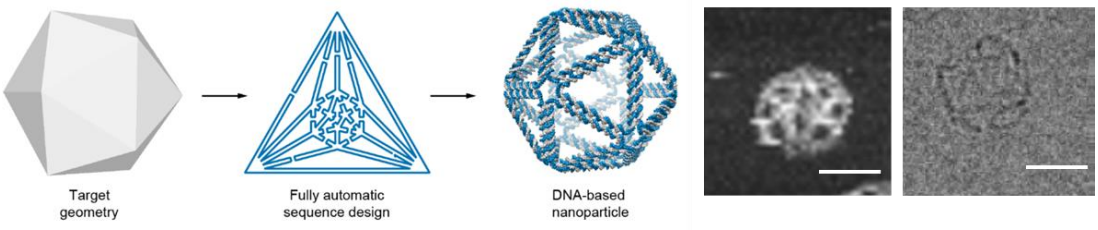

Figure 1.13 Process of the design, synthesis and AFM, cryo-EM characterization of DNA origami platonic solid using DEADALUS (scale bar 20 nm) (figure taken from [26]).

.

Mark Bathe's group demonstrated a versatile synthesis strategy to self-assemble complex nanoparticles which are stable in different buffers and in physiological conditions, offering the opportunity for their potential use in numerous *in vitro* or clinical applications **[26]**.

1.3 DNA origami Functionalization and Application

The extraordinary properties of nucleic acids, like the programmability, the bp-affinity and the mechanical flexibility, allow the precise design and synthesis of multi-shaped objects with nanometer resolution. Oligonucleotides are also easy to modify by the addition of chemical groups, as thiol, amine, fluorophores and chemotherapeutic molecule. The annealing of few modified oligonucleotides in a DNA origami structure allows to precisely address molecules or more complex polymers to a focused binding site. Thanks to this, DNA origami has found a variety of applications, ranging from the engineering of devices to research on fundamental mechanisms in nanoscience.

1.3.1 DNA origami for drug delivery

Because of its biocompatibility, minimal cytotoxicity, programmability for targeted and controlled release, DNA origami is considered one of the most promising technology for drug delivery. Anyway, the DNA has to overcome the barrier of being digested by cellular nuclease, enzyme designated for the protection from host attacks through DNA fragmentation. It is indispensable that DNA origami remains intact in cellular environment before completing their delivery mission. In this way, Yan's group observed that DNA origami structures survival for at least 12h in a cell lysate **[27]**. Moreover, the stability is maintained in tissue culturing **[28]**, serum **[29]**, in the presence of chaotropic agents **[30]** and organic solvents **[31]**. The aforementioned properties stimulated researchers to develop nanorobot for the transport of focused drugs that could kill cancer cells. Ding and coworkers loaded different shape of DNA origami with a doxorubicin chemotherapy molecule **[32]**. The latter intercalates DNA double helix inhibiting the cell proliferation. The load capacity is consistently high because of the numerous double helices present in the structures. This system has been able to kill specifically both the adenocarcinoma cells and tumor cell Dox-resistant, demonstrating a good antitumor efficacy also in a mouse model of the tumor. DNA origami is associable with other therapeutic methods as photothermal and photodynamic therapy. Ding and colleagues, associated a triangular shape DNA architecture with a gold nanorod and delivered the hybrid structure to MCF-7 tumor cells **[33]**. By infrared irradiations, they generated an heating of the metal particle, able to kill tumor cells. The latter responds to the near infrared photothermal therapy and also improves the imaging qualities of tumor tissue. To demonstrate the use of DNA origami also for photodynamic therapy Zhuang and colleagues loaded the photosensitive

agent BMEPC through intercalation delivering the complex into the cell **[34]**. BMEPC produces free radical and singlet oxygen upon light irradiation to kill cancer cells and simultaneously destroys the DNA origami structure through photocleavage (Figure1.14a).
The DNA origami before being a good carrier for drugs, is a good hauler for nucleotides. In nature there are some specific sequences able to stimulate immunosystem response. CpG islands are present with high frequency in bacterial genome with respect to mammalian's one. Liedl and coworkers functionalized a DNA origami tube with 62 cytosine-phosphate-guanine sequence to study immunoresponce on spleen cells **[35]**. The mammalian system is able to recognize them as foreign bodies and trigger the immune response. Thanks to this, CpG can be used as immunestimulatory response to improve the mammalian resistance from viral or bacterial attacks. CpG sequences directly injected in the organism are immediately degraded from nucleases, while the link with DNA origami not only protects them from digestion but enables the cellular membrane crossing, stimulating an important immunoresponse (Figure 1.14b).

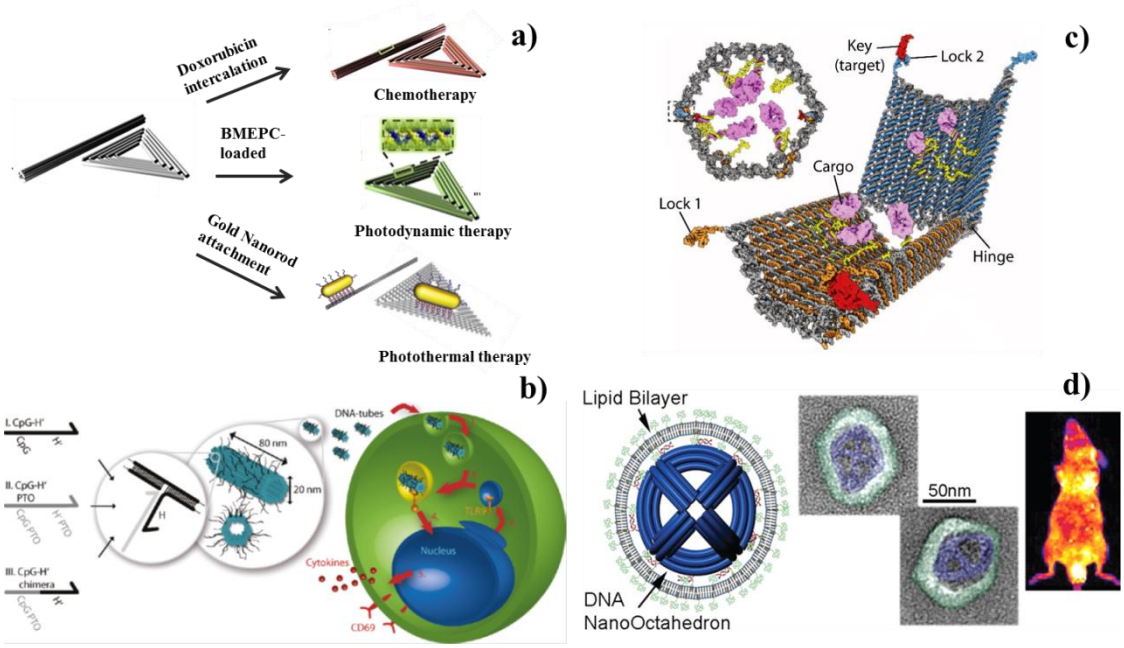

Figure 1.14 DNA origami for drug delivery: **a)** DNA origami triangle and nanotube can be used to load chemotherapic molecule, photosensitizer for photodynamic and gold nanorods for photothermal therapy (figure taken from [32,34,33]); **b)** DNA origami tubed loaded by CpG island stimulate immoresponse (figure taken from [35]); **c)** nanorobot with aptamers controlled-release containing antibody against leukocyte (figure taken from [36]); **d)** lipid bilayers coating of DNA origami octahedron to increase cell uptaken and to reduce the immuneresponse (figure taken from [37]).

To improve the target delivery specificity Douglas and colleagues built an aptamer-gated nanorobot (Figure 1.14c). Aptamers are specific DNA sequences which have high affinity for various molecular targets as proteins, virus and cells **[36]**. The DNA origami robot contained antibody fragments which fight leukocyte cells (HLA)-A/B/C. In the absence of the proper molecular target, the robot was inactive, but if it encounters the right key, it opened and exposed the antibodies. The antibodies can attack the receptors on the cell surface blocking the proliferation of the tumor. Bare DNA origami is scarcely uptaken by cells, because it presents some difficulty in the translocation across the cell membrane. Mikkida and coworker presented a method to incorporate DNA origami inside a viral capsid, increasing the internalization efficiency of more than 10 times **[38]**. Shih and colleagues, coated the surface of DNA structures using PEGylated lipid bilayers enhancing the pharmakokinetic bioavailability by a factor of 17, reducing by 2 orders of magnitude the immune activation (Figure 1.14d) **[37].**

1.3.2 Nucleic acid detection

Molecular biology offers the possibility to analyze DNA or RNA fragments substantially through the (RT-) PCR amplification of the targets. The use of DNA origami as a chip for a punctual detection of the oligonucleotides arouses the interest to the analysis at single molecule level through microscopy.

Single nucleotide polymorphisms (SNP) are the most common type of genetic variation among people. They have been found in the DNA between genes and they can act as biological markers, helping to locate genes that are associated with disease. Moreover, when SNPs occur within a gene or in a regulatory region near a gene, they may play a more direct role in disease by affecting the gene's function. Seeman's group, used a visual method to recognize SNPs based on a strand displacement reaction and AFM origami patterns **[39]**. One single strand hybridized a ssDNA protruding from a double strand helix end thanks to a partial or full complementarity. Initially the hybridization involved single strands parts, also called toehold and continued with branch migration to displace the shorter helix forming the initial double strand. The branch migration process is strongly affected by the length of the toehold as well as the perfect complementarity between strands. The presence of a mismatch could dramatically reduce the hybridization process acting as a kinetic trap. A rectangular shape DNA origami chip, containing four different

alphabetical patterns of strands overhung from the surface, was designed and synthetized (Figure 1.15a).

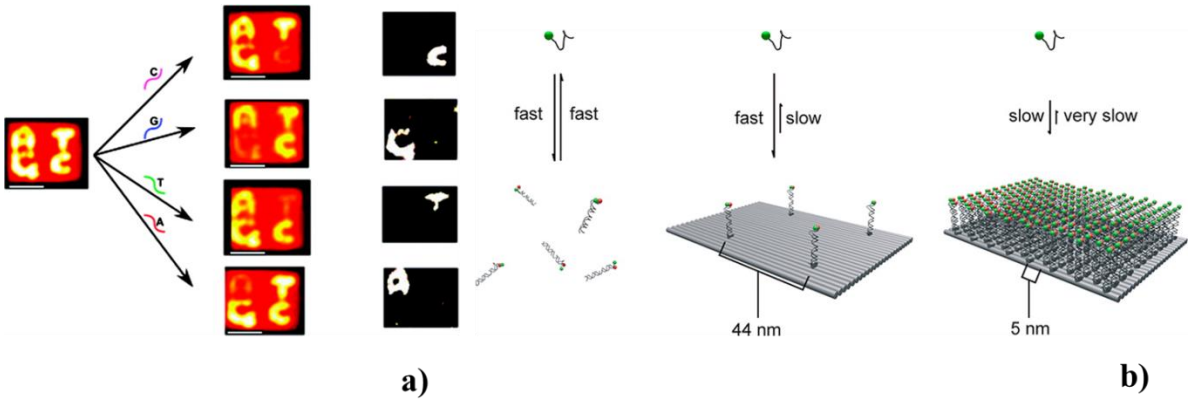

Figure 1.15 Nucleic acid detection: **a)** of SNP using a DNA origami array patterned with 4 letter containing ssDNA protruding from the surface which differ just from 1 base, the presence of SNP in the ssDNA added dramatically decreases the hybridization inducing the disappearance of the letter (figure taken from [39]); **b)** hybridization kinetic in DNA origami array where oligonucleotides are spaced 44 nm and 5 nm detected through FRET (figure taken from [40]).

Each pattern is made up the same DNA sequence but with a single nucleotide in the same position. The invading DNA strand can match just with the fully complementary sequence on the alphabetic pattern, inducing the disappearance of the letter under AFM.

To improve the knowledge of the kinetic behavior of the DNA hybridization, Walter and co-workers studied through FRET the rate of ds pair/unpair both in a crowded neighbor environment and in an empty surrounding **[40]**. Single target strands are positioned in a DNA origami array separated by 44 nm in the empty chip while 5 nm in the crowded one. They figured out that the dissociation rate of a target strand is reduced by an order of magnitude in the densest oligo array. Two mechanisms were proposed to explain the slow dissociation: the movement and the hybridization between adjacent sequences on the origami surface and the salt bridges attractive electrostatic interactions of the oligos with the DNA origami pegboard (Figure 1.15b).

1.3.3 Biophysical study using DNA origami

The forces investigation on the biological sample is useful for a complete knowledge of sophisticated mechanisms. The most commonly used techniques are atomic force microscopy or optic/magnetic tweezers. Necessary to analyze the elasticity of the cell

membrane or the dehybridization of the dsDNA, they suffer for limited data throughput and require for a physical connection to the macroscopic world. The design of a nano-spectroscopy can overcome these disadvantages, allowing the forces analysis at single-molecule level. Nickel and colleagues designed a force clamp to study the mechanical forces involved in the molecular interaction **[41]**. The structure used (Figure 1.16a) resembles to a potato peeler in which the supporting structure is made with rigid DNA origami and the blade is represented by a ssDNA spring. The entropic spring behavior of the ssDNA was used to exert controlled tension in the low piconewton range on a molecular system, whose conformational transitions were monitored by single-molecule Förster resonance energy transfer. They first tested the device with the conformer switching of a Holliday junction as a benchmark to study the TATA-binding protein-induced bending of a DNA duplex under tension. The observed bending suppression of above 10 piconewtons provides further evidences of mechanosensitivity in gene regulation.

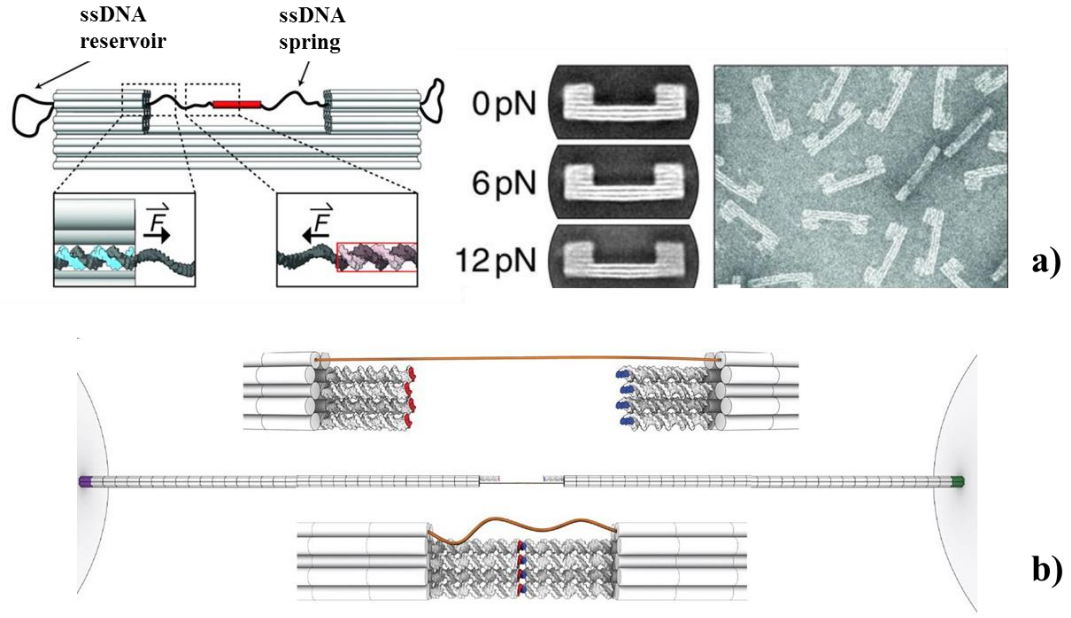

Figure 1.16 Biophysical study with DNA origami: **a)** molecular force spectroscopy using DNA origami nanoclamp, in the right side each constant-force variant, individual origami samples were assembled (figure taken from [41]); **b)** measurement of base pair stacking force through rigid DNA origami bundles (figure taken from [42]).

Dietz and coworkers used a DNA origami architecture to study the forces of base stacking at single molecule level **[42]**. They substituted a DNA origami structure to an optical tweezers to precise position blunt end of helices and to measure the weak base stacking forces (Figure 1.16b). The system was composed by two sets of parallel helices used to study the base pair stacking forces and by a rigid bundle of DNA origami supporting the

blunt end which reduced the background present at low forces range. One flexible connection mildly joined the two counterparts in order to increase the frequency of binding/rebinding. The hybridization of the bases was studied in different Mg^{2+} concentrations: 20 mM, which represents the in vitro environment concentration for the DNA origami synthesis and 500 mM which represents the cell contents. In this way they demonstrated that in both conditions the forces exerted present a sequence dependent rule: a stronger stacking (-3.42 kcal/mol) occurred with GC/CG and a weaker stacking (-0.81 kcal/mol) between AT/TA.

1.3.4 DNA origami templated architecture

DNA origami nanotechnology offers the possibility to rearrange with nanometer-scale precision nano-object as carbon nanotubes, metal particles and metal rods. The fine organization of metal particles in well-defined geometries and distances permits to exploit their unique optical and electrical properties. Metal nanoparticles can be chemically modified with DNA sequences which specifically recognize the strand protruding from the DNA origami surface. To ensure a robust bond and to address with higher precision the object on the DNA origami structure, more than one strand come out from the binding site on the surface. Yan and coworkers found a novel method to arrange gold nanoparticle on a triangular shape DNA origami, demonstrating that they can control the position and the number of the nanoparticles attached (Figure 1.17a) **[43,44]**. This pioneering work, opened the way for the analysis of novel properties. DNA origami, for example, was used to study the distance-dependence of single fluorophore quenching **[45]** by gold nanoparticles. Liedl and coworkers, utilized a rigid DNA origami scaffold as a linker to assemble metal NP, quantum dots and organic dyes into hierarchical nanocluster with planet-satellite-type shape (Figure 1.17b). Using DNA origami with different length, it was possible to tune the inter-particle distance of 5-200 nm. Moreover nanoscale components can be positioned along the radial DNA spacers of the nanostructures, which allows short- and long-range interactions between nanoparticles and dyes to be studied in solution **[46]**. To better control the geometry of the NPs arrangement, Gang et al assembled nanoparticles into crystalline and open 3D frameworks by connecting them through designed DNA-based polyhedral frames (Figure 1.17c). Polyhedral 3D DNA origami frames, whose vertices connected DNA-encoded NPs **[47,48]**, facilitated the establishment of local particle coordination that results in the formation of 3D ordered NP–DNA frameworks. Five

different DNA origami polyhedral frames, including octahedron, cube, elongated square bipyramid, prism and triangular bipyramid geometries, were built using six-helix-bundle edges with lengths (depending on the frame shape) from 30 to 45 nm. The designed DNA frames thus connect NPs at their vertices, establishing the overall lattice topology based on frame geometry. The different crystal lattice achieved were characterized both with cryo-EM and with small angle x-ray scattering analysis confirming the construction of the 3D nanoparticle lattice. Metallic nanoparticles, have surface plasmonic resonance affecting a small surrounding area. Mie and Prodan **[49]** predicted that the metal nanoparticle can absorb light and a plasmonic coupling can occur if the distance between them is short enough. In particular, the plasmonic coupling requires the edge-to-edge distance to be less than 2.5 times the particle diameter **[50]**.

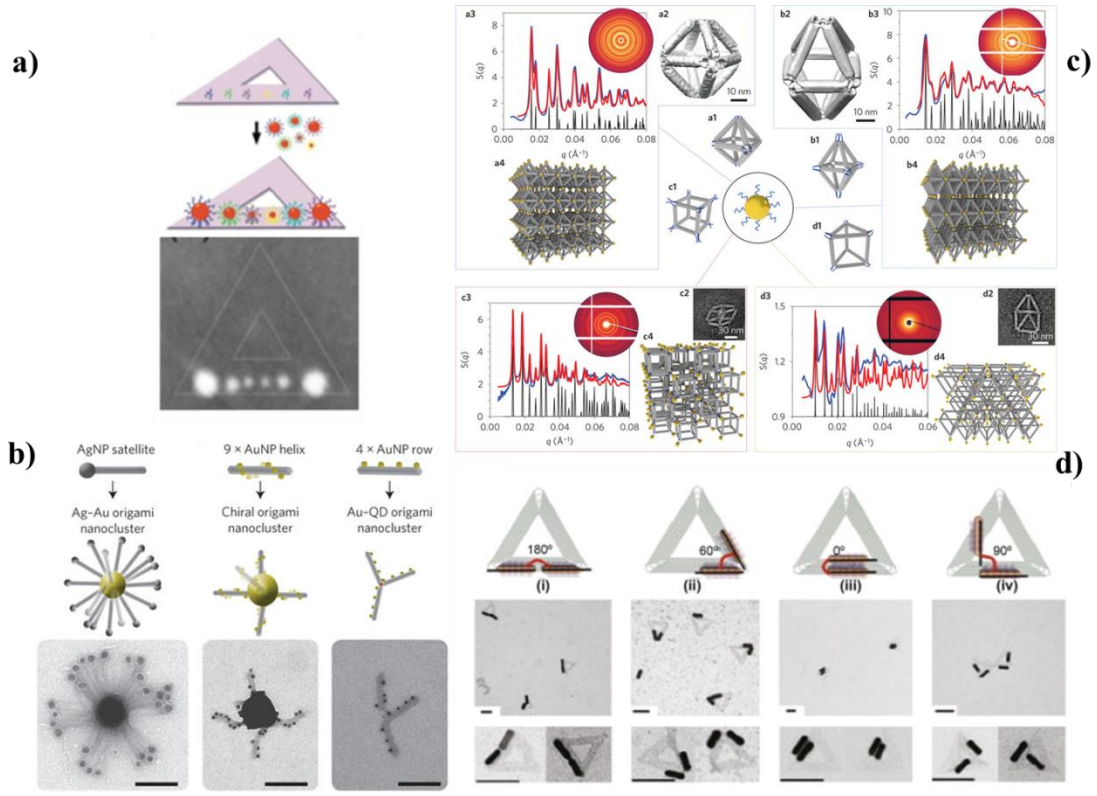

Figure 1.17 a) Gold nanoparticle arrangement in a triangular shape DNA origami platform (figure taken from [43]); **b)** Rigid DNA origami scaffold as a linker to assemble metal NP, quantum dots and organic dyes into hierarchical nanocluster with planet-satellite-type shape (figure taken from [46]); **c)** ssDNA functionalized AuNP linked to the vertices of DNA origami polyhedral frames: octahedron (a1), elongated square bipyramid (b1), cube (c1) and prism (d1) and X-ray scattering structure factor, S(q), extracted from the 2D SAXS pattern (abcd-3) and the proposed superlattice structures (the experimental scattering profile is in blue and the model fitting is in red) (figure taken from [48]). **d)** nanorods arranged in a triangular DNA origami with different inter-rod orientation inducing a red-shift of the absorbance peak position respect to the monomeric construct (figure taken from [51]).

DNA origami is an ideal platform to address the assembling of plasmonic nanostructure with new optical properties. Klein and coworkers, for example have used a DNA origami scaffold to align a series of 10 nm gold nanoparticles separated by 14 nm for visible spectrum subdiffraction plasmonic wave-guiding **[52]**. When the metal-nanostructure assembly is asymmetric, its plasmonic coupling can interact with the incident light according to the chirality of the assembled plasmonic structure. Yan's group reported a DNA origami-templated plasmonic nanostructure by arranging gold nanorod dimers in different inter-rod angles (Figure 1.17d). UV/vis spectra showed that angular orientations between the rods of 180°, 60° induced a red-shift of the absorbance peak position with respect to the monomeric construct, 0° on the other hand causes 5.5 nm blue-shift **[51]**. The simulated model well matches with experimental results. Chiral plasmonic structures were obtained also through the arrangement of gold nanoparticles or rods in helical superstructures. Liedl and coworkers have helically organized 9 binding sites for the nanoparticle attachment in a 24-helix bundle. The optical response can be tuned in handedness, color and intensity **[53]** in accordance with the theoretical model. The same effect was obtained by folding a rectangular shape DNA origami with a diagonal 10 nm gold nanoparticles-arranged in a tubular way **[54]**.

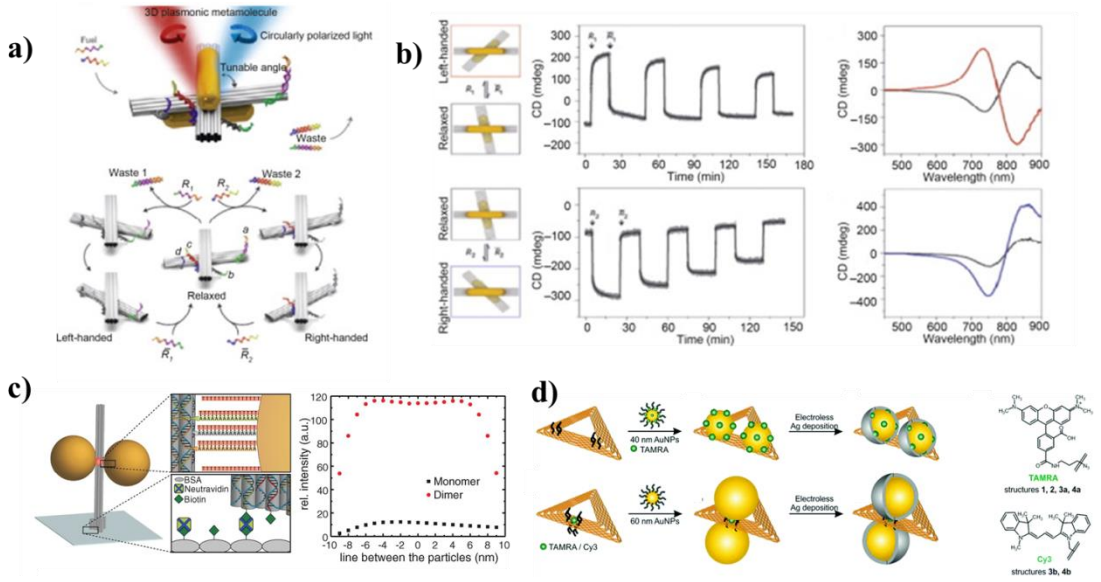

Figure 1.18 a) DNA origami metamolecule: the strand displacement induces the angle change of the AuNR, generating **b)** the switchable variation of the CD signal attributable to either a left- or right-handed state (figures a and b taken from [55]). **c)** Nanoantenna DNA origami with 2 AuNPs spaced several nm enhanced the fluorescence intensity in a plasmonic hotspot (figure taken from [56]). **d)** DNA origami decorated with a AuNP dimers to enhance Raman signal; optimization of the size and Au-Ag shell composition increases Raman enhancement by 10^{10} (figure taken from [57]).

Strand displacement reaction makes the plasmonic structure reconfigurable and dynamic. Liu and co-workers have created reconfigurable 3D plasmonic metamolecule using a dynamic DNA nanostructure, consisting of two connected DNA bundle, to organize two gold nanorod (AuNR) (Figure 1.18a).

Fueled by specific strands, the device movement caused the relative angle change between the AuNR, generating the switchable variation of the CD signal attributable to either a left- or right-handed state (Figure 1.18b) **[55]**.

Plasmonic structures can create a strong local field that enhances the brightness of the dye's fluorescent emission when the dye is placed at a specific local spot, called hotspot. The nanoantenna concept, indeed, enhances the excitation field in a very small local area, to direct single-molecule emissions **[58]** and to increase quantum yield for the detection of quantum yield-dye **[59]**. Tinnefeld and colleagues constructed a nanoantenna by positioning two gold nanoparticles with a distance of several nanometers on a DNA origami to enhance the dye fluorescence intensity in a plasmonic hotspot **[56]**. A 220 nm long and 15 nm wide pillar-shape DNA origami is attached to a surface through biotin-streptavidin interaction. Two AuNP and a fluorescent dye were immobilized in a defined positions imposed by the capturing strands. When the dye was positioned in a gap of 23 nm between a dimer of 100 nm AuNP, the fluorescence was enhanced of 117-fold (Figure 1.18c). They demonstrated that this system can be used for the single-molecule analysis to detect the binding or the unbinding events of a short strands, as well as the dynamic conformational changes of the DNA Holliday junction dyed with FRET reporters. Improvements on this DNA-based nanoantenna allowed to reach 5000-fold fluorescence enhancement, achieving a single-molecule detection limit of 25 μm. A Surface-Enhanced Raman Spectroscopy signal can be amplified using the same system. Bald's group, indeed, used a triangular shape DNA origami as a platform for the positioning of AuNPs dimers with a gap distance of 25 nm. Thanks to this approach they revealed several molecules by SERS **[60]**. Optimizing the size and the composition of Au-Ag-core shell nanoparticles, they reached a Raman enhancement of 10^{10} (Figure 1.18d) **[57]**.

1.3.5 Moveable DNA origami structures

DNA origami structure can be also reconfigurable: the accurate design of the components constituting the whole project allows various structural rearrangements and conformational changes. This fundamental property can be exploited with a double purposes: the creation

of a nanorobot which switches after the appropriate stimuli, and the plan of a dynamic device which is able to detect specific targets. One pioneering work in this field has been the design of a 3D box made up by the assembling of 6 DNA origami squares with a dynamic lid **[61]**. It had a "lock-and-key" system to control the closing and opening of the lid based on the hybridization of ssDNA positioned both on the edges of the lid and on the main structure (Figure 1.19a). At the initial point the box was closed because the ssDNA of the lid duplexes with the sticky-end extensions to provide a toehold for the strand displacements. The key, represented by a ssDNA, separated the hybridized strands and opened the lid. The box can be loaded and it specifically released its cargo after a proper stimulation. Marini and coworkers **[62]** demonstrated the autonomous and reversible motion of a DNA origami hatch which contained an internal moveable disk (Figure 1.19b). The internal flexibility of the disk is caused by unpaired regions, the hybridization with an hairpin ssDNA complementary to a DNA probe caused the wings aperture. Adding a linear competitor strand with more affinity for the probe than the target, the wing closed and the initial configuration was reestablished. The system was initially detected through FRET and AFM imaging.

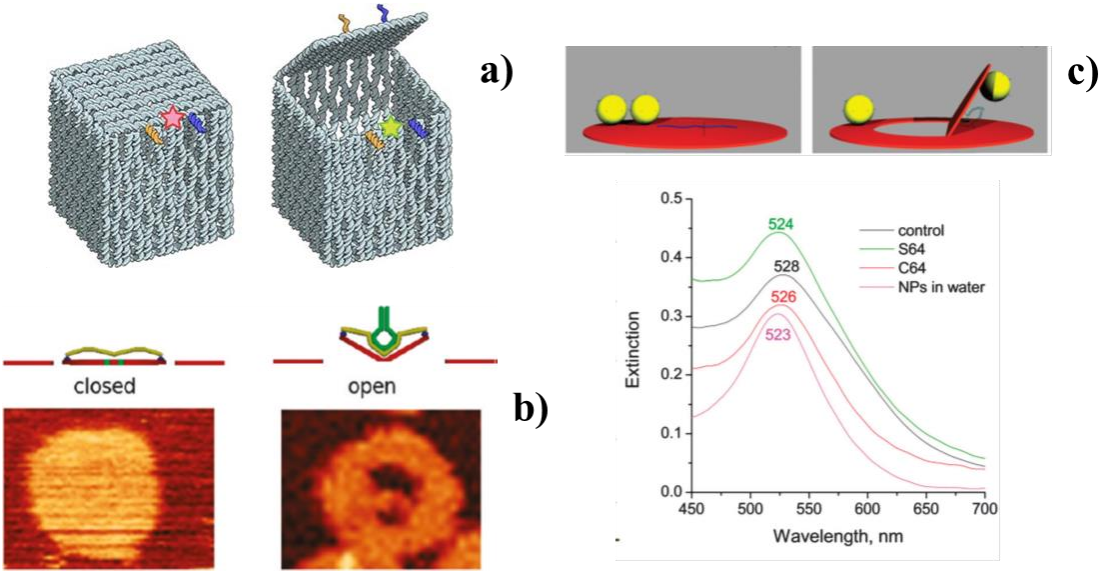

Figure 1.19 a) DNA origami box with lock-and-key system to control the opening of the lid (figure taken from [61]). **b)** Reconfiguration of a DNA origami hatch through strand hybridization, detection is performed with FRET (figure taken from [62]). **c)** DNA origami hatch with one moveable wing, decorated with two 20 nm- AuNP positioned between the hatch aperture. The addition of a specific target hybridizing the actuator strand induce the hatch aperture, increasing distance between NPs determining a blue-shift in the peak position of the absorbance. The system is reversible (figure taken from [63]).

AFM analysis showed the hole upon the addition of the hairpin molecule; the mechanism was implemented by Piantanida who used a similar structure with only one wing decorated

with two gold nanoparticles, positioned between the hatch aperture (Figure 1.19c) **[64]**. The motion induced by the addition of different strands (target/competitor) was detected through LSPR analysis: a blue shift is visible for all the targets with respect to the control. The plasmonic metamolecule planned by Liu and coworkers and described in the previous paragraph is an example of how switchable DNA origami structures can be used to reconfigure plasmonic properties. Castro and colleagues implemented the mechanical principle of macroscopic engine to plan nanomachineries capable of complex 3D motion. These DNA origami robots are made up three constituents: a hinge, a slider, and a crank-slider **[65]**. A ssDNA was used as a connection cable to control the slider by varying its length, determining different stiffness and range of motions (Figure 1.20a).

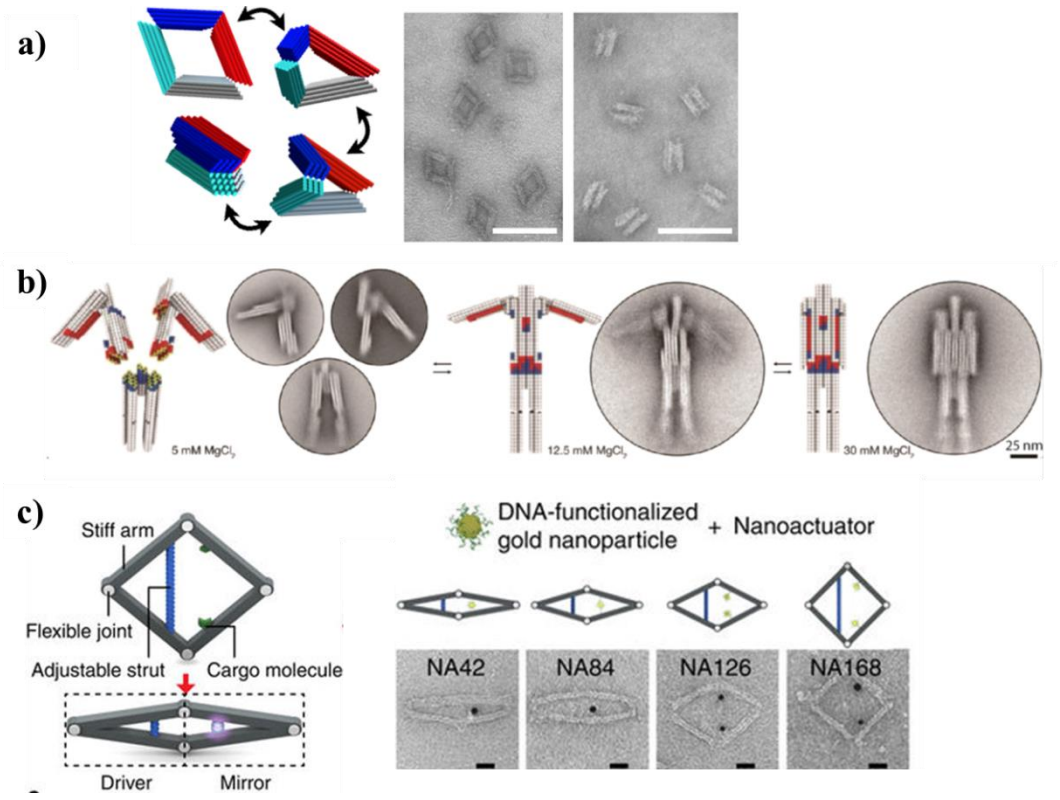

Figure 1.20 DNA origami nanorobot: **a)** ssDNA controls the slider by varying its length, determining different stiffness and range of motions. TEM images confirm the expected behavior (scale bar 100 nm) (figure taken from [65]). **b)** Dynamic nanorobot made up by heterotrimeric constituents differently assembled, by the changes of Mg^{2+} concentration, switching between three state: disassembled, assembled with open arms and assembled with closed arms (figure taken from [66]). **c)** A DNA origami robot consisting of four arms in a rhombus shape that can control distances between interacting molecules (figure taken from [67]).

The design with shorter connections resembled a linear spring with a stiffness of 0.42 pN/m, while the design with longer strands exhibited a non-linear force/extension trend with a stiffness of 0.07 pN/m at a shorter extension and 0.21 pN/m at a longer extension.

Dietz and coworkers planned a reconfigurable dynamic nanorobot made up by heterotrimeric constituents which can be differently assembled by the changes of Mg^{2+} concentration **[66]**, switching between three states: disassembled, assembled with open arms and assembled with closed arms (Figure 1.20b).

Ke and colleagues designed a nanoactuator which consisted of four rigid arms of DNA origami connected in a rhombus shape (Figure 1.20c). DNA origami nanoactuator used mechanical linkages to copy distance changes induced on one half ('the driver') to be propagated to the other half ('the mirror'). To actuate the surface two different mechanisms were used. A locking ssDNA hybridized the strands protruding from two of the four arms, regulating the distance between the connecting sites and the angles of rhombus. The addition of an hairpin target induced a long range conformational change to the device. This system was checked to induce the formation and the separation of a split green fluorescence protein demonstrating tunable fluorescent behaviors via long-range allosteric regulation. The second mechanism, indeed, considered the use of a compressed spring to maintain the system closed, locking it in two different positions. The locking can be due to molecular interactions, RNA-RNA hybridization or G-quadruplex formation **[67]**.

1.3.6 Other DNA origami application

Different research fields found DNA nanotechnology favorable. Thanks to its fine programmability at nanoscale level and to its versatility, it was used for variegated applications.

Lithography is a technique used to transfer a pattern from one object to another. The DNA origami exploitation can effectively improve the resolution of the technique itself.

Liu's group employed a DNA origami shape to be transferred in an inorganic pattern in one-step process **[68]**. The presence of DNA origami structures can modulate the vapor-phase of SiO_2 at molecular level. In the HF-etching of the SiO_2, the water acts as a catalyst of the reaction. DNA origami can adsorb a huge amount of H_2O molecules, reaching 100% if the humidity is relatively high, inhibiting the diffusion of HF in SiO_2 surface and consequentially increasing the etching of the surface.

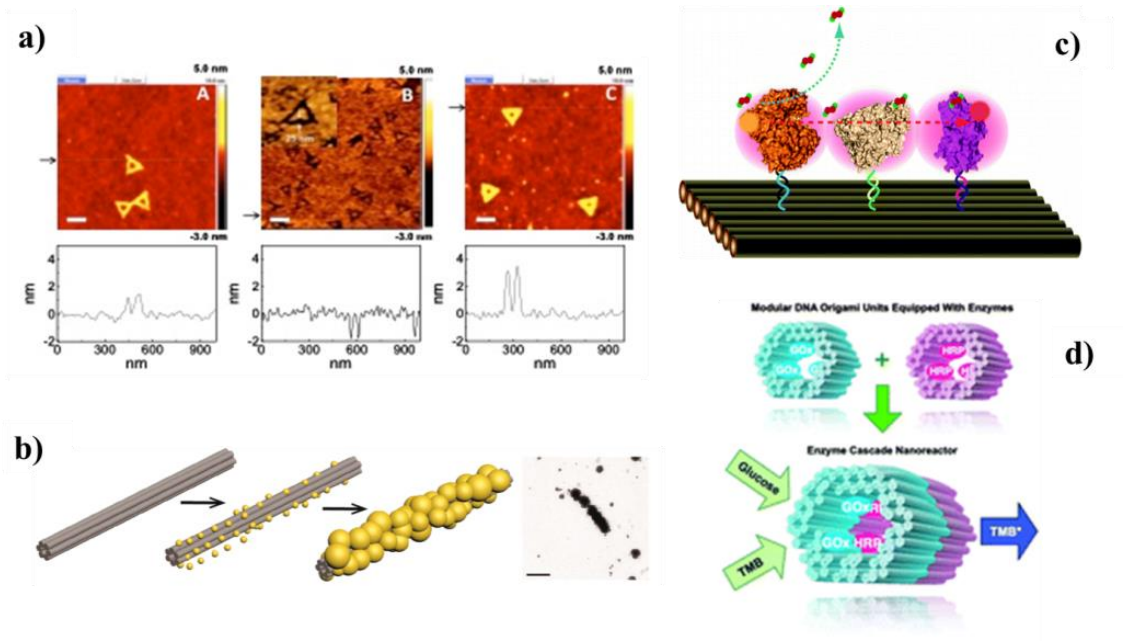

Figure 1.21 a) DNA origami used as a mask for lithographically pattern transferred to Silicon oxide surface: triangular shape on a SiO_2, concave pattern transferred, convex pattern transferred (figure taken from [68]). **b)** DNA origami for the growth of non DNA material (scale bar 200 nm) (figure taken from [69]). Enzyme cascade study using glucose oxidase (Gox)/horseradish peroxidase (HRP): **c)** positioning the enzymes on DNA origami array (figure taken from [70]) **d)** introducing the enzymes in two modular DNA origami tubes (figure taken from [71]).

By regulating the humidity conditions, the time and the speed of the reaction, DNA structures can be transferred in silicon wafer, enhancing or reducing the etching process and so the sub-ten-nanometer depth of patterns. To control the orientation and the position of the DNA origami structures on the surface, an electron beam lithography and dry oxidative process was developed. In particular, DNA origami-binding sites were created on a SiO_2 surface through lithography. DNA structures attached the binding site with the proper orientation and position forming a nano-ordered pattern. The possibility to control the 2D and 3D shape of DNA origami gave the opportunity to use it for the programmable synthesis of inorganic material. By designing a set of DNA origami, Liedl and coworkers induce a shape-controlled metallization **[69]**. The negatively charge backbone phosphate is bound by 1.4 nm gold cluster positively charged as a seed for the growth of the gold cluster. The nanoparticles continued to metalize the DNA origami reproducing accurately the shape. To improve the size and the resolution in the shape, Seidel and colleagues used a DNA origami as a mold which contained a gold nanoparticle acting as a seed **[72]**. The seed in the box-like mold would grow until it fills completely the box. Using this method it was possible to create different 3D metal shape as sphere, cube an Y-shape structure.

The possibility to precise position nano-objects enables to use the DNA origami as a platform for the study of enzyme cascades. All the metabolic processes inside the cell are maintained by a set of enzymes involved in the same pathway. Enzymes, target molecules and intermediates are usually localized in the same compartmentalized area in order to facilitate the efficiency of the working mechanism. Yan and coworkers used a DNA origami chip to link glucose oxidase (Gox)/horseradish peroxidase (HRP) **[70]**. Gox oxidizes the glucose to gluconic acid and produces hydrogen peroxide H_2O_2. The latter is the substrate for the HRP which transforms $ABTS^{2-}$ to $ABTS^{-}$. Positioning the two enzymes at variable distances, they observed the distance-dependence of the mechanism: the HRP activity decreased if it is up to 20 nm far from Gox, but increasing the distance between them, did not highlight a strictly relation due to their separation. The phenomena was explained through a 2D restricted diffusion when the enzymes are in close proximity, while for long distances between the pairs, the Brownian diffusion dominates the scene.
An evolution of this work was performed by Linko and colleagues through the design of two tube-like DNA origami containing separately Gox and HRP **[71]**. The connection of the two tubes, induced the formation of a DNA origami nanoreactor in which the diffusion is considerably reduced.

1.4 Aim of the thesis

The biological environments are complex frameworks in which chemical and physical stimuli synergistically operate in order to modify, digest and definitively remove externals body. The careful analysis of the constitutive material, the structural design and its resistance against modification and degradation induced by the operational environment are, indeed, fundamental parameters for the design of a successful device which is expected to operate within an biological organism.
DNA origami technology was proposed for numerous biological and medical applications because of its peculiar properties. Among them, the compatibility with biological environments, the programmability at nanoscale level and the precise addressability of nano-compound as drug molecules, metal particles or antibodies are noteworthy. Drug delivery devices actuated by specific molecular recognition or contrast medium are two examples of how DNA architectures can contribute to the technological development in medicine and pharmacologic field, aiming to more focused treatments and reduced side effects (cytotoxicity).

The shape of the device assumes a strategic role and should be finely designed considering not only the final objective, but also the conditions imposed by surrounding environments: different shapes can in fact produce different responses in the organism. A tetrahedral DNA structure benefits from a great nominal robustness and its successful internalization in living cells was demonstrated in several studies. These nanostructures are characterized by high mechanical rigidity and stability against nuclease degradation; moreover, they seem to be compatible with most cell uptake mechanisms **[73]**. By exploiting these properties Hemmi and coworkers used a DNA tetrahedron nanostructures to carry cytosine-phosphate-guanosine (CpG) oligonucleotides into macrophage like RAW264.7 cells **[74]**. By modifying the termination of each of the four DNA sequences composing the tetrahedron with CpG islands, they stimulated the Toll-like receptor 9 (TLR9) and induced immune responses. The secretion levels of certain cytokines (TNF-α, IL-6 and IL-12) stimulated by these CpG-tetrahedral nanostructures were dramatically higher than those by single-strand CpG oligonucleotides even with the help of transfecting agents. In another work, Andersen's group showed the transport efficacy of small interference RNA sequences in tetrahedral DNA cage. siRNA sequence are usually composed by few ribonucleotides able to hybridize a specific gene silencing it. They are efficaciously used for gene therapy but once in the cell, they are quickly degraded by nuclease. The loading of siRNA sequence inside a tetrahedral cage with the help of folate, improved the efficacy of RNAi and increased the blood circulation time with respect to that of isolated siRNA ($t1/2 \approx 24.2$ min vs $t1/2 \approx 6$ min) **[75]**.

DNA origami technology enhances structural stiffness and functionalization. The tetrahedral DNA origami can be differently designed in accordance with the final purpose. Varying the helix number and their disposition, the vertex design, the dimensions, and the typology of the desired polyhedron (wireframe or full structure), it is possible to plan architectures with different mechanical properties.

The aim of this project is the design, the synthesis and the characterization of a biocompatible sensor which changes its conformation in response to a molecular target recognition. The device presents a wireframe tetrahedral DNA origami shape, providing for a structural stability in different environments and at the same time characterized by a great flexibility. To monitor the target-induced motion we have planned to integrate a plasmon ruler, built through the suitable decoration of the tetrahedron with two 20 nm-gold nanoparticles. The DNA origami will operate as a molecular-switchable nanomachine

which tunes the inter-particle distance, providing a spectral response univocally linked to the state of the origami that transduces a molecular recognition event into an optical shift.
In our lab, we had already planned a plasmon ruler system as described in the paragraph 1.3.5. but it presented some critical issues: the flap-motion was strongly influenced by adhesion forces when deposited on a substrate and by thermal fluctuations in liquid environment. Moreover, when hybrid structures are forced to pass through the agarose gel net in an electrophoretic migration, the gel itself could induce a closure of the system.
The purpose of this work is the design and the validation of a DNA-origami nanostructure able to:

- switch its configuration in response to an external stimulus, that in our case will be a complementary DNA single strand;
- transduce a configuration change at the nanoscale to a macroscopic signal that can be read from remote, that in our case will be the optical shift of the LSPR absorbance spectrum;
- maintain its functionality also after the mechanically-harsh purification protocols that may be required by the adopted synthesis scheme, in our case mainly agarose gel filtration;
- maintain its functionality independently from the operative medium, that may have, as in the case we tested, solid, liquid, or gel character.

The wireframe DNA origami tetrahedron is composed by six DNA bundles connected at the vertices by flexible joints. The wireframe tetrahedral shape provides the necessary stability while preserving the required flexibility, overcoming the problems arisen in the previous structure. The decoration with two gold nanoparticles allows the transduction of the conformational change in a LSPR shift.

2 Materials and methods

2.1 DNA origami design

The design of the DNA origami structure has been implemented through CaDNAno software **[76]** arranged on a square lattice scheme (Figure 2.1). After the plan of the geometrical shape, parallel helices of scaffold strands are designed, imposing a central seam which enables the folding of a circular scaffold strand. The software suggests the crossover positions in order to avoid significant global twisting. Moreover it automatically generates a set of short helper stands (staples) after the input of few basic information as the crossover inter-distance (multiple of 16 bases) and the average bases number. Inter-helix crossover can be rearranged in order to minimize the overall stress and to increase the stability of the system. Oligonucleotides length is then leveled out at ~32 bases. Shorter oligonucleotides are also possible but the hybridization stability and uniqueness can be affected, on the other hand an excessive length could reduce the staples diffusion and interaction rate in the self-assembly process.

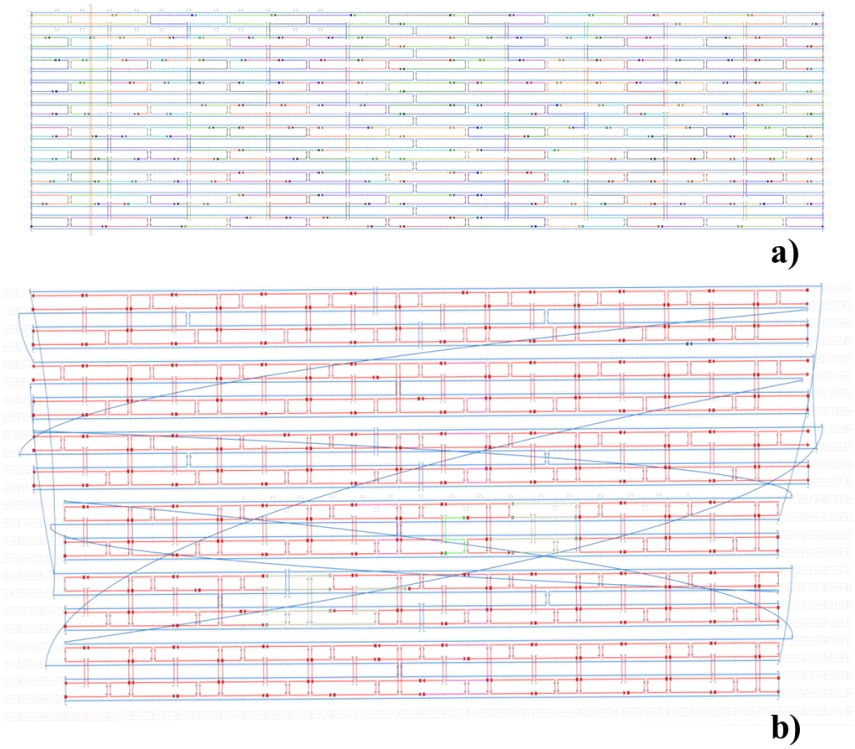

Figure 2.1 Design of DNA origami structure using caDNAno software: **a)** rectangle shape and **b)** tetrahedron shape. The horizontal blue lines represent scaffold strand helix, colored segments are staple strands which anneal scaffold strand to induce its folding through the arrangement of periodic crossover. Blue line protruding from the extremity of the structure in b) represent the scaffold junctions between different struts.

The insertion of scaffold strand sequence as M13mp18 determines the sequence of complement strands, exported in an excel file in which is specified the 5′ and 3′ points and the colors consistent with the one in the design (the staple sequences are listed in appendix 1).

CanDo **[77]** is an online sources which simulates scaffolded or non-scaffolded DNA origami 2D and 3D and the flexibility of single- and multi-layer structures to enhance their design process, starting from the input provided by the caDNAno design above. Through CanDo it has been possible to evaluate both the correct folding of the DNA origami structure and the thermal fluctuations of the system (Figure 2.2).

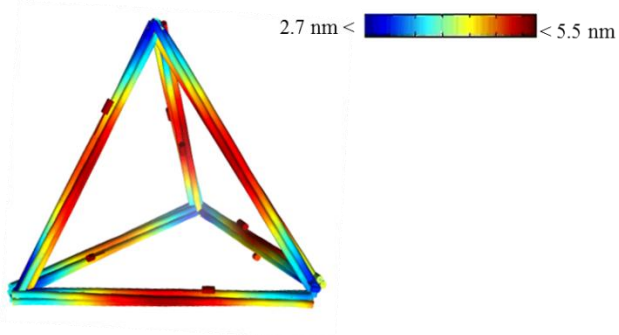

Figure 2.2 CanDo simulation of a tetrahedron shape DNA origami made of 6 four-helix struts; the bar associates the color with the thermal fluctuation of the structure (nm).

The probe or actuator strand and the catchers strands coming out from the DNA origami structure for AuNP anchoring, have been built following the rules of avoiding self-annealing, avoiding loops in each sequence, limiting the number of strong GC pairs, and checked using the online tools of IDT's Oligo Analyzer® v.3.1. Exceptions has been made for the target as it includes a 18 bp GC clamp (Table 2.1) **[63]**.

Actuator	5′-CGATCCGACCTTCCTCCCTCCTCCTCTTCCC TTGGGTCGAACATTGCTCGTCGTCACTGGGT CCTGCTCATATTGGGTTTACAGCTCACATAG GTAGACTTTAGCTTCCCGGGCTCGCAG-3′	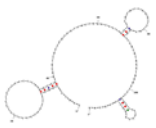 ΔG = - 5.44 kcal*mol^{-1}

Target	5′GGGCGGGGCGGGGGCGCGAAAGTCTACCT ATGTGAGCTGTAAACCCAATATGAGCAGGAC CCAGTGACGACGAGCAATGTTCGACCCAAGG GAAGAGGAGGACGCGCCCCCGCCCCGCCC-3′	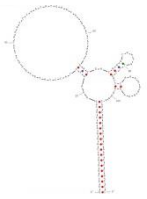 ΔG = - 27.8 kcal*mol^{-1}

Table 2.1 Sequences of the actuator strand and the target equipped by a stem and loop structure, the stem is obtained with CG pair (underlined sequences); on the right side of the box it is shown the most probable secondary structure of actuator and target strands and the relative Gibbs energies.

2.2 DNA origami synthesis and purification

The DNA origami synthesis is based on one-pot reaction where the whole set of staples and the scaffold strand are mixed together in a buffer solution containing Mg^{2+}. Staples are added 5 or 10 time in excess with respect to the scaffold strand and the synthesis buffer is composed by Tris (40 mM), acetic acid (20 mM), EDTA (2 mM), and $MgCl_2$ (12.5 mM) forming the TAE 1× + Mg^{2+}. The annealing path consists in a cooling down ramp obtained in a standard thermocycler: the sample is initially heated to denature DNA double strands; the temperature is then slowly reduced until room temperature with steps of - 0.1 °C. The cooling process duration is a critical point, and it has been largely examined by Shih and colleagues **[78]** in correlation with the bivalent cations concentration. It has been observed that multilayered DNA origami structures need longer annealing ramp probably because they traverse more kinetic traps, owing to the larger density of crossovers. The bivalent cations reduce the hybridization time neutralizing and consequentially stabilizing the final structure. Efficient Mg^{2+} concentrations range from 10 to 16 mM and the cooling process can last up to 173 h.

The purification of the freshly prepared DNA origami from excess of staples removes useless material which can interfere with well-folded sample. The purification can be reached in different way, in this work we explored the Amicon filtration and the direct extraction of DNA origami from agarose gel.

In the first method we remove extra oligo using Amicon Ultra 0.5 ml 100 kDa filters (Millipore, Massachusetts), adjusting the protocol supplied by the constructor. Briefly, TAE 2× / Mg^{2+} solution was added in the same amount of sample volume; capped Amicon Ultra were centrifuged four times refilling each time with 450 µl of buffer solution for 1.5 minutes at 14000 × g. Concentrated samples have been eluted spinning the inverted filters

in a clean vial at 2000 × g for 3 minutes. The second purification method allows the selection of the well-folded and single structure from dimers, aggregates and free oligonucleotides. The sample is previously separated through agarose gel electrophoresis and then the band of interest is cut, crushed and filter in a Freeze and Squeeze tube for 10 min at 10000 × g. At this point the gel matrix is confined inside the filter, while the DNA origami structure are extracted in few µl of buffer.

2.3 Agarose Gel Electrophoresis

Agarose gel electrophoresis is a method used in molecular biology to separate DNA fragments or protein based on their size and charge. Since nucleic acid molecules or structures are negatively charged, can be separated by applying an electric field in the agarose matrix. DNA origami analysis is performed using two references: the ladder as molecular weight standards for agarose gel electrophoresis and the scaffold strand M13mp18 which runs faster than the folded DNA origami (Figure 2.3, lane 2). The estimated time varies according to the temperature and the typology of the sample: in particular complex 3D DNA architectures require to run about 2 h at low voltage (50 V) in order to avoid the overheating and the consequently degradation of the sample.

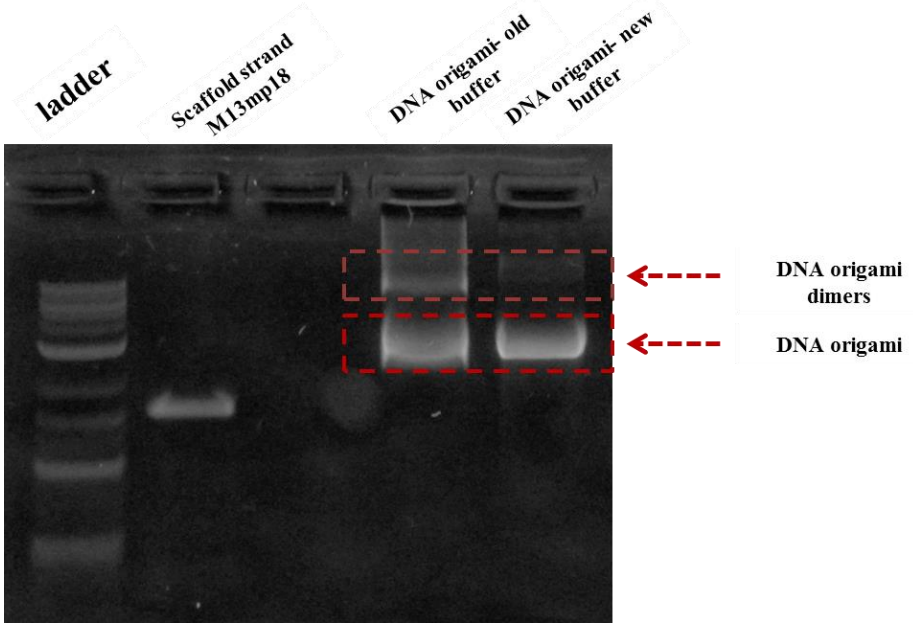

Figure 2.3 Example of agarose gel image exposed at UV light, post-processed with Image J software showing the migration of: ladder, scaffold strand M13mp18, DNA origami freshly synthetized using old and new buffer. The old buffer induced both a dimerization of DNA origami structure and both general aggregation (smear), at the contrary, with the new buffer this effect is reduced.

The gel is prepared mixing agarose powder (derived from algae agar agar) and TAE buffer in the right proportion for obtaining 1% mass/volume, boiling it in microwave oven until it dissolves and adding 1 × GelRed™ staining which intercalates inside DNA double helix and emits fluorescence if excited by UV light. The visualization of the bands produced by the electrophoretic separation is obtained through an UV transilluminator, recorded with a camera, and analyzed through post processing software, as Image J or similar (Figure 2.3).

2.4 DNA functionalization of Gold Nanoparticles

The functionalization of the gold nanoparticles surface increases the possible applications in order to exploit their peculiar optical properties. Small single strand oligonucleotides chemically modified with one thiol group at 5′ or at 3′ ends can fully cover the gold spherical surface through the formation of Au-SH bind. The 20 nm gold colloids (AuNP) are supplied in water with trace amounts of citrate which stabilized the negative surface charge **[79]** (extinction coefficient: 9.406 E^8 M^{-1} cm^{-1}, OD: 1 at 520 nm, particle/mL: 7.0 E^{11}) Ted Pella, Inc. First a coating with BSPP (Bis(p-sulfonatophenyl) phenylphosphine dihydrate dipotassium salt) has been carried on following published procedures **[80-82]**.

12 mL of colloids solution incubated overnight with 3.2 mg of BSPP. Then the particles are precipitated adding gradually NaCl until the solution changes color from ruby red to blue/gray. After the centrifugation at 10000 × g for 10 min, the transparent supernatant is removed, rinsed with BSPP 0.5 mM, concentrated and resuspended. Buffer exchange is achieved with another centrifugation step adding 50% in volume of methanol to induce the precipitation of the NP and then resuspending the concentrated sample with a solution of BSPP 2.5 mM in approximately 2 mL of final volume. The concentration of the AuNP in BSPP 2.5 mM is evaluated through absorbance analysis preformed in a spectrophotometer, diluting 1:20 the highly concentrated solution with ultrapure water into a quartz cuvette. The NPs concentration is determined through the Lambert-Beer's law, taking the max value of the peak at 520 nm and using the extinction coefficient provided by the manufacturer company (Ted Pella, Inc.). The ssDNA are designed and purchased from Sigma Aldrich; the average length is 22 nt and they are chemically modified with a disulfide bond at one end. Depending on the concentration, on the length and on the specific modifications, oligonucleotides are purified through HPLC or desalting. Before facing the NPs gold surface, the thiol group of 40 μM of oligonucleotide is reduced with 0.3 M 1,4-Dithiothreitol (DTT), 0.3 M NaCl and SPB buffer (0.01 M NaH_2PO_4/Na_2HPO_4, pH 7.04). All the material have been purchased from Sigma Aldrich unless specified. The

solution is aged on a tube rotator for at least 2 h and after the removal of DTT salt through NAP 5/10 columns filtration to avoid reducing environment, activated oligonucleotides are mixed with gold nanoparticle with a typical ratio DNA/NP of 3500-4000.

The following salt ageing process will provide for the necessary ionic strength for DNA strands stability and will avoid the aggregation of AuNP through the gradual addition of NaCl and SPB to reach a final concentration of respectively of 0.1 M and 10 mM. After the stabilization of AuNP- DNA complex, the centrifuge step in Amicon filter concentrates the sample removing the extra oligonucleotides that have not adhered to the surface and allowing the resuspension of the sample in TAE 1× + 0.1 M NaCl. The final concentration estimation is performed through the spectrophotometer.

2.5 Gold Nanoparticles anchored on DNA origami

The presence of catcher strands coming out from DNA origami structure provides for a site-specific anchoring of gold nanoparticles covered with complement ssDNA. The protocol, optimized by Piantanida and coworkers **[83]**, is based on the proportional mixing of the solution containing DNA origami structure with the AuNP solution in a ratio between binding site present on DNA architecture and AuNP of 1:2. In order to promote the hybridization, the sample is maintained at 50 °C for 45 min and it slowly cools down over night. The anchoring success is firstly checked with agarose gel electrophoresis (AGE); the result obtained can be confirmed by the visible pink / ruby red color of the gel band containing DNA origami (detected at UV light).

2.6 Hybrid structures purification through density gradient centrifugation

The separation of non-attached AuNP through AGE is an efficient method but if the sample is gel-extracted, the recovery yield is less than 100% and the desired structures may also be damaged. These limitations led to find other purification protocols capable of preserving the structural properties with high recovery yield that delivers purities of >90% **[84]**. Rate-zonal centrifugation separation is performed by loading the sample solution in a narrow single layer on top of a gradient medium inside 2 mL tube. The centrifugal step is performed selecting the gradient medium density, the viscosity and the proper acceleration to reach the separation in few hours in bench-top microcentrifuge. The particles sediment under the influence of: centrifugal force, buoyant force and drag force (proportional with the hydrodynamic radius). The density gradient contains 9 layer of density/viscosity

gradient of iodixanol (density = 1.32 g cm^{-3}, dynamic viscosity = 14.3 mPa s for 60 % iodixanol in water) from 15% to 50% mass concentration of iodixanol in TAE 1×. The 9 layers are prepared one day in advance in order to stabilize the gradient. The day after the AuNP-DNA origami hybrid structures are gently pipetted on the top of the iodixanol density gradient and then centrifuged at 7000 × g for ~ 3 h in a swing-bucket rotor centrifuge. Most of the times we obtain two separated red bands which represent the conjugated NP with DNA (upper band) and free AuNP (lower band). We basically collect with a micropipette the band of interest but frequently also the other band (free AuNP) to check the precision in separation of this protocol. Filtering the obtained sample with TAE 2× buffer + 25 mM $MgCl_2$ through Amicon centrifuge step, the viscous medium which affected the SEM images is removed.

2.7 Functionalized substrate for a controlled adhesion of the particles

The particles adhesion on a substrate is strictly correlated with the properties of substrate and of the samples. The deposition control in terms of number and disposition of the adhered structures favorites the single-particle detection and the detailed architectural analysis. For example the dark-field detection of single or dimer AuNP is feasible only if AuNP are not in close proximity. AuNP dimers DNA origami conjugated, if properly interspaced in a surface can be exploited as SERS **[57]** substrate or can induce a Raman signal enhancement **[60]**.

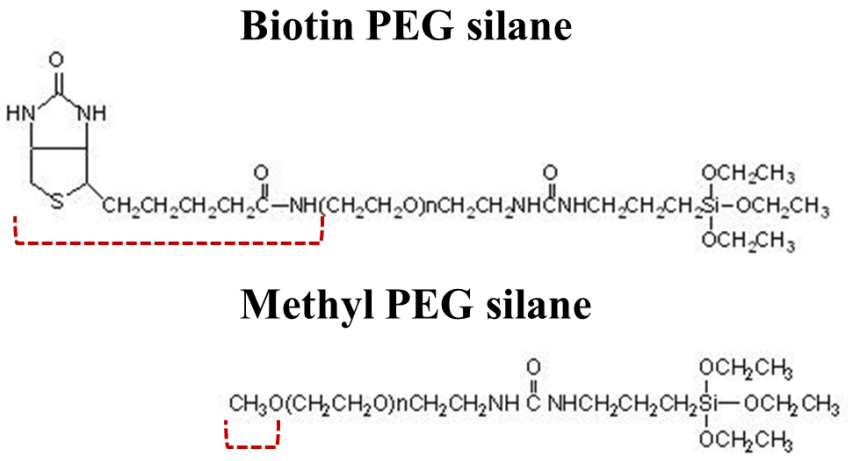

Figure 2.4 Chemical formula of Biotin-PEG-silane and Methyl-PEG-silane.

The substrate functionalization protocol is based on the proper mix of methyl-PEG-silane (2000 Da) and biotin-PEG-silane (3400 Da), both purchased from Sigma Aldrich (Figure 2.4). Hydrophilic polymer chains, poly(ethylene glycol) (PEG), are attached on the silicon surfaces by silylation of the silanol groups with the trimethoxysilanes of the polymers (Figure 2.4). We consider these tethered polymer chains to resemble to self-assembled monolayers (SAMs) of PEG since the grafting process is entirely spontaneous. All the preparation steps are performed in glove box to avoid the increasing reactivity of silanol groups. The two PEG molecules are separately dissolved in 97% of Ethanol + 30 mM HCl, and they have been freshly mixed before each incubation with the substrate. We prepare two different proportions of mPEG-silane and biotPEG-silane, 98:2 and 99.9:0.01, obtaining a total concentration of PEG molecules of 500 μM in a final volume of 5 mL using EtOH-HCl as solvent. The incubation of the two different solutions with the silicon wafers is performed at room temperature overnight. In parallel, a negative control in which the incubation of the silicon wafer is done with a solution of mPEG-silane 490 μM in EtOH/HCl has been realized. All consecutive steps involve both sample and control.

Washing steps with EtOH/HCl solution have been done the day after to remove all the non-attached molecules. Surface passivation is obtained after 1 h 30 of incubation with 2% BSA. The BSA is then removed with three successive washing steps with TAE 1×. Then 160 nM of streptavidin in TAE 1× solution is incubated for 2 h. Streptavidin is a tetrameric protein which binds biotin with high affinity ($Ka = 10^{15}M^{-1}$) and specificity and it is able to link more than one biotin simultaneously. After the streptavidin excess is removed through another washing with TAE 1× buffer. Finally, 1.8 nM of 20 nm biotinilated-AuNP is spotted and incubated in wet chamber for 1 h and then the sample is washed three times with MilliQ water. Once the sample is dried, functionalized silicon wafers have been imaged through SEM. The AuNP count and the statistical analysis of each picture has been performed through Image J software.

2.8 LSPR analysis direct in agarose gel

UV-Vis characterization has been performed on inverted optical microscope (Axiovert 200, Zeiss) in transmitted light illumination (HAL 100 illuminator, Zeiss) coupling a microscope with 750 mm long spectrometer (Shamrock SR-750, Andor Technology plc.). The agarose gels resulting from the electrophoretic procedure with distinguishable bands have been placed onto clean glass coverslip that was mounted on XY sample stage. The light transmitted through the sample has been collected by 100x immersion objective (NA

1.45, α Plan-FLUAR, Zeiss), directed into a spectrometer, split by a diffractive grating of 600 lines/mm, and finally analyzed using TE-cooled EMCCD (Newton DU971-UVB, Andor Technology plc.).

A basic equation to calculate the actual extinction spectra is:

$$A + S + R + T = 1 \quad (1)$$

where A is absorption, S is scattering, R is reflection and T is transmission of the light and A+S= E represents the extinction. Neglecting the difference in the light reflection from the surface of clean gel and the one with AuNP, E = 1- T. Thus, the final equation to calculate the extinction is:

$$E = (I_0 - I_i)/(I_0 - I_{bg}) \quad (2)$$

where I_i is the corresponding intensity of light passed through each band, and I_0 is the intensity of light passed through the clean gel in a position without origami and nanoparticles. I_{bg} is a dark thermal noise of CCD. At least 5 different positions along each band have been characterized and finally averaged **[63]**.

The resulting spectra show a peak in the range of 525-535 nm which is attributed to the LSPR in single gold NPs or dimers. The spectra also demonstrate a different extinction at low wavelengths complicating an estimation of LSPR position. Since the gel density, gel hydration and AuNP size in each series of experiment are supposed to be constant the difference in the extinction is caused by a variable gel thickness of the lanes. To determine the LSPR position we applied two steps procedure. At first step, the background corrected for the gel thickness was plotted for each spectrum and then subtracted. Second, the resulted spectra were fitted with two Gaussian functions in the range of 450-700 nm considering i) LSPR in spherical gold NPs at about 530 nm **[85]**, and ii) an additional peak in the range of 560-600 nm (Appendix 2). The last one is caused either by a non-sphericity of gold NPs **[86]** or possible plasmon coupling effect **[87]**, which cannot be distinguish in our case.

2.9 Scanning Electron Microscope characterization

Scanning electron microscope (SEM) is a type of electron microscope that produces images of a sample by scanning the surface with a focused beam of electrons. The accelerated electrons (1-30 kV) interact with the atoms in the sample, producing scattered electron with different energy and intensity depending on the surface topography and composition. The electron beam is scanned in a raster scan pattern, the scattered electrons are collected and amplified with the aid of detectors positioned at fixed angles, their

intensity is associated to the position of the primary beam in the sample, and finally the image is reconstructed point by point. The specimens should be observed in high vacuum. SEM can theoretically achieve resolution better than 1.6 nanometer, but not all the samples can be imaged with that resolution. The chemical nature of the sample, the presence of a metal coating which can enhance the scattered signal and the voltage applied can reduce it dramatically. Biological samples for instance, are imaged in a ultra-vacuum conditions, so dehydration and metallization are required. Small biological sample such as vesicles, proteins or DNA structures are usually deposited on silicon wafer which is the material of election for SEM measurements because it is a flat semiconductor material. The surface previously cleaned with ethanol or isopropanol and acetone, is then physically activated with Plasma Oxygen treatment. To make the surface hydrophilic, we physically / chemically modify the surface using the suitable protocol. The same activation has been obtained using different instruments: Reactive Ion Etching and a bench plasma cleaner. With reactive plasma etching it is possible to control all the parameters of plasma oxygen treatment. Bench plasma cleaner, instead, can control only of the power applied, while chamber pressure and consequently the BIAS and the oxygen flow remain unknown. However we got a successfully activation with both instruments. Oxygen plasma cleaning, in principle, produces an energy which is very effective in the breaking of most organic bonds of surface contaminants. A second cleaning action is carried out by the oxygen species created in the plasma (O_3, O, O^+, O^-, ionized ozone and free electrons). These species react with organic contaminants to form H_2O, CO, CO_2, and exhibit on the surface OH groups making the surface more hydrophilic.

The oxygen plasma obtained with Plasma Cleaner, has been performed applying a power of 40 W and a constant flow of oxygen for 2 min. The same protocol performed with RIE, provide for a precise control of the Bias (maintained stable at 100 V) and of the oxygen flow (fixed at 30 sccm). The oxygen plasma cleaning, in principle, can destroy the carbon layer on the top of the TEM grid. For this reason we developed a less incisive treatment which is based on a disposition of the grid inside a metallic holder maintaining the grid in an oblique position. The latter produces a weaker effect of the plasma because it reduces the gas molecule entrance. Moreover, we have decreased both the power applied from 80 to 20 W and the BIAS from 100 V to 45 V. At the same time we extended the treatment from 2 to 5 min, achieving the same effect obtained with silicon wafer. If the procedure is effective, the drop should spread immediately across the substrate, otherwise it maintains its shape because of the hydrophobic repulsion. 5 μl drop of DNA origami sample with and

without gold nanoparticles is left adsorb on the activated surface (silicon wafer or TEM grid) for 7-10 min before being washed twice with ultrapure water. After drying, the samples are imaged with scanning electron microscope Supra Zeiss 40 at 2 kV of acceleration voltage, a working distance between 2-5 mm and a filament current of 2.3 A.

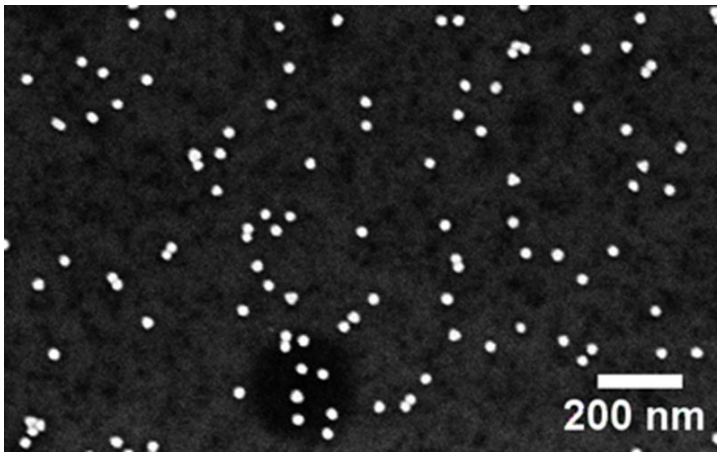

Figure 2.5 Gold nanoparticle adhered to a silicon substrate functionalized with an organic polymer, imaged at SEM using an energy of 2 kV and a working distance between 2-5 mm.

Electrons seriously damages DNA origami structures after few second of exposition, so the measurements must be acquired rapidly. Gold nanoparticle, instead, are imaged with greater precision (Figure 2.5), so we exploit the numerous pictures obtained to measure the dimers inter-particle distance (from center to center) in order to estimate the average gap length.

2.10 Atomic force microscope characterization

Atomic force microscope (AFM) is a scanning probe microscopy (SPM) with a nanometric resolution that overcomes the optical diffraction limit.

AFM provides a 3D profile of the surface on a nanoscale, by measuring the interaction between a sharp probe (<10 nm) and a surface at very short distance (0.2-10 nm probe-sample separation). The AFM cantilever "gently" touches the surface and records the small force between the probe and the surface through a raster scan in a x-y plane. The motion of the probe across the surface is controlled through the feedback loop and the piezoelectronic scanners. The feedback loop has the cantilever deflection as input, and its output controls the distance along the z axis between the probe and the sample. The deflection of the probe is typically measured by an optical lever method: a semiconductor diode laser is bounced off the back of the cantilever and onto a position-sensitive photodiode-detector which

measures the bending of cantilever during the tip scanning over the sample. The measured cantilever deflections are used to generate a map of the surface topography, the signal achieved is plotted in a pseudocolor image, in which each pixel represents an x-y positions on the sample and the color represents the recorded signal. The AFM resolution is strictly dependent on the radius of curvature of the tip apex (typical 5-20 nm) and for this reason, compared with electron microscopy, the achievable resolution is much lower in x-y axis but it is sub-nano-metrical in z axis. AFM can operate in three different modes: contact, intermittent contact and non-contact mode. In contact mode the tip follows the samples exploiting repulsive forces, while in intermittent contact the tip oscillates up and down at its specific resonance frequency exploiting attractive forces. The oscillation amplitude and frequency are usually maintained constant but the interaction of forces acting on the cantilever when the tip comes close to the surface (Van der Waals forces, dipole-dipole interactions, electrostatic forces) causes the amplitude of the cantilever's oscillation to change as the tip gets closer to the sample. While in non-contact mode, the tip of the cantilever doesn't interact with the sample surface and long-range forces that extends above the surface act to decrease the resonant frequency of the cantilever.

The DNA origami AFM characterization can be performed both in liquid and in air. Visualization of biological sample benefit from the development of the intermittent contact mode in liquid for different reasons. First the tip does not deform the soft sample, second the bio-sample weakly adheres to the surface and the tip contact can modify or display it, and third the liquid conditions reproduce the physiological conditions of the sample. However the oscillation of a cantilever in a liquid presents important differences compared with oscillation in air or ultrahigh vacuum.

The cantilever motion drags the surrounding liquid, leading to an increase of the effective mass and a corresponding decrease of the resonant frequency. And the strong hydrodynamic interaction between the cantilever and the liquid produces a very low quality factor (Q) of 2-10, about two orders of magnitude lower than in air. We observed that the DNA origami imaging can be performed in liquid as well in air without modification of the sample proprieties. Moreover the measurements in air increases both the final resolution of the picture and the stability of the sample that can be analyzed better also after few days from the sample preparation.

The election substrate for the DNA origami imaging is freshly cleaved mica substrate which is extremely even, flat and negatively charged. The DNA origami particles are immersed in a saline buffer TAE 1× containing 12.5 mM of Mg^{2+} cations, which act as

bridges between the negatively charged phosphate backbone of the DNA and surface, thereby increasing the adhesion of the DNA onto the mica surface **[88]**. The addition of 1 mM of $NiCl_2$ solution in the final volume implements the adhesion between DNA nano-structures and mica substrate. After 15 min of incubation the drop can be dried with a tissue, washed twice with a buffer solution to remove the not attached particles and rinsed with 1.5 ml for in liquid measurements (Figure 2.6b) or washed directly with ultrapure water and dried with a nitrogen stream for few seconds (Figure 2.6a).

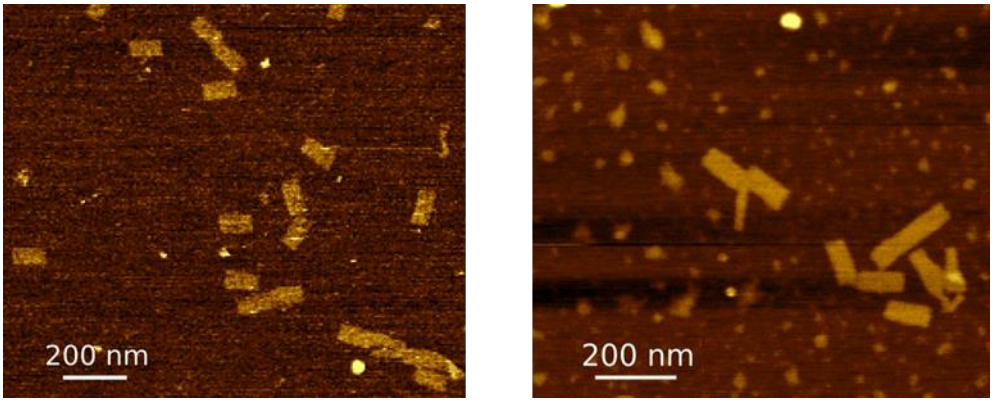

Figure 2.6 AFM topography DNA origami rectangular shape deposited on mica: **a)** in air **b)** in liquid. The images are performed with JPK AFM using a pyramidal cantilever. The pictures are both post-processed using Gwyddion software.

The AFM images have been recorded using a JPK Nanowizard II, operated in liquid phase in tapping mode or in air in contact mode using Olympus OMCL-TR400PSA tips with a nominal force constant of 0.08 N/m and a resonance frequency of 34 kHz (in air).

2.11 Transmission electron microscope characterization

The transmission electron microscope is a type of electron microscope where the electron beam is transmitted through a specimen to form an image. The specimen, with a thickness ranging from few to hundred nanometers, lays on a TEM grid. The electrons beam (50-200 kV) focused with a condenser system passes through the sample. The final image is reconstructed and magnified through lenses and it is finally recorded on a fluorescent screen or a charge-couple device (CCD).

Materials with electron densities that are significantly higher than amorphous carbon are easily imaged. These materials include most metals (e.g. silver, gold, copper, aluminum) characterized by heavier atoms which scatter more electrons and therefore have a smaller electron mean free path than lighter atoms.

In general, samples must therefore be stable under vacuum, and so are traditionally prepared in the solid state. The water content of biological sample (cells, matrix, or proteins, etc.) requires other strategy for TEM visualization. Because biological material essentially consists of atoms of low atomic number, the contrast and consequently the signal-to-noise ratio (SNR) is generally low in cryo-EM. To increase the contrast of the bio-sample, uranil acetate and formate staining are commonly used.

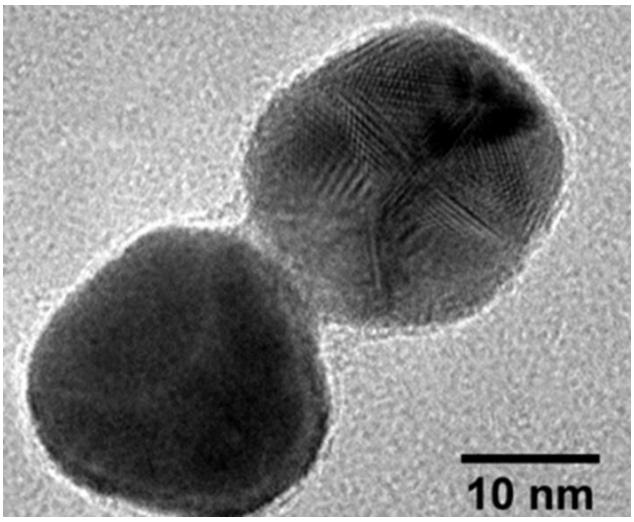

Figure 2.7 TEM picture of two 20 nm gold nanoparticles with a full coverage of ssDNA.

TEM imaging has been largely used for the characterization of DNA origami-gold nanoparticle hybrid structures. In particular, copper grids covered with a thin carbon layer have been activated with a plasma cleaning treatment for 5 min at 20 W (45 bias). A drop of solution is then deposited on the surface and after 5 min it is removed with a paper wipers and rinsed twice with ultrapure water. When it is completely dried, it is possible to image it (Figure 2.7).

2.12 Cryo-electron microscope characterization

TEM measurement is useful method to examine with high resolution biological samples, but it presents few negative points. During the drying process of the sample, for example, the structures can collapse and the superficial tension forces can draw near the structures close to each other.

Cryo-electron microscopy is a method in which the sample is frozen instead of dehydrated and then imaged at cryogenic temperatures by electron microscopy. The possibility to freeze the samples allows the keeping of the physiological condition, avoiding destructive

treatments. The specimen are prepared in standard buffered media and a drop of 4 µl is applied to an EM grid (200-mesh grid, EMS, Hatfield, PA). The grid is blotted for 3 sec and immediately plunged into a cryogenic liquid (ethane); this step called vitrification, prevents the rearrangement of water molecule into a crystalline lattice **[89]**. Plunge-freezing of the cryo-EM grids has been performed using Leica EM GP (Leica, Buffalo Grove, IL) that incorporates a chamber to control the humidity (80%) and the temperature (8°C) for blotting and thus the evaporation. The sample is stored in nitrogen and remains always below -140°C to avoid devitrification. Hydrated, unstained samples are sensitive to electron irradiation because higher doses lead to progressive alterations of molecular structures **[90]**. Consequently, cryo-EM images have been recorded at low electron exposures, limiting their signal-to-noise ratio (SNR).

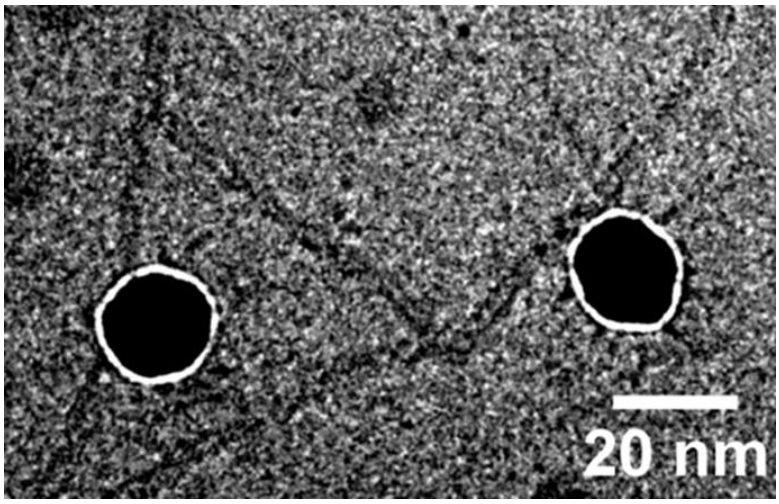

Figure 2.8 Cryo-EM image of DNA origami bundles organized in a triangular shape decorated with 20 nm-gold nanoparticles.

The DNA origami architecture decorated with gold nanoparticle have been imaged with Zeiss Libra 120 transmission electron microscope (Carl Zeiss SMT GmbH, Oberkochen, Germany) equipped with a LaB6 gun operating at 120 kV, an in-column energy filter, and a 4 k × 4 k Gatan UltraScan 4000 CCD camera (Figure 2.8).

Numerous techniques can be used in cryoelectron microscopy, one of the most popular is the electron cryo-tomography which consists in a set of electron micrographs (tilt series) acquired at different angular orientations of the sample. Tilt series images are then aligned and computationally merged into a 3D image (tomogram).

2.13 Small angle X-ray scattering characterization

Small-angle X-ray scattering (SAXS) is a powerful method for the structural characterization of both ordered and disordered macromolecule in solution. It provides nanoparticle size distributions, resolves the size and shape of (monodisperse) macromolecules, determines pore sizes, characteristic distances of partially ordered materials under various experimental conditions varying from extreme (e.g. high pressure or cryo-frozen) to nearly native. This is achieved by analyzing the elastic scattering behavior of X-rays when travelling through the material and recording their scattering at small angles (typically 0.1 - 10°). It is done using hard X-rays originated from a source of synchrotron radiation with a wavelength of 0.07 - 0.2 nm. If the angles considered are between 10 - 90 °, this technique is called Wide Angle X-ray Scattering (WAXS).

The setup of a SAXS experiment is conceptually simple: a solution of particles usually placed in a quartz capillary is illuminated by a collimated monochromatic X-ray beam, the intensity of the scattered X-rays is recorded by an X-ray detector (Figure 2.9). The scattering pattern of the pure solvent is collected as well and subtracted from the sample solution scattering leaving only the signal from the particles of interest. SAXS allows the analysis of different biological systems: mesoporous structures, polymer and proteins, colloids and nanoparticles but also gels. Thanks to this, we performed SAXS measurements of the DNA origami structures with AuNP in the original mix solutions, from agarose gel band and after the gel extraction. We used Au nanoparticle dimers with an interparticle distance comparable with the one in our DNA origami structure as a reference system.

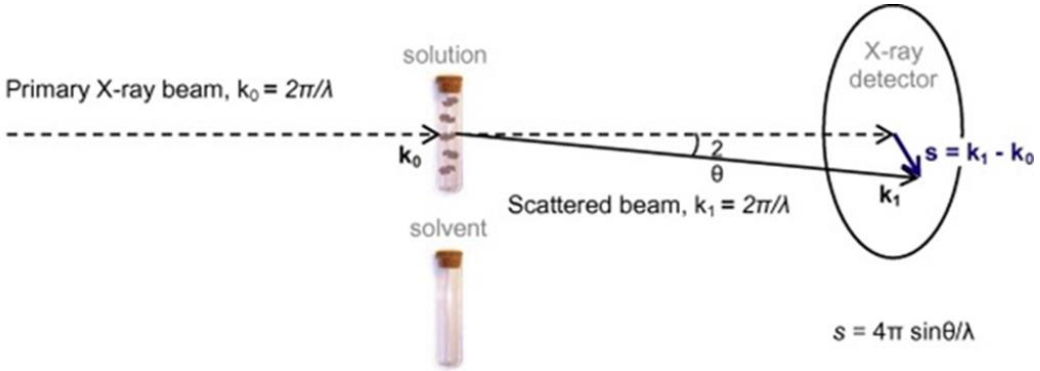

Figure 2.9 Working principle of SAXS analysis: x-ray primary beam crosses the solution containing the particles of interest; the x-ray beam will be partially scattered and the scattering pattern is then collected; subtracting from the scattering pattern of the solution the one of the pure solvent, it is possible to obtain the signal from the particles of interest.

The dimers have been obtained from the incubation of AuNP functionalized with two complementary sequences: the number of nucleotides (16 nt, 21 nt, 27 nt, 54 nt) composing the sequences would influence the interparticle distance.

Small Angle X-ray Scattering (SAXS) measurements have been performed at the SAXS beamline of Elettra Sincrotrone in Trieste **[91,92]**. SAXS images have been collected with a Pilatus 1M detector (Dectris, CH) in a q-range from 0.058 nm^{-1} to 5 nm^{-1}, at a photon energy of 8 keV. Sample-to-detector distance was 1381 mm. The liquid samples have been filled into flow through glass capillaries of 1.5 mm diameter (WJM-Glas / Müller GmbH, Berlin-Pankow, DE) and then have been measured at room temperature. The samples in gel, have been crushed and filled into a closed cell at both sides with mica substrates. Scattering data obtained have been corrected for the fluctuations of the primary beam intensity and sample transmission. The background has been subtracted with a corresponding buffer measurement. The conversion into 1D SAXS pattern is done with Fit2D. Data fitting analysis has been performed using IGOR Pro (Wavemetrics) with custom-made functions based on the literature. We used the following models: Schulz distribution for the size distribution for spherical particles and Sticky Hard Sphere structure factor (SHS) **[93,94]**.

3 DNA origami test bench

3.1 Rectangular DNA origami

DNA origami technology allows the design of complex structures as 3D cubes, wireframes and polyhedra. The precise positioning of different nanoparticles makes the DNA origami a wide-range technology, exploitable for physical, chemical, biological and also medical studies.

Hybrid DNA-origami-AuNP structures present many critical points. For this reason the possibility to use a test bench is an important opportunity. A stable platform, characterized by defined mechanical properties, high stability, easy to recognize thanks to its unique shape can be considered a very good control to define experimental conditions. We have selected a 120 nm × 60 nm rectangular shape DNA origami both to fix the working conditions and to have a comparison with the more complex device planned. The rectangular shape DNA origami has been re-designed in our lab but it has been reported in several other study. The founding father was Paul Rothemund who firstly synthetized and characterized through AFM this shape, defining also its problem: the stacking among structures **[13]** which often occurs through bridges formation in linear edges which share a common path of staple strands. Anyway, the rectangle remains one of the most stable DNA origami structure and can be exploited as a platform to verify the positioning of gold nanoparticles.

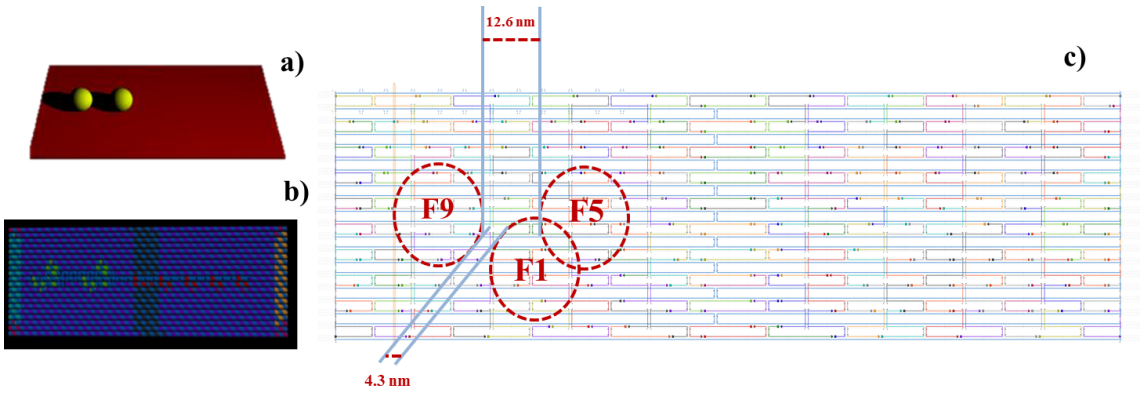

Figure 3.1 DNA origami rectangle: **a)** sketch of the structure decorating with two gold nanoparticle; **b)** Autodesk Maya rendering of the caDNAno design; **c)** caDNAno design in which the three AuNP binding sites and the respective interparticle distances are presented.

We defined three binding sites for three differently covered gold nanoparticle separated by 12.6 nm and 4.3 nm as shown in figure 3.1c. The final shape of the design performed with

caDNAno software, has been checked with Autodesk Maya (Figure 3.1b) which integrates the CAD file rendering helical disposition. The synthesis protocol lasts ~ 5 h and the cooling down ramp consists in a constant temperature decrease from 90 °C to 25 °C. Agarose gel migration as shown in figure 3.2 produced a smear of the band which usually does not influence the DNA origami quality.

The DNA origami rectangle has been purified through Amicon filtration following the protocol explained in paragraph 2.2. The agarose gel electrophoresis has been performed on the sample before and after the filtration step. The image displayed in figure 3.2 shows an increase in brightness of the DNA origami rectangle band after the purification which corresponds to an increase in concentration. To calculate the concentration we post-processed the images obtained with a standard camera. Considering the intensity of the non-filtered sample equivalent to 1.6 nM, which is the scaffold strand concentration, we proportionally calculate the intensity of the band brightness after Amicon filtration. The concentration often reaches 4-5 nM which is 2-3 times higher than the initial one.

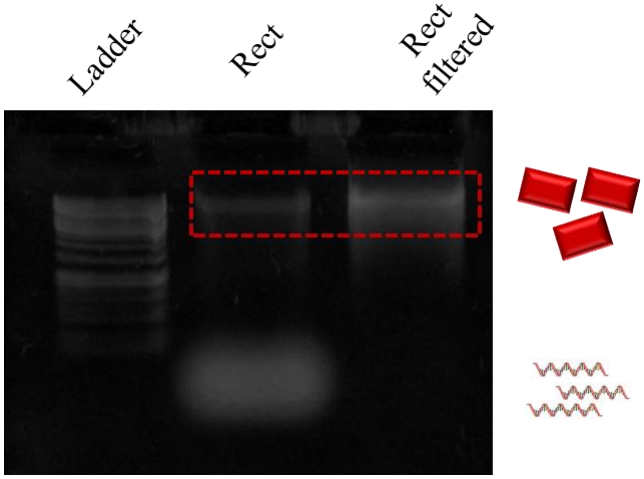

Figure 3.2 Agarose gel electrophoresis of DNA origami rectangular shape before and after the Amicon filtration. The lowest band represents free staple strands which are removed through filtration.

3.2 AFM sample preparation, analysis and preservation

Rectangular shape DNA origami have been used for studying DNA hybridization kinetics **[40]** as well as chemical reaction through the specifically displacement of biotins **[95]**. Most of these studies are based on the topographical detection of the DNA origami structure performed though AFM characterization. Rectangular DNA architecture is suitable not only for the investigation of molecular mechanism but also for the in depth-

analysis of adhesion mechanism to the substrate, of the sample stability in liquid and in air, and its preservation over the time.

The immobilization of DNA nanostructures on a surface is a key step for the integration of DNA-based material for electronic applications. Fritzsche and coworkers studied the effect observed when already immobilized and dried origami were again rehydrated under certain conditions, resulting in a certain ordering of densely packed origami structures **[96]**. In our case we used the rectangle to optimize a protocol to stably anchor DNA origami structures to the surfaces.

The sample has been initially spotted on a freshly cleaved mica substrate for 5 min and then ~1 mL of TAE 2× + 25 mM $MgCl_2$ has been added before AFM analysis. With this protocol we obtained high resolution images, in which it is possible to see the central seam of the DNA origami. However we observed that after 1-2 h, the structures did not adhere anymore to the substrate and were dragged from the AFM tip. To avoid this phenomenon, we improved the adhesion adding 1 mM of $NiCl_2$, which resulted in a prolonged stability during the time.

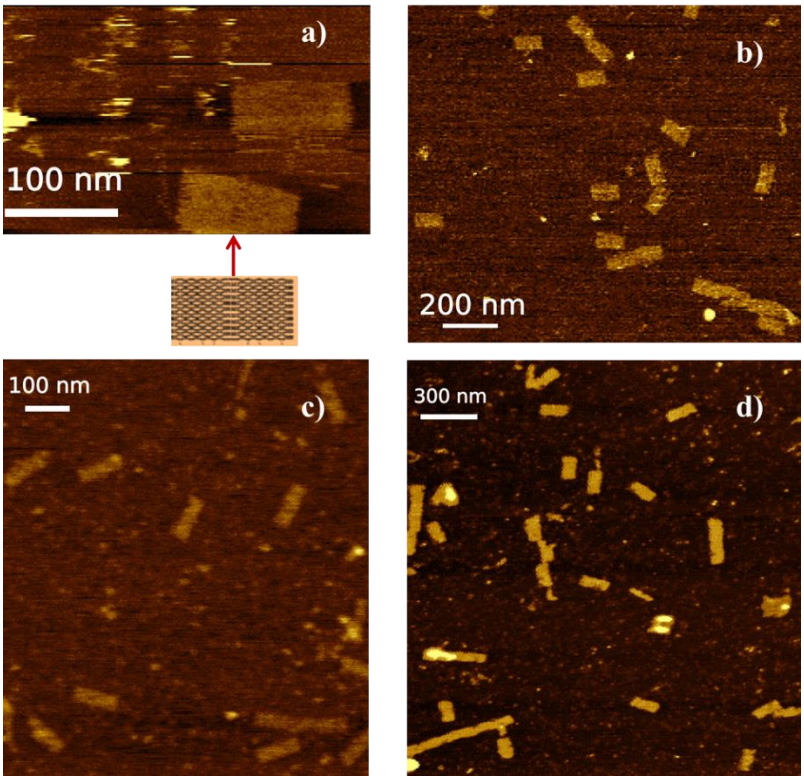

Figure 3.3 a) AFM of DNA origami rectangles in intermittent contact imaged in liquid showing the central seam of the structure. Evaluation of the DNA origami stability **b)** in liquid with a freshly prepared sample (intermittent contact); **c)** in air with one day sample (contact mode); **d)** in air with 2 months-old sample (intermittent contact).

We analyzed the sample through AFM topography in liquid on the freshly prepared sample (intermittent contact), one day after we repeated the same measurement on dried sample (contact mode), after two months we performed on the same sample the measurement in air (contact mode). The images demonstrated that the time and the drying process did not affect the structure of the DNA origami (Figure 3.3). Even if buffer solution is considered determinant for the maintenance of the biological molecules in the physiological conditions, in this case it was not crucial for preserving DNA origami shape.

Moreover we investigated also the adhesion strength of DNA origami on the silicon surface (after plasma cleaning treatment) performing AFM topography. A comparison analysis has been done with SEM. The images showed that DNA structures strongly adhere to silicon thus allowing AFM measurements.

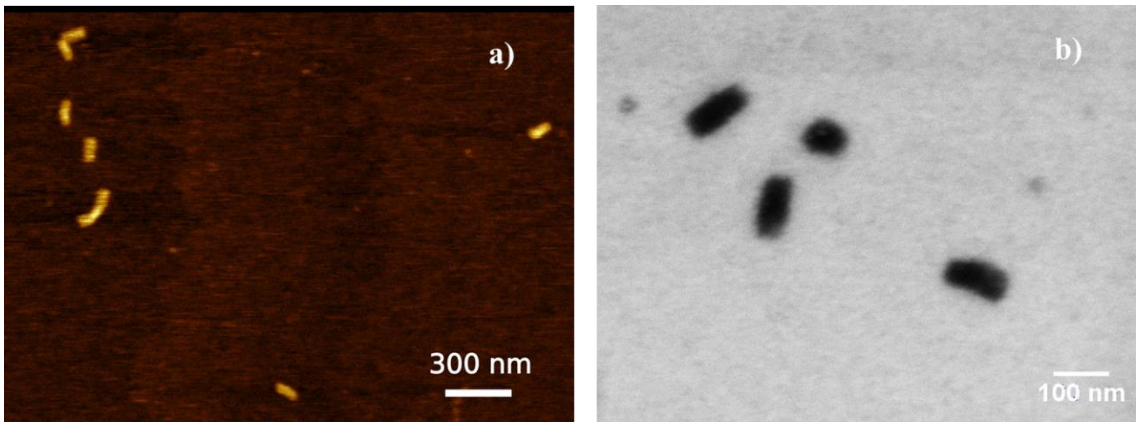

Figure 3.4 Rectangular shape DNA origami on silicon imaged with **a)** AFM performed in air (contact mode); **b)** SEM.

3.3 DNA coverage of gold nanoparticles

The ssDNA coverage of gold nanoparticles has been done using an already optimized protocol described in the paragraph 2.4 **[83]**. A good covering of gold nanosphere is correlated with the typology of the bond and with the reactivity of the molecules arranged on the surface. The number of molecule involved on the coverage strongly influence its reactivity. In particular, if the molecule density is high, the ssDNA are highly packed because of the stacking interaction along the molecular chains. A reduction in the number of molecules, instead, could generates a large non-homogeneity on the surface that prevents the correct stand up position leaving most molecules laying down **[97]**. This effect produces a large portions of gold surface exposed and available for electrostatic interactions such as, for example with the ions contained in the buffer solution. Since the

gold surface is negatively charged it tends to generate aggregation between NP through the formation of an electrostatic salt bridge between exposed gold surface portions. The success of the functionalization procedure, therefore, is correlated with a sufficient number of molecules attached on the surface to allow the NP neutralization in buffered ionic solutions.

In our functionalization protocol, we used one of the most common way to produce a full DNA coverage of the gold sphere, consisting in the formation of sulfur-gold bond. Sulfur atom, in fact, strongly interacts with a cell of four gold atoms of the nanosphere providing for a strength bond similar to the covalent one (Figure 3.5a) **[98]**.

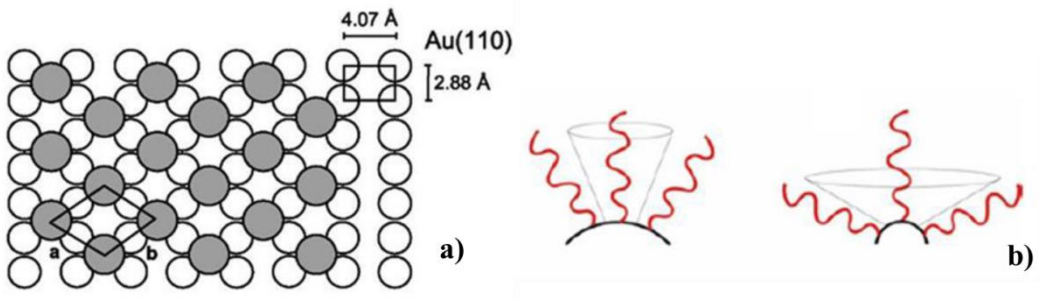

Figure 3.5 a) Representation of sulfur-gold bond: the S atom strongly interacts with 4-Au atoms cell (figure taken from [98]); **b)** The radius of curvature of a spherical surface induces a different arrangement of the molecules which determines the angle between molecular chains affecting the stacking interactions.

In literature there are many examples of Self Assembly Monolayer (SAM) in which thiol modified molecules react with gold planar surfaces to create a monolayer with a controlled degree of order. The radius of curvature of a spherical surface induces a different arrangement of the molecules which determines the angle between molecular chains affecting the stacking interactions (Figure 3.5b). The substitution of sodium citrate, used for gold colloids synthesis, with BSPP (Bis(p-sulfonatophenyl) phenylphosphine dihydrate dipotassium salt) is fundamental to passivate the gold colloids surface. Moreover, BSPP can be easily replaced by thiol reactive groups.

Single strands DNA are modified with thiol reactive group at one extremity. But the presence of a disulfide bond (oxidation of two thiol groups that bind together) is thermodynamically favorite in solution and prevents the premature disulfide bond formation in solution between the DNA strands. For this reason, the thiol group is synthesized with a protective chemical "cap" making the extremity not reactive. The reduction reaction to break disulfide bonds can be carried on with several reducing molecules. Among them, we selected dithiothreitol (DTT) because, as widely reported in literature **[99]**, it is able to reduce the disulfide bond producing two -SH (thiol)

terminations. Immediately after DTT de-protection, the DNA molecules have been mixed with a proper ratio with gold colloids previously coated with BSPP (DNA concentration/ NP concentration = 3500-4500). The salt-ageing process in which the NP are kept stirred and a small salt (NaCl) amounts are added step by step to reach 0.1 M concentration which gradually stabilizes the link of DNA strands on the gold surface. Thanks to this slow process, DNA strands can acquire all the ionic charge needed to strengthen the interaction with the surface, avoiding aggregation caused by rapid salt amount addition.

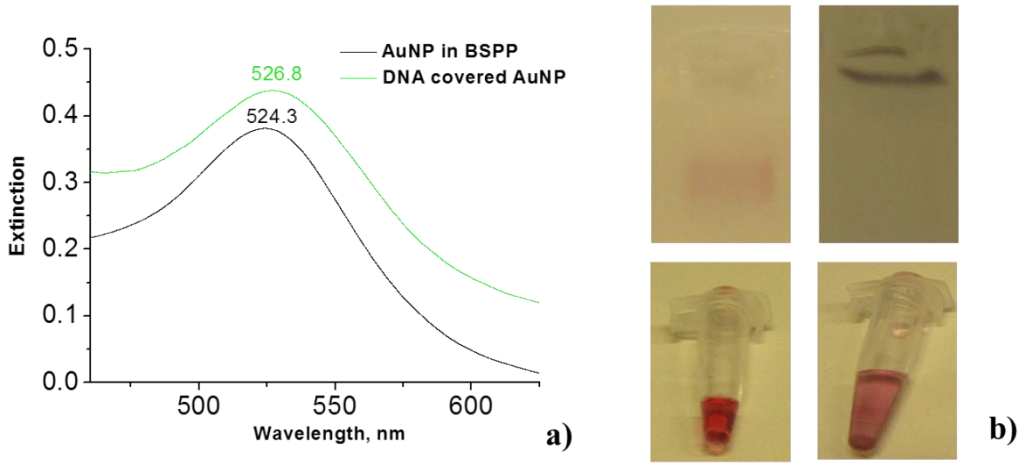

Figure 3.6 a) Extinction spectra of (i) 20-nm gold nanoparticles in BSPP (peak max = 524.3 nm) and (ii) 20 nm gold nanoparticles DNA functionalization. The latter induces a red-shifted plasmonic peak associable with a change of permittivity. **b)** Functionalized gold NP are characterized by a ruby red color which becomes violet/gray after the formation of aggregated complex; the agarose gel migration is avoided if functionalized NP aggregate forming a violet line inside agarose well.

The solution stability is primarily checked controlling the color that should remain ruby red and transparent (Figure 3.6b). The same color should be maintained also after agarose gel electrophoresis migration. If functionalized gold colloids are stable also inside buffer solution, they enter in the gel producing a clear red colored band otherwise they don't enter inside the well producing a violet/ gray line (Figure 3.6b). The UV-Vis spectra performed with the gold colloids in BSPP shows a peak maximum at 523 nm, after the functionalization with DNA, the peak position is slightly red-shifted to 527 nm because the permittivity is changed (Figure 3.6a).

3.4 Functionalized substrate for nanostructures anchoring

Biotin-functionalization of DNA origami structures as well as DNA covered-AuNP, introduce anchor points to specifically deposit the particles on a substrate. Thus, the

substrates modification with organic molecules which are able to bind both the substrate and the nano-particle of interest. In our experiment, we functionalized a silicon wafer with two different PEG-silane one modified with methyl-group and the other one with biotin. Overnight incubation in non-oxidizing atmosphere was sufficient to fully recover all the silicon piece. We mixed methyl-PEG-silane and biotin-PEG-silane in different proportions (ratio 1 = 98:2 and ratio 2= 99.9:0.01). The height profile of the layer was determined in dried sample through AFM topography, repeated also after the scratch of a small area to calculate the layer thickness. The height profile of different scratched area presents an height average of 1 nm (Figure 3.7), demonstrating that there was an organic layer laying on the surface.

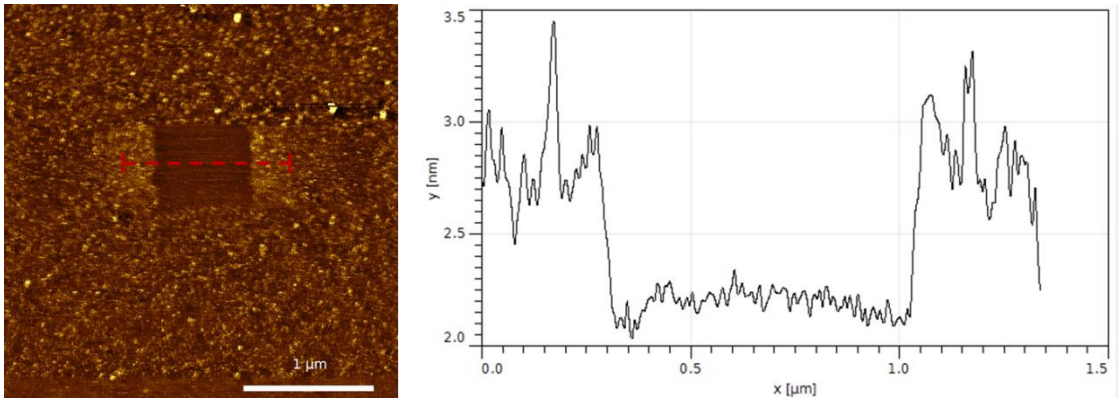

Figure 3.7 AFM image of PEG-silane functionalized substrate with the central scratch performed with AFM tip; the profile measurement shows a step of ~1 nm.

To understand the relation between the biotinilated-PEG concentration in solution and biotin deposited on the surface, we functionalized gold nanoparticles with an oligonucleotide biotin-modified. The streptavidin addition and the washing steps have been performed for each ratio (methyl-PEG-silane and biotin-PEG-silane) in parallel both for the sample and for the negative control represented by a substrate functionalized only with methyl-PEG-silane. After the incubation with biotinilated-AuNP we counted through SEM their density (Figure 3.8). The statistical analysis evidences that AuNP average number in the negative control was 20 times less than the sample containing 0.01% of biotinilated-PEG. The sample containing 0.01% of biotinilated-PEG shows an half number of particles with respect to the sample containing 2% of biotinilated-PEG. The aspecific binding of AuNPs observed in negative control remained constant in all the experiments.

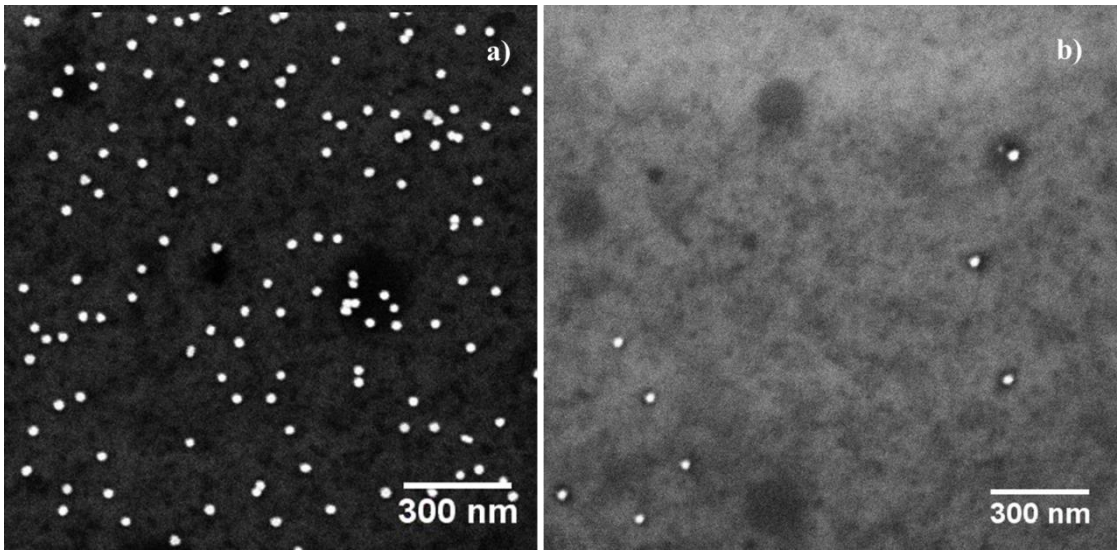

Figure 3.8 SEM picture representing biotinilated-AuNP incubated on functionalized substrate with: **a)** 99.9 : 0.01 of metil-PEG-silane and biotinilated-PEG-silane; **b)** 100% metil-Peg-silane.

3.5 A platform for AuNP arrangement

Rectangle DNA origami allows different rearrangement of AuNP. We organized three binding sites for gold nanoparticle functionalized with a different DNA sequence (F5, F9 and F1) as shown in figure 3.1c. Each binding site is composed by three catchers strands protruding from the surface interspaced ~ 10 nm (AuNP radius). Our purpose was to increase the precision in positioning, and to strengthen the bond. However only two NP can be attached to the origami at the same time because of the partial overlapping of two binding sites (Figure 3.1c). The decoration protocol is usually performed mixing the DNA origami and the AuNP with a ratio of 2 NPs to each binding site. If the initial concentration of the NP is not sufficient to satisfy the ratio, an aliquot of NP solution is centrifuged to pellet the NPs and the volume of the supernatant is reduced as many times as necessary. The resuspended particles are then added to DNA origami and incubated at 45 °C/ 50 °C for 45 min, and cooling down overnight. The long cooling down ramp, should avoid thermal shock that can modify the structure. The presence of conjugated AuNPs and DNA origami has been confirmed by gel electrophoresis (Figure 3.9).

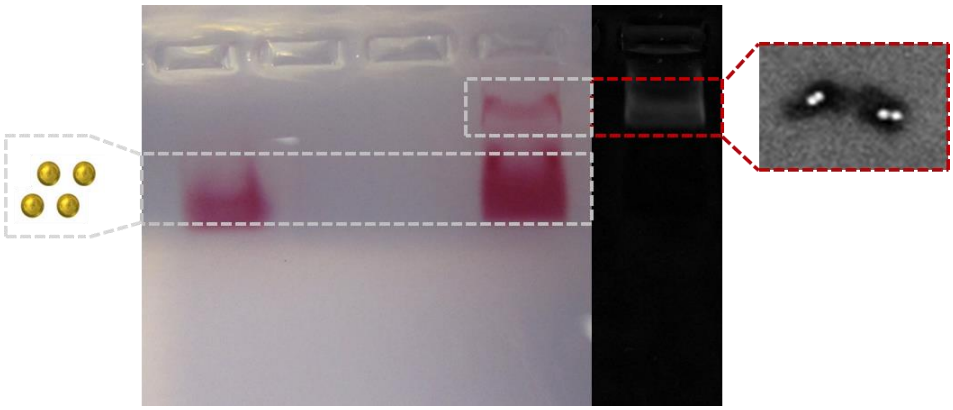

Figure 3.9 Agarose gel electrophoresis of DNA origami rectangle decorated with two AuNP, imaged with visible light and UV lamp, shows the band of the product functionalized and the band of free NP.

The samples decorated with one or two NPs have been imaged both with SEM and STEM as shown in figure 3.10. The purification of DNA origami rectangle from excess of free NPs has been performed using different protocols. In gel extraction the ruby red band corresponding to DNA origami-AuNP is cut and centrifuged in Freeze and Squeeze filter. The SEM imaging of purified AuNP-DNA rectangles showed the dirt produced by agarose gel residues as displayed in figure 3.10b. Most of the structures were trapped inside gel matrix and the concentration was extremely reduced. The further proof of a decrease in concentration was the color of the sample which became transparent after gel extraction.

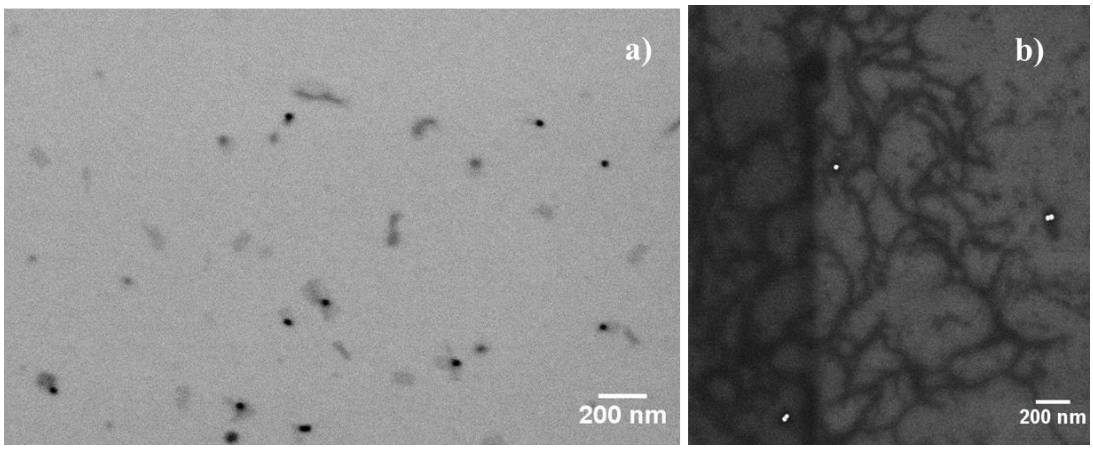

Figure 3.10 a) STEM image representing DNA origami rectangle decorated with one AuNP; **b)** freeze and squeeze gel extraction of the DNA origami rectangle linked with two AuNP.

These critical points encouraged us to find another way to purify the AuNP-decorated DNA origami using a completely new method exploited by Liddle's group **[100]**. The protocol is based on a density gradient separation which employs a viscous liquid (iodixanol) to purify DNA origami rectangles decorated with 1, 2 and 3 AuNP in discrete

bands after a 2 h long centrifugation step. In all the experiments we performed, after the centrifugal step we obtained two pink bands both analyzed through SEM imaging. A successive Amicon filtration with TAE 1× containing $MgCl_2$ removed the viscous liquid improving the quality of SEM images (Figure 3.11). Through this protocol we successfully separated most of the free AuNP from AuNP conjugated DNA origami but we didn't succeed in the separation of DNA origami with 1 NP from 2 NPs. Moreover the protocol was barely reproducible, so we concluded that it is not appropriate for further experiments.

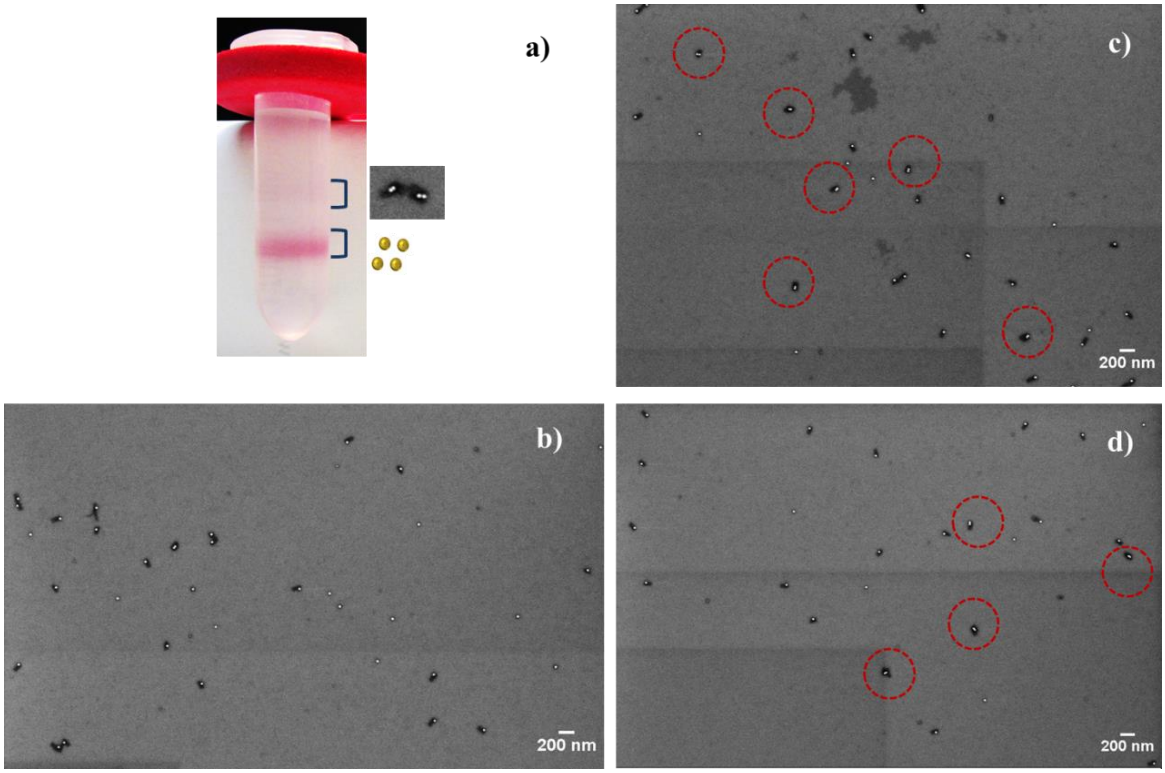

Figure 3.11 Iodixanol separation and purification of AuNP decorated-DNA origami rectangles: **a)** iodixanol density gradient shows an intense red band and a pale band representing free AuNP and AuNP-DNA origami; **b)**, **c)** and **d)** SEM images of pale red band shown in a). Red circles surround DNA origami anchored by 2 AuNPs while all the other particles are DNA origami with 1 NPs attached. Few free NPs are present.

The LSPR analysis on the samples purified with the iodixanol method has been performed using a spectrophotometer. In the graph shown in figure 3.12 we have measured free AuNP and DNA origami rectangle decorated with AuNP in both combination: F9-F5 and F9-F1. Data are not normalized to highlight the different signal intensities. In the origami the intensities are strongly reduced because of the purification step after the decoration with AuNP, where most of the structures were lost. The three peak positions are overlapped, thus confirming that most of the structures observed possess only one AuNP as shown in

figure 3.11. For this reason the optical response of the particles linked to the DNA origami is comparable with the free AuNP response and no LSPR red-shift is observed.

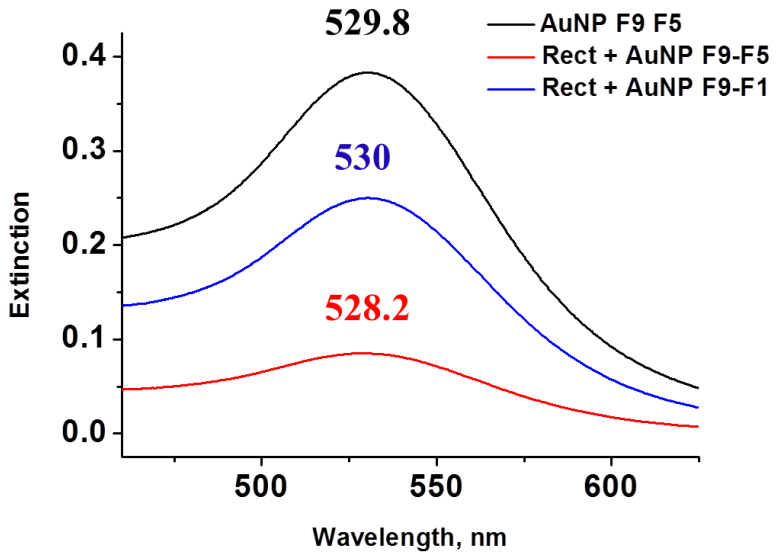

Figure 3.12 LSPR analysis of free AuNP and DNA origami rectangle with two different combination of AuNP; the peak position does not evidence relevant red-shift after the conjugation of AuNP with DNA origami rectangle.

4 Plasmonic-based tetrahedral DNA origami device

4.1 Tetrahedron design

As mention in the thesis aim, I focused my attention to a wireframe DNA origami tetrahedron. Each edge is composed of four dsDNA helix ~90 nm long and is connected to the other two neighboring edges at the vertices by flexible joints. The scaffold strand, coming out from the struts, crosses each vertices twice. The connection points between the struts are composed by 5 bases left at single strand. The number of bases composing three of the six struts slightly differ to fold completely the scaffold strand. Three of the struts have been designed with a central seam which separates the two half of the pillar itself, so we properly prolonged the staples strands tuning their pairing to build a cage around the seam in order to reinforce the central part. In the three pillars left, the scaffold strand still forms a central seam but the external helix extends along the entire length of the pillar maintaining the struts more solid (Figure 4.1).

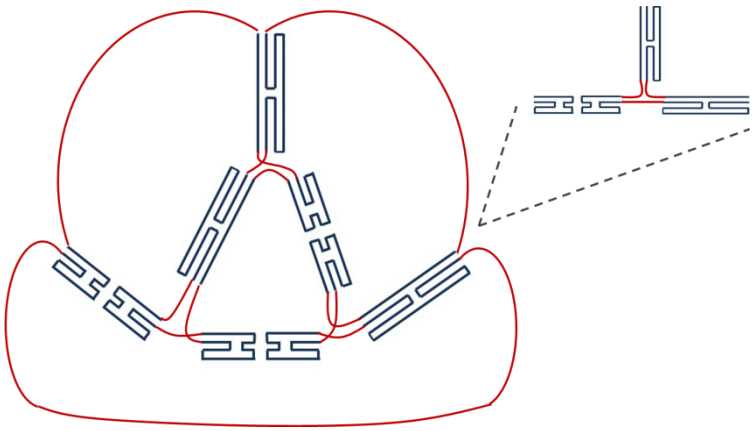

Figure 4.1 Visual model of the scaffold strand folding path: six 4-helix bundles in blue, the flexible connections at the vertices in red. There are two different types of struts: the two half struts typology and the strut with a central seam. On the right side, a focus of the vertex connection.

In order to tune the mechanical properties of the bundles, we designed three different set of staples which induced the formation of weakened points on two of the six struts. The three sets of staple strands include staple strands which: (i) anneal the entire scaffold strand of the bundle (0ss), (ii) anneal the scaffold strand except 4 bases of one of the four helix (1ss), (iii) anneal the scaffold strand except 4 bases of three helices composing the bundle (3ss) (Figure 4.2).

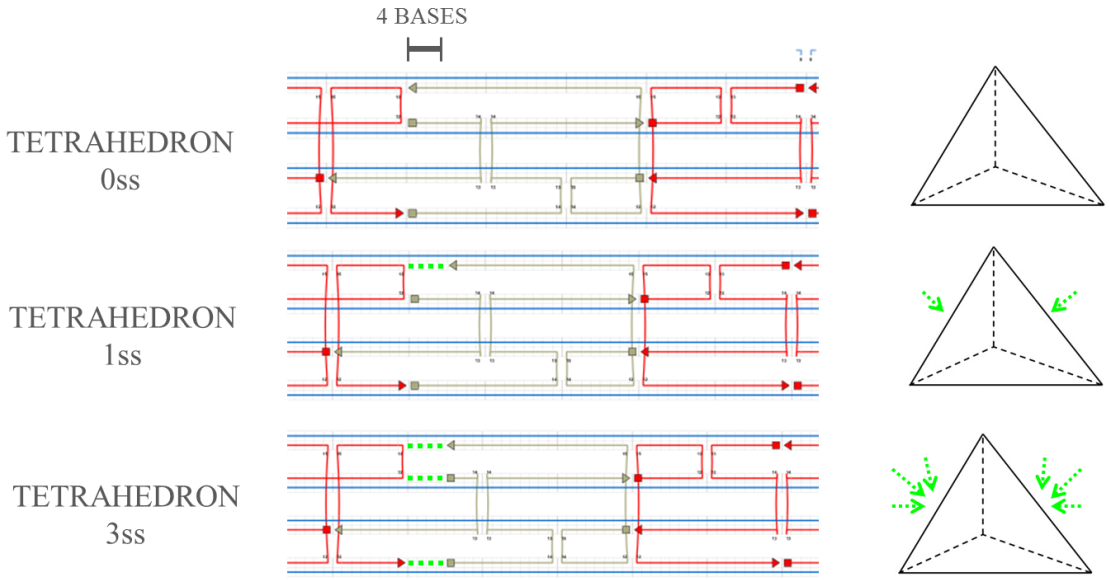

Figure 4.2 Three set of staples containing: 0 base single strand (0ss), 4 base single strand in 1 helix (1ss), and 4 bases single strands in 3 helices (3ss). The scaffold strand is blue, the structural staples strands are red, the staples involved in the variable part of the struts are gray, and the green dotted segments are the 4-bases gaps where the scaffold strand is left unpaired. On the right, the arrows indicate the position and the number of weak points.

The three structures have been separately designed through the help of design-assisted software caDNAno as described in section 2.1. The success in the proper folding of the structures has been estimated using CanDo simulation software. The three structures share the same tetrahedral shape but they are differently colored (Figure 4.3).

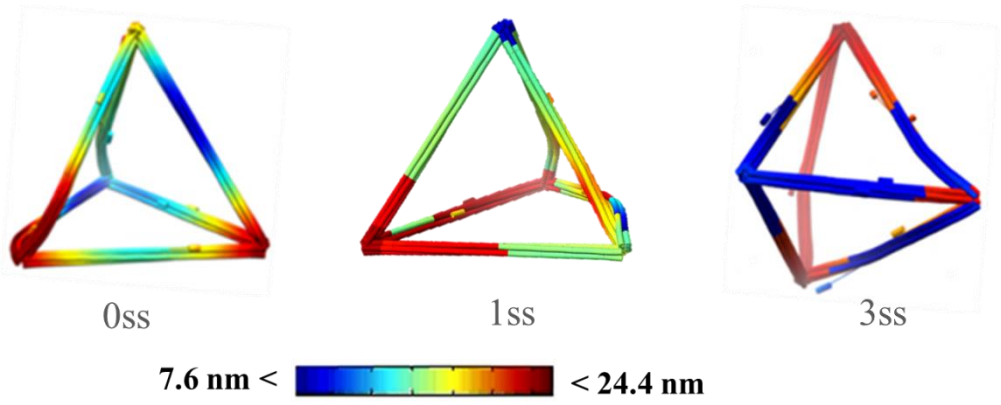

Figure 4.3 CanDo simulation of tetrahedral DNA origami 0ss, 1ss and 3ss. The color bar represents the thermal fluctuation (nm) of the structures.

The CanDo simulation provides a qualitative information about the deformation induced by thermal fluctuations experienced by the DNA origami. The zones in which the deformations are higher highlight the regions where the conformational changes are more

likely to happen. Tetrahedron 3ss show a completely different colors pattern respect to 0ss and 1ss. 0ss and 1ss present red zone in two vertices while the rest of the structure is approximately stable; 3ss, instead, exhibits red parts in an entire strut and in three of the four vertices, but the other pillars are more stable than in 0ss.

The purpose of 1ss tetrahedron design and synthesis was to use it for SAXS measurements, since its behavior should be too similar to 0ss to be detected with other technique.

In order to bind two gold nanoparticles to the tetrahedron, we extended oligonucleotides from the original design, creating "catchers" strands. Each AuNP has three anchor points coming out from three different struts of a tetrahedral facet. The length of the catchers strands has been accurately defined to position the NP in the middle of the facet with a nominal interparticle distance of 10 nm from surface to surface.

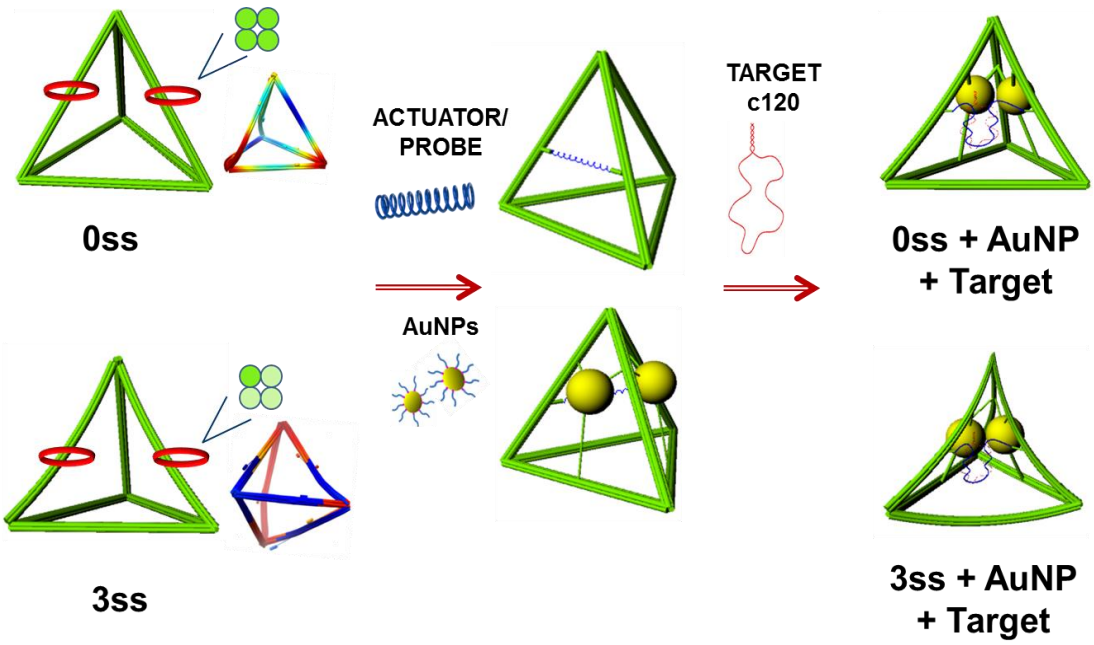

Figure 4.4 4 helix-bundle DNA origami tetrahedron 0ss and 3ss (4 nucleotides gap), represented with the CanDo simulation, are decorated with an actuator strand and with two 20 nm- gold nanoparticles positioned in the center of two opposite tetrahedral facets with an planned interparticle distance of 10 nm (30 nm from center to center). The addition of molecular target induces a conformational change of the structure reducing the gap between AuNP.

A third tetrahedron facet is modified by the addition of the "actuator" strand, which represents the probe of the DNA origami device. One long ssDNA, connects two of the six struts of the tetrahedron through two catcher strands complementary to the 5′ and 3′-ends of the actuator strand. The complementary sequence is 18-bases long. The target has a stem and loop configuration, complementary with the actuator strand sequence. The annealing

of the target loop with the central part of the actuator strand reduces the actuator length pulling the tetrahedron from both sides. The partial collapse of the structure, decreases the gap between AuNP and changes the optical properties of the system (Figure 4.4).

4.2 Synthesis of DNA origami structure

The synthesis of DNA origami structure has been performed in one pot-reaction through the addition of three different staple mix. The synthesis condition are described in the session 2.2 **[18,25]**, some optimizations of the original protocol have been done modifying the cooling down ramp, the Mg^{2+} and the scaffold/staples strands concentrations in order to improve the quality and the quantity of the tetrahedron DNA origami.

We firstly have used a scaffold strand concentration of 1.6 nM; the latter determines the concentration of folded DNA origami. The purification step was performed through centrifugation in Amicon filter, described in paragraph 2.2, which removed the excess of staple strands and increased the DNA origami concentration from 1.6 nM to 2.8 nM, calculated with the same method presented in paragraph 3.1.

In figure 4.5a is shown an agarose gel: in the first and in the third lanes we can observe the migration of the ladder and of the M13mp18 while the forth and the fifth wells were filled with DNA origami tetrahedron respectively before and after the Amicon purification. The red box in figure 4.5a identifies the gel bands corresponding to the well folded origami. After the purification step the origami concentration was increased (band brightness enhancement). Meanwhile we assist to the formation of two slower bands which correspond to larger constructs, derived from the aggregation of two and three tetrahedrons. SEM characterization confirms the agarose gel indications: in fact, most of the tetrahedrons analyzed were aggregated (Figure 4.5b,c) or broken in different places, probably because of the harsh purification step.

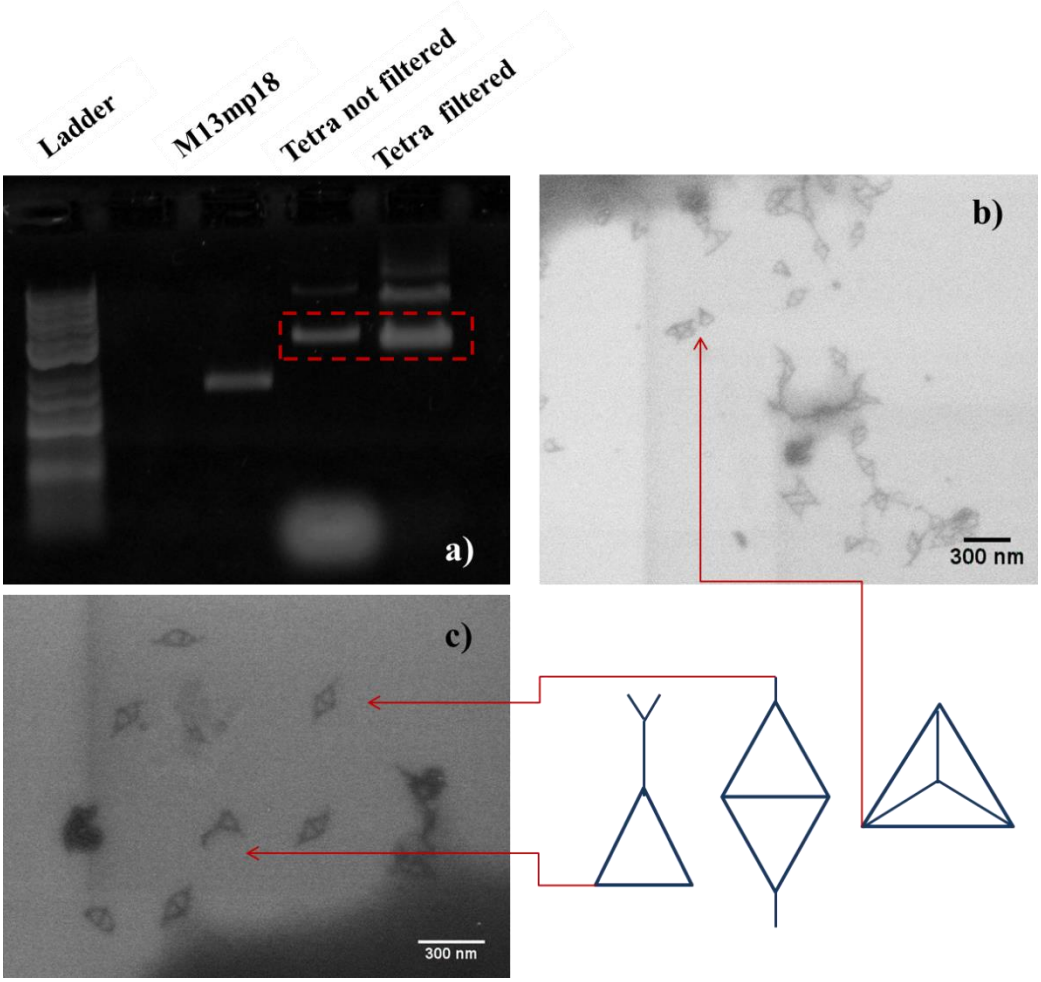

Figure 4.5 a) Agarose gel electrophoresis of DNA origami tetrahedron shows the concentration and the aggregation enhancement after Amicon purification, M13mp18 is used as a control of the folding success; **b)** and **c)** SEM pictures in which there are well-folded tetrahedron, broken and aggregated DNA architectures.

Reducing the centrifugation speed of Amicon filtration from 14000 × g to 4000 × g, the gel band resolution and position are not modified, but the presence of free staples highlights an insufficient purification. The addition of the "actuator" strand does not induce any additional aggregation. However, the structural instability of tetrahedron demonstrate that further improvements of the synthesis protocol are required. The purification step has been avoided and synthesis protocol adjusted, reducing both the incubation time from 48 h to 40 h and modifying the cooling down ramp. Instead of an homogeneous decrease from 90 °C to room temperature lasting 48 h, the ramp starts at 80 °C, reaches 60 °C in 20 min, and slowly decreases in the following 40 h, reducing the time in which the high temperature can degrade DNA filaments.

The cooling down ramp time, as described by Carlos Castro **[18]**, varies from few hours for single-layer to several days for multi-packed structures. DNA origami tetrahedron is

intermediate because it is composed by the folding of only 4 helices. For this reason, we tried also the fast synthesis which consists in a 3 h-long protocol, with a constant cooling down ramp from 80 °C to 25 °C. The agarose gel electrophoresis showed a band comparable with the one obtained with the 40 h-long protocol. However, SEM analysis indicates that the structure stability is strongly affected by the duration of the protocol, and the stacking among the structures is increased for the shorter one.

Therefore we concluded that the 40 h-long folding protocol is the more appropriate to obtain a reproducible DNA-origami. To increase the amount of the synthesized origami we increased the scaffold concentration from 1.6 to 10 nM and proportionally the concentration of the staple strands mixture (up to 100 nM). The analysis in agarose gel and at the SEM shows that the resulting origami are well folded and separated as shown in figure 4.6.

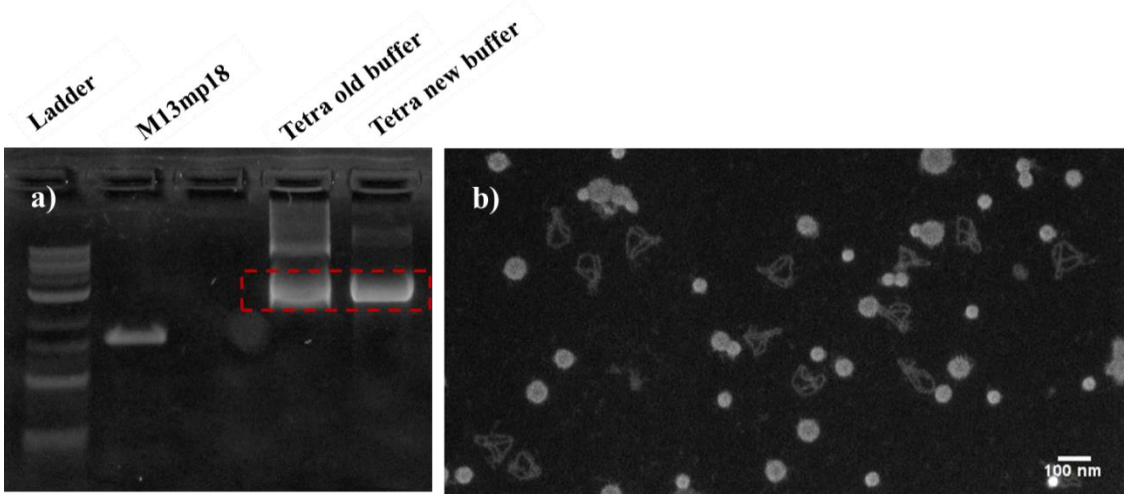

Figure 4.6 a) Agarose gel analysis of tetrahedron 3ss synthetized with 2-week old buffer and freshly prepared buffer; the latter produced a more confined band reducing the number of aggregation (upper part of the gel). **b)** SEM images of tetrahedron 3ss deposited on carbon coated grid; white spots represent salt residues.

The final DNA origami concentration was calculated using ImageJ software: the brightness of the whole lane can be assumed proportional to the M13mp18 initial concentration (10 nM), so the ratio between the brightness of the origami band and of the entire lane is equivalent to the ratio between the concentration of the tetrahedron and of the scaffold strand. Moreover, we investigated the ageing effect of the used chemical and solutions. In particular we compared the use of freshly opened buffer, with respect to a buffer bottled opened three weeks before and then stored at room temperature. We observed that freshly prepared buffer instead of old buffer (3 weeks old) may influence the output of the synthesis as shown in figure 4.6a. The old buffer, in fact, induced the formation of a

second band and a smear representing the dimerized structures and aggregated ones . The characterization of DNA origami 0ss, and 3ss performed through agarose gel electrophoresis and SEM did not evidence structural differences among them. The same sample deposited on the grid used for the SEM imaging shown in figure 4.6b has been also imaged with TEM (Figure 4.7), confirming the results already obtained with SEM. Even if TEM increases the structures magnification, the absence of a negative staining reduced dramatically the contrast of DNA which appears more defined in SEM images.

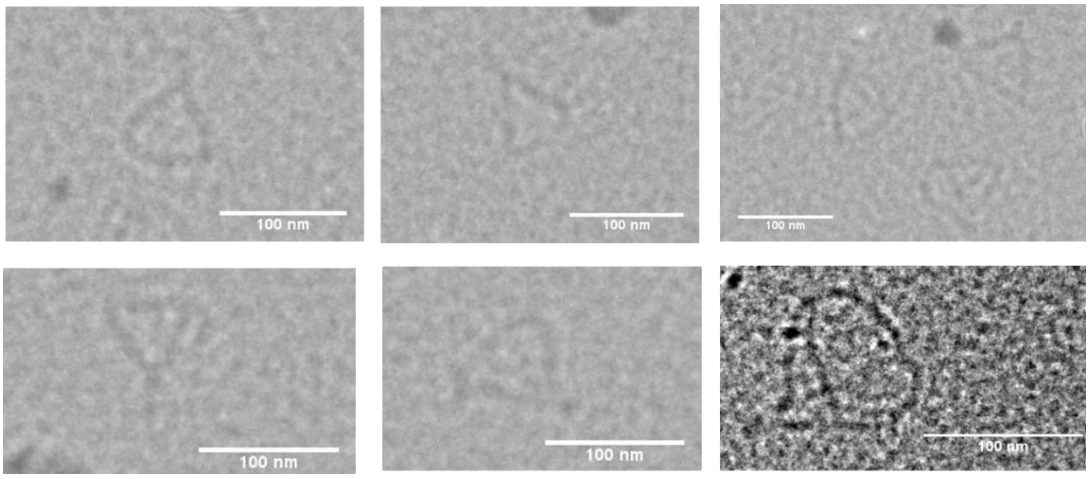

Figure 4.7 TEM images representing well-folded tetrahedrons (thanks to Mattia Fanetti).

4.3 AFM characterization of DNA origami tetrahedron

SEM characterization is an helpful and rapid method to simultaneously check the correct folding of numerous DNA origami, but it provides a partial information especially considering the three-dimensionality and the flexibility of the structure of choice. SEM imaging is a destructive technique in which organic sample are rapidly damaged: this does not allow the detailed characterization of the origami. Even if low voltage energies are used, the measuring time is still limited. Thus, a complementary analysis with AFM imaging is usually required. Because of its flexibility and wireframe configuration, the full 3D structure of this DNA origami cannot be properly reproduced using AFM. For this reason we intentionally flattened the tetrahedron by preparing a staples mix in which 6 staples involved in the seam reinforcement of one of the six pillar, are omitted. In this way, we obtained in a controlled way, an homogeneous sample in which almost all the structure are 2D. We performed the flattening both for 0ss and for 3ss tetrahedron inducing the

formation of a kite-like structures, obtaining primary information on the pillars height and width (Figure 4.8a).

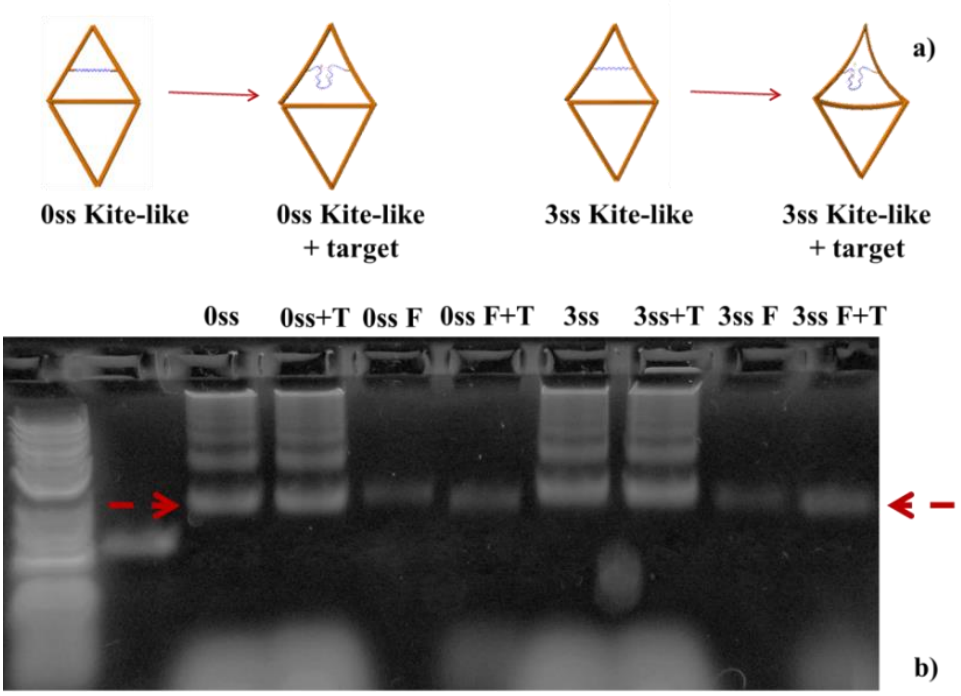

Figure 4.8 a) The omission of few staples strands in the one-pot synthesis protocol induced the formation of kite-like structures (0ss and 3ss); **b)** after the synthesis of the DNA origami kite-like we performed the agarose gel analysis in both structures before and after the addition of the target; purified samples show an electrophoretic migration comparable with that of the not-purified samples.

After the folding of DNA origami Kite-like, achieved with the same protocol of the 3D tetrahedron, we purified the product of interest from excess of staple strands. 2D DNA origami, did not require the same precaution of the 3D tetrahedron: both gel extraction and the Amicon filtration did not influenced structural properties even if the latter, exactly as in the 3D shape, introduced kites aggregation (Figure 4.9c).

Agarose gel analysis of the 0ss and 3ss samples after the extraction from a previous agarose gel produced a fine selection of the product of interest, as shown in Figure 4.8b, without perturbing the migration but it reduced the concentration and introduced dirt originated from agarose gel fibers as shown in SEM pictures (Figure 4.9d). AFM imaging has been performed in air because of the prolonged sample durability and of the higher resolution with respect to the liquid environment; moreover, the topographic analysis in air is faster and easier than in liquid. After the measurements performed on the rectangular DNA origami structure I have established that the drying process doesn't affect the samples shape and position (paragraph 3.2).

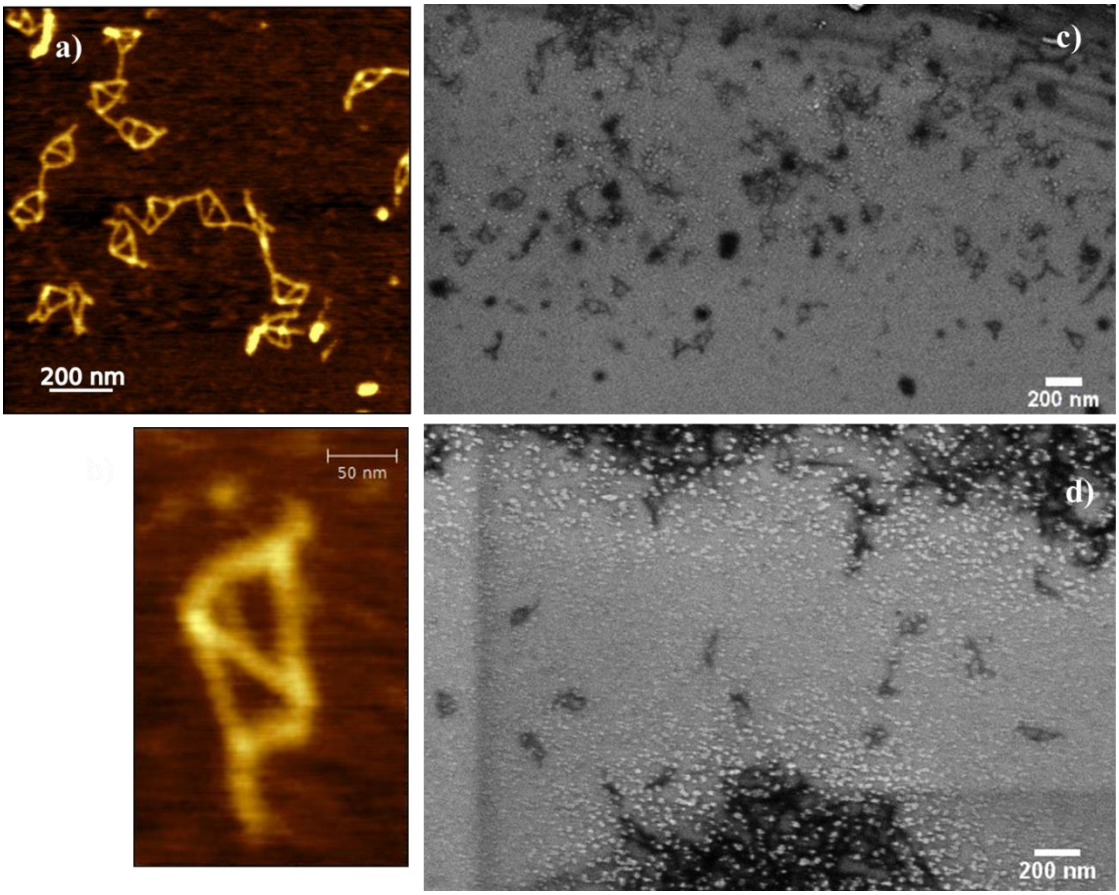

Figure 4.9 a) AFM images performed in contact mode (dried samples) of kite-like structures and **b)** zoom in on a DNA kite-like structure; SEM images of: **c)** kite-like DNA origami filtered in Amicon, **d)** kite-like structures gel extracted.

AFM showed that almost all the structures are in the flat configuration, except few of them which are folded down on themselves (Figure 4.10a), probably because the scaffold strand can still pull the two halves of the broken strut together. Moreover, the flexibility of the vertices provides enough degrees of freedom to allow the folding of the structure on itself even if it is statistically less favorably placed configuration due to the electrostatic repulsion between the origami struts. The profile of the kite DNA origami deposited on mica as measured from the topographic images, post-processed with Gwyddion software, highlights an average strut height of 2 nm which is substantially lower than 2 double-helix value in solution (between 4 and 5 nm) (Figure 4.10b,d) **[101]**. The apparent width of the ds-DNA molecules is strictly correlated with the tip used, but it was always exceeding the 2 ds-DNA diameter in solution, which is to be expected for tips with apex radii exceeding substantially the molecular diameter (Figure 4.10c).

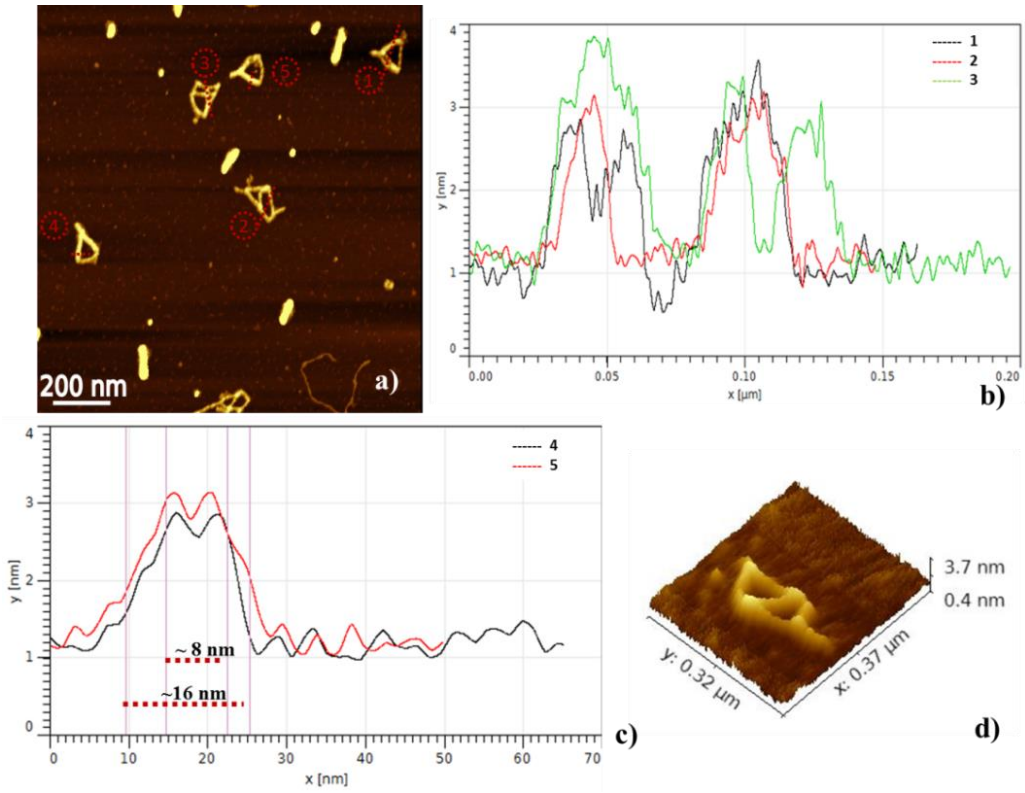

Figure 4.10 a) AFM images in which there are kite-like DNA origami, few of them are folded on themselves; **b)** height profile of the structures shown in 3.10a; **c)** wide of the kite-like struts using Gwyddion tool; **d)** 3D image of a kite-like DNA origami.

4.4 DNA origami gold nanoparticle-decoration

DNA origami tetrahedron provides for two binding sites which consist of 3 oligonucleotides protruding from 3 different struts. If connected by the three catchers strands, each AuNP will be positioned at the center of a tetrahedral facet. When two AuNP are anchored to the tetrahedron at two opposite facets, the calculated distance between them is 10 nm from surface to surface or 30 nm from center to center (of the NPs). Catchers strands are made up of three domains: one 16-mer complementary to the DNA origami structure and one 22-mer complementary to the ssDNA sequence attached to the AuNP and a third domain between the former two which provides the length required to position the nanoparticle in the exact center of the facet. The decoration protocol is performed mixing DNA origami and NP with a ratio of 2 NPs for each binding site. AuNP were then added to DNA and incubated at 45 °C/ 50 °C for 45 min, and cooled down over night. The presence of hybridized AuNPs on the DNA origami has been confirmed by gel electrophoresis. The agarose gel migration of DNA origami decorated with gold nanoparticles, both 0ss and 3ss, before and after the target addition, induces the appearance

of ruby red gel bands. The UV light image of the same gel highlights the DNA staining, provides a clear correspondence between the specific bands of hybrid structures with the band of DNA origami (Figure 4.11a). The targets are usually mixed in excess of 200 times respect the DNA origami concentration, to induce complete hybridization to DNA origami. To increase the AuNP band, we doubled AuNP concentration, as shown in figure 4.11b, and we got a more intense ruby red gel bands which correspond to DNA origami decorated with NP, before and after the actuation with the target c120, but a lot of free NP which were trapped in between. The excess of unbound NPs can be observed as the broad red band in all the lanes and is negative upon DNA staining.

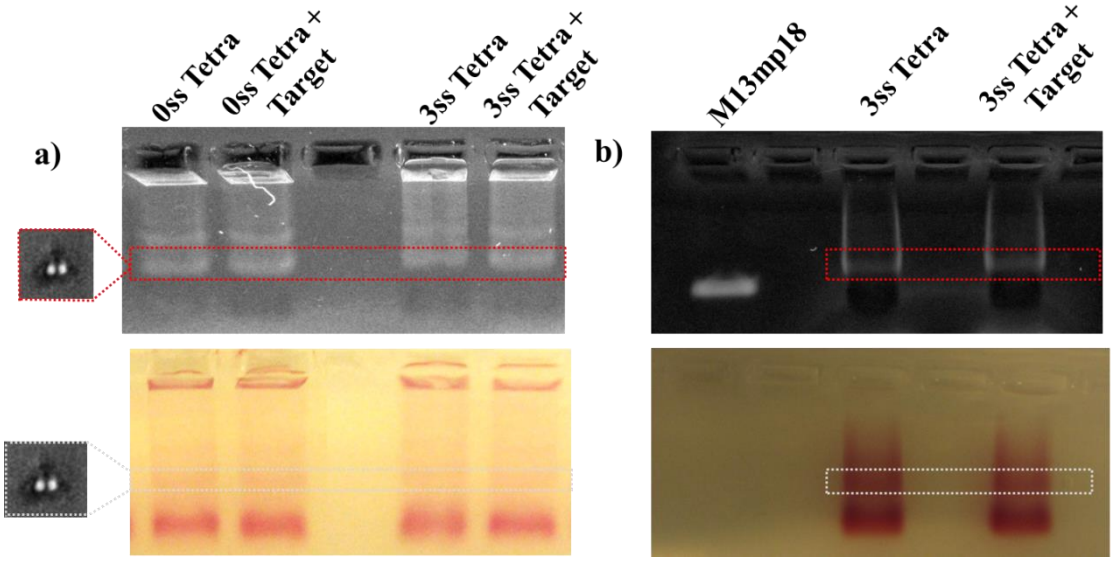

Figure 4.11 Agarose gel Uv/vis representing the migration of DNA origami-gold nanoparticles hybrid structures. The AuNPs functionalization induces a smear of the band. The presence of gold nanoparticles allows the formation of a visible band. Agarose gel electrophoresis showing the migration of: a) tetrahedron 0ss and 3ss decorated with AuNP (ratio 1 DNA structure :5 NP) not previously filtered from free staples strands before and after the target addition; b) tetrahedron 3ss decorated with AuNPs (ratio 1 DNA structure: 10 AuNP) not previously filtered before and after the addition of the target strand.

No differences have been observed in the bands position between the Au-NP decorated DNA origami and the two DNA target-actuated constructs. The structural differences induced by the target hybridization are not large enough to produce an appreciable electrophoretic migration delay. A slowly moving bands attributed to the formation of DNA origami superstructures (dimers, aggregates) can be observed. These results have been also confirmed by SEM characterization.

4.5 SEM/TEM characterization of the DNA origami/NP hybrid structures

After the functionalization of DNA origami with gold nanoparticles, SEM imaging has turn out to be useful in the characterization of the samples. While DNA origami alone doesn't provide enough electronic contrast to be efficiently characterized with this technique, the presence of gold nanoparticles produces a good contrast which is meaningful for a statistical analysis of the interparticle distance. We deposited the samples on different types of substrate as silicon wafers and TEM copper grid carbon. The latter were preliminary checked at SEM before being analyzed at TEM, producing a good contrast of the images.

In order to selectively decorate the DNA origami structure with one or two gold nanoparticles, we initially synthetized it using only one set of catchers strand which are involved in the binding of one AuNP.

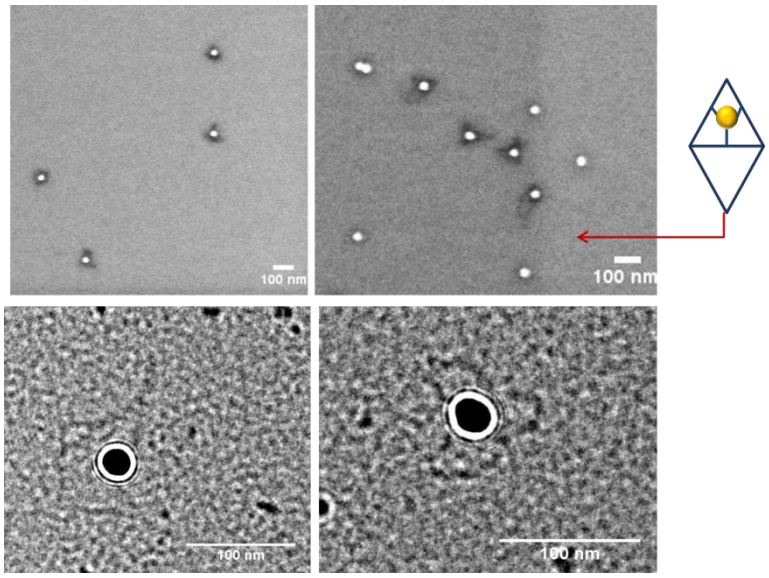

Figure 4.12 DNA origami tetrahedron conjugated with 1 AuNP; (up) SEM images with a broken tetrahedron in which is visible the right AuNP positioning; (down) TEM images (thanks to Mattia Fanetti).

The conjugation of one AuNP to the DNA tetrahedron, still allows to visualize the tetrahedral shape. Moreover, the presence of kite-like structure, as in figure 4.12, evidences the precise positioning of the AuNP in the center of a tetrahedral facet.

The further functionalization of the tetrahedron with two gold nanoparticles has been performed through the addition of two sets of catcher strands, which recognize the same AuNP functionalization, during the DNA origami synthesis. The presence of a second NP

attached to the tetrahedral architecture, further increases the signal background, coming from secondary electrons scattered by the two nanoparticles, thus outshining the signal generated by the origami itself. However, sometimes we noticed a triangular shadow, that we attributed to DNA origami (Figure 4.13).

The imaged sample has not been previously purified because, as explained in paragraph 4.3 and 4.4, any kind of purification may break, aggregate, and in some case dilute the sample, with the introduction of dirt.

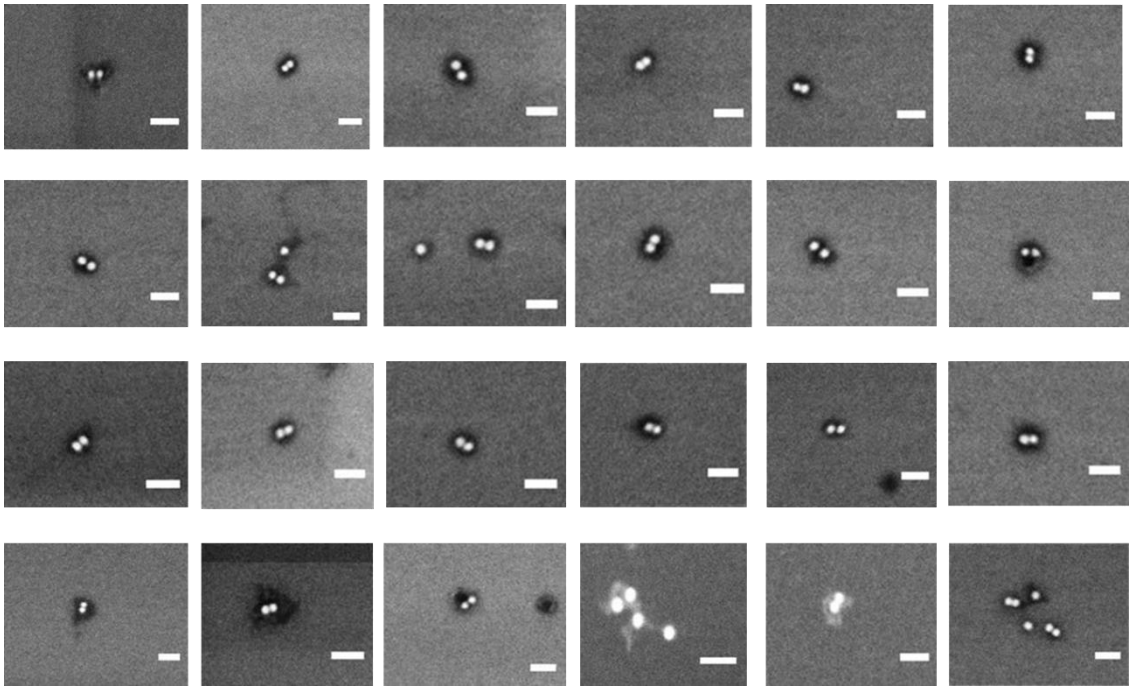

Figure 4.13 Dimers of gold nanoparticles with a triangular like shadow representing DNA origami tetrahedron with two gold nanoparticles (Scale bar 100 nm).

The SEM analysis showed a huge number of gold nanoparticles dimers which have been counted and analyzed to evaluate the interparticle distance on the 3ss tetrahedron before and after the addition of the target. The distance analysis, has been performed on more than 100 particles for both the samples (3ss and 3ss + target), measuring the distance between the NPs from center to center (Figure 4.14a,b). In this way, the AuNP dimension variability does not affect the measurements. The statistical analysis evidenced two different trends of the interparticle distance for actuated and not actuated structures. Before the addition of the target, the interparticle distance is subjected to great variability. In particular the center-center distance can be described by two Gaussian distribution centered at 27 nm and 33 nm respectively. After the addition of the target, a single

Gaussian can be used to reproduce the interparticle distance, peaked between 23 nm and 24 nm.

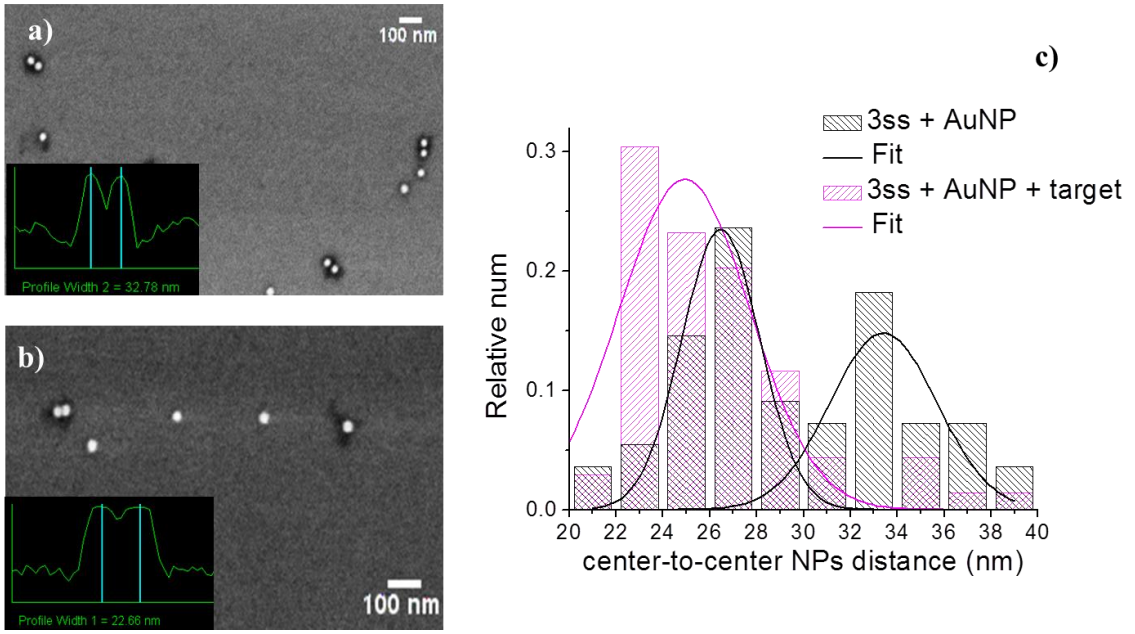

Figure 4.14 a) Representative SEM image of not purified DNA origami sample before target hybridization. Well-folded 3ss tetrahedron decorated with two gold nanoparticles are identified and distinguished from the free AuNPs also present in the solution. In the inset a representative profile used to evaluate the interparticle distance. **b)** Representative SEM image of not purified DNA after target hybridization. In the Inset a representative profile used to evaluate the interparticle distance. **c)** Statistical distribution of interparticle distance (center-to-center) of 3ss dimers before (black) and after (magenta) the hybridization of target. The interparticle distances were evaluated measuring the profile width through SEM SUPRA software. Before hybridization the distribution is broad with a bimodal character peaked at 26nm (AuNP in quasi-contact) and 33 nm (equilibrium configuration). After target hybridization, the distribution become monomodal peaked at 23-24 nm.

This outcome can be motivated by the flexibility of 3ss structure which allows numerous configurations, determining a change of the interparticle distance in a range of 20 nm. The equilibrium configurations are closed to the designed ones (interparticle distance of 30 nm from center to center). The addition of the target pulled the struts closer and stabilized the configuration in which the two particles are 3-4 nm far from each other. The actuation mechanism of tetrahedral device was further investigated and confirmed through LSPR analysis.

4.6 Plasmon ruler actuation

The optical response of the DNA origami tetrahedron before and after the actuation with target strand has been studied through LSPR measurements. The analysis, of 0ss and 3ss,

has been performed directly in agarose gel with the setup described in paragraph 2.8. The electrophoresis allows the separation of the DNA origami tetrahedron from dimer, trimers, aggregated structures and free AuNP. The gel extraction, in fact, reduces the concentration of the DNA origami-AuNP hybrid structures modifying the structural properties. In our lab, we have already demonstrated the possibility to perform LSPR measurements of DNA origami/NP in agarose gel, obtaining absorbance peak positions univocally associable with a specific interparticle distance **[64]**. We recorded extinction spectra for each structure both in liquid and directly in the separated gel bands to minimize cross band contamination. In figure 4.15 are displayed the extinction spectra of AuNPs in BSPP, DNA coated gold NPs in water and the tetrahedrons 0ss and 3ss decorated with gold nanoparticles. Measurements in liquid have been performed because in previous experiments we have noted a tight packing of NPs in gel and this, associated with higher dielectric permittivity of the gel, results in significant red shift of LSPR peak and its broadening due to a plasmon coupling effect in respect to origami with gold NPs **[87]**.

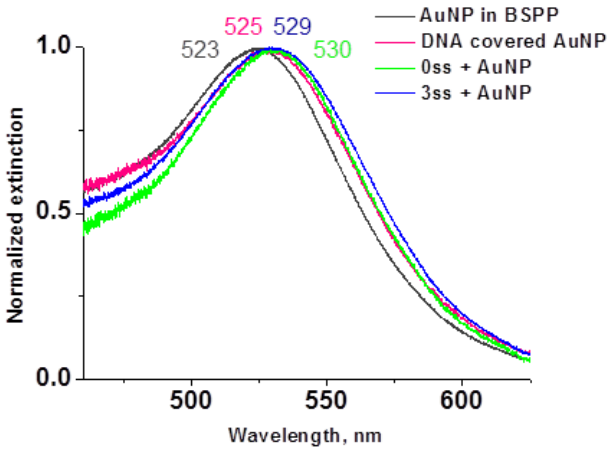

Figure 4.15 AuNP LSPR analysis in solution. Spectra from pure AuNP, DNA coated AuNP, 0ss and 3ss origami are displayed. A spectral red shift is observed, as expected, because of the increased dielectric constant of the AuNP environment from pure, DNA covered, and DNA origami environment. The shift from 0ss to 3ss structure is due to the higher thermal fluctuation in the latter that reduce the average interparticle distance.

Extinction spectra showed that the DNA-covered gold NP red shifts respect to AuNP in BSPP solution because of the change in permittivity of the medium around the nanoparticle (see also paragraph 3.3). A further red-shift for non-actuated tetrahedrons is due to the reduction of interparticle separation driven by the tetrahedron structure. The larger red-shift of the 0ss with respect to the 3ss and the larger broadening of the latter can

be explained by the higher flexibility of the 3ss tetrahedron which can assume a broader range of conformations.

The spectra before and after the target addition, recorded in separated gel bands, are shown separately for 0ss in figure 4.16a and for 3ss in figure 4.16b. The spectra showed that the target triggers a change in the optical response only on tetrahedron 3ss, inducing a further red-shift of the peak position. The two curves representing 0ss actuated and not actuated by the target, instead, are peaked in the same position.

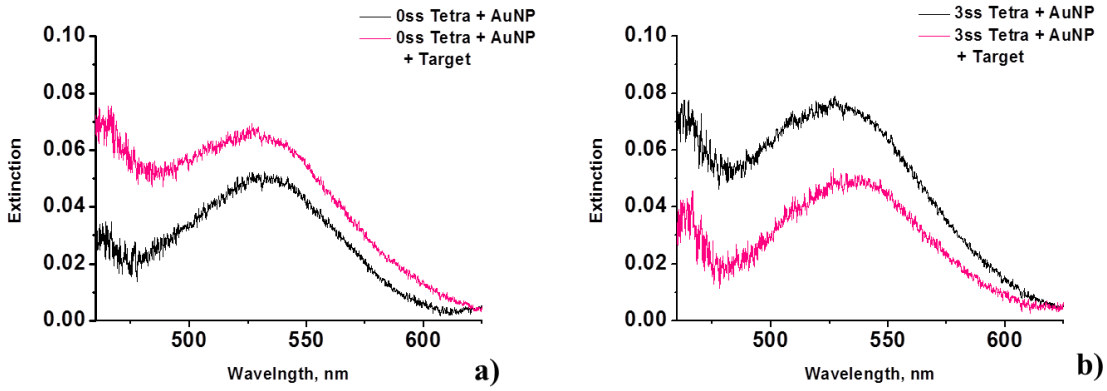

Figure 4.16 AuNP LSPR analysis in agarose gel, after band selection. Spectra from **a)** 0ss and **b)** 3ss structures with and without target. A significant red shift is observed only in 3ss after target addition and it is attributed to the interparticle distance reduction due by the target-probe hybridization.

The normalization of the data to 1 at the peak maximum facilitates the visualization of the peak positions, highlighting the plasmonic shift of the tetrahedron 3ss after the hybridization with the molecular target (Figure 4.17a,b).

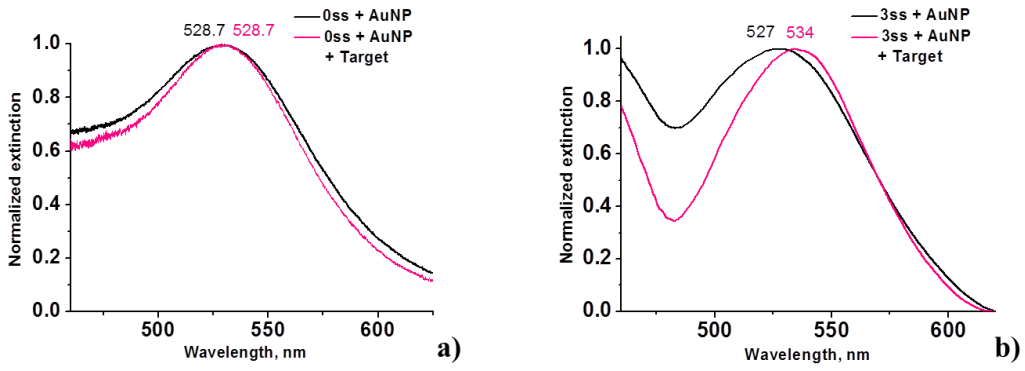

Figure 4.17 Normalized spectra of: **a)** AuNP LSPR analysis in solution. Spectra from 0ss structures with and without target; no spectra shift is observed. **b)** 3ss structures with and without target displaying a significant red-shift is observed after the target-probe hybridization.

Before the addition of molecular target, LSPR peaks are centered at 528.7 nm for 0ss and 527 nm for 3ss. Using Mie theory and considering single NP, we evaluated the value of effective dielectric permittivity that is 1.8. Using this value, the interparticle distance in the tetrahedron 3ss is estimated to be 9 nm before the reaction with the target. After the interaction, the LSPR peak does not change for 0ss while 3ss is red-shifted to 534 nm. This 7 nm LSPR red-shift is proportional to a distance reduction of 5 nm. These data match with the interparticle distance distribution defined with SEM analysis. All the extinction spectra have been fitted for background subtraction with two Gaussian curves as shown in Appendix 2. In the fitted data, the absolute peak position is slightly red-shifted in all the graphs but it does not influence the results since I consider only the shift between the peaks, which is not affected by the fit.

The same analysis has been performed on the 3ss tetrahedron in which the concentration of the AuNP was double with respect to the previous experiment to ensure that all the binding sites present on the tetrahedral structures were linked to a nanoparticle (Figure 4.18).

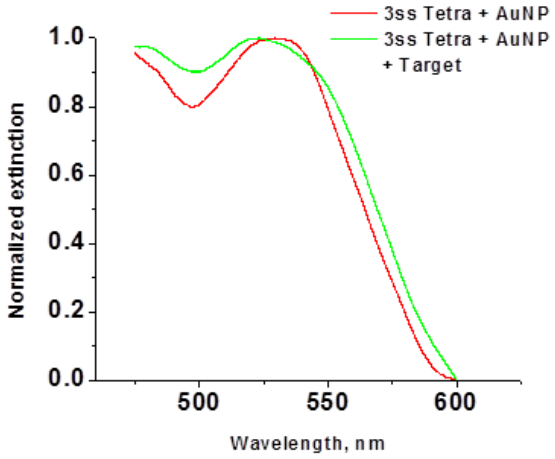

Figure 4.18 LSPR graph representing the extinction of tetrahedron 3ss before and after the actuation with the target c120 measured in agarose gel. The excess of free AuNP superimposed to DNA origami-AuNP structures strongly influences the curves shape.

The identification of the LSPR peak is made more difficult by the superposition of the stronger component of the free AuNP, for this reason I separated the single peaks composing the curves through multi-Gaussian fit. The fit has been applied to non-normalized data.

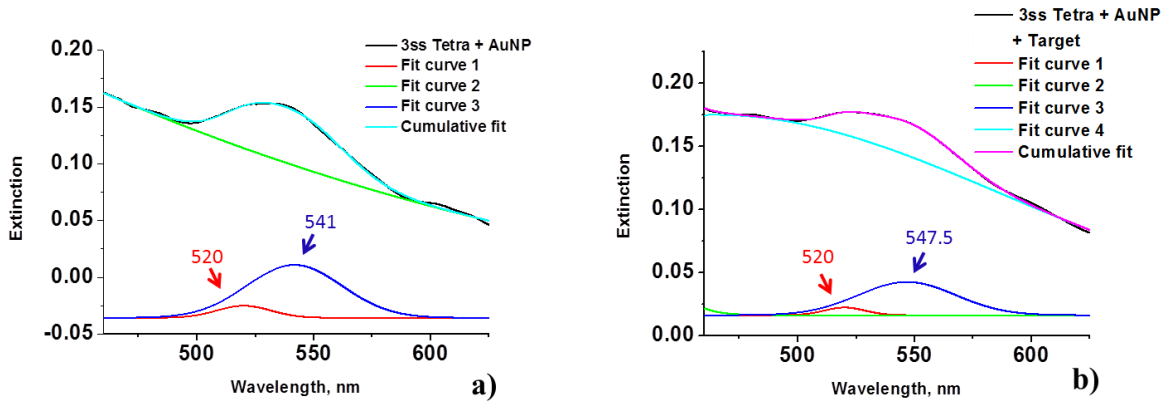

Figure 4.19 Fit of the plot in figure 4.18 representing 3ss tetrahedron before **a)** and after **b)** the addition of the target. The multi-Gaussian analysis performed with 3 elements in a) and 4 elements in b) highlights a common component at 520 nm associable to the free AuNP absorbance and another major curve (blue) which is presumably related with the tetrahedron-AuNP dimers which red-shifts 6.5 nm after the target hybridization.

The fit of the 3ss before and after the addition of the target highlights the present of a strong component at 520 nm which can be reasonably associated with free AuNP absorbance (Figure 4.19). The other main component (blue curve fit) has been associated with the LSPR of the dimers linked to the tetrahedron: the position of this component after the addition of the target resulted shifted by 6.5 nm with respect to the 3ss sample before the target addition. This value is in accordance with the previous experiment and demonstrates the successful actuation of the DNA origami structure.

4.7 Small angle x-ray scattering

We probed the structures of AuNP dimers-DNA origami hybrid constructs by in situ small-angle X-ray scattering (SAXS). SAXS allows the structural analysis and the distance determination with nanometer resolution. The measurements have been performed at SAXS beamline at Elettra Synchrotron. We measured about 77 samples previously checked through agarose gel electrophoresis.

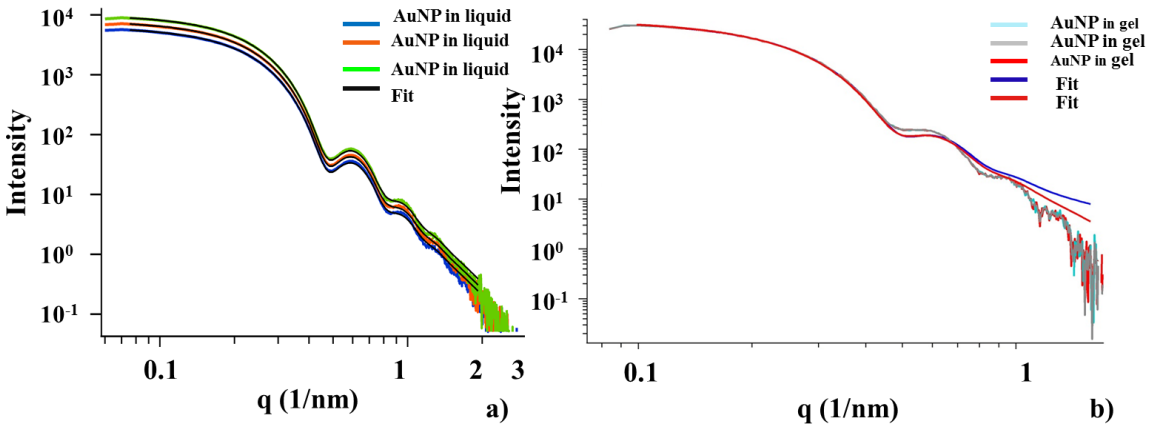

Figure 4.20 a) Comparison of three different measurements of the nanoparticles dispersion with the corresponding fit. The fits have been performed using form factor for spherical particles adding a Schulz sphere size distribution with Sticky Hard Sphere Structure factor (black solid lines). Data are shifted for clarity. **b)** Comparison of three different measurements of the nanoparticles in agarose gel with the corresponding fit. The fits have been performed using form factor for spherical particles adding a Schulz sphere size distribution with Sticky Hard Sphere Structure factor (blue and dark red lines).

Half of them was in liquid, and half was measured directly in agarose gel. In a preliminary analysis we noticed that gel-migrated AuNP were detectable through SAXS (4.20 b).

The signal produced and the intensity, in fact are comparable with the one of the AuNP in liquid represented in figure 4.20a. Thanks to these measurements, we predicted that tetrahedron 0ss, 1ss and 3ss decorated with 2 AuNP could be analyzed before and after the actuation with target directly in agarose gel to reproduce LSPR measurements conditions. The same samples have been measured also after the gel extraction to analyze the structural changes of the samples after gel purification to precisely evaluate the conformational change attributable to this process. Only for SAXS measurements, we designed three more targets which differ from target used for the previous experiments (Target c120) both for the secondary structures and for the complementary region with the actuator/probe strand (Table 4.1).

Name	Sequence	Secondary structure
Target 1	5′AGGAGGAGAAGGGAACCCAGGGGGGGGGG GGGGGGGGGGGTTTTTTTTTTCCCCCCCCCCCC CCCCCCCCTCGAGTGTATCCATCTGAAA 3′	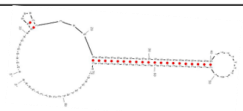 ΔG= -34.44 kcal/mol
Target 2	5′AGGAGGAGAAGGGAACCCAGCTTGAACGA GGGGGGGGGGTTTTTTTTTTCCCCCCCCCCAAC CAAATGTCGAGTGTATCCATCTGAAA 3′	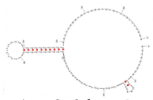 ΔG= -15.26 kcal/mol
Target 3	5′AGGAGGAGAAGGGAACCCAGGGGGGGGGG GGGGGGTTTTTTTTTTCCCCCCCCCCCCCCCCTC GAGTGTATCCATCTGAAA 3′	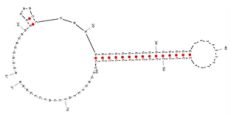 ΔG= -23.69 kcal/mol
Target c120	5′GGGCGGGGCGGGGGCGCGAAAGTCTACCTAT GTGAGCTGTAAACCCAATATGAGCAGGACCCA GTGACGACGAGCAATGTTCGACCCAAGGGAAG AGGAGGACGCGCCCCCGCCCCGCCC-3′	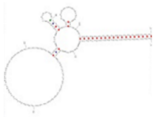 ΔG= -27.8 kcal/mol

Table.4.1 Target strands designed for SAXS measurements. Sequences in red represent the regions complementary to the actuator strand while underlined sequences are GC stems. Target 1, 2, 3 have a central T-loop and 5′ and 3′ ends –are complementary to the ends of the actuator strand. Target c120, instead, has a central loop which is complementary with the central part of the actuator strand.

The samples in gel before and after gel extraction have not been sufficiently concentrated and the background produced by the different agarose matrices could not be subtracted. While, the measurements performed in the not purified samples in liquid, displayed an interesting signal variation after the addition of the target c120 to the tetrahedron 3ss; the hybridization of the target with the actuator strands, in fact, induces a reduction of the interparticle distance. We examined in depth this behavior repeating SAXS analysis in solutions both for tetrahedron 0ss and for 3ss before and after the addition of target 1 and target c120. The raw data of the 3ss tetrahedron before and after the addition of the target c120 have been normalized to 1 at 0 cm^{-1} as shown in figure 4.21a. The samples analyzed have not been previously purified from excess of free AuNP. For this reason, the data obtained from functionalized AuNP are then subtracted from data of the tetrahedron with and without target to remove free NPs contribution, highlighting the differences between the two samples as shown in figure 4.21b. The black arrow in the plot, shows the region of interest (30 nm from center to center), while the biggest differences in the initial parts of

the curves are not considered because they describe longer order range which are attributable to supramolecular structures.

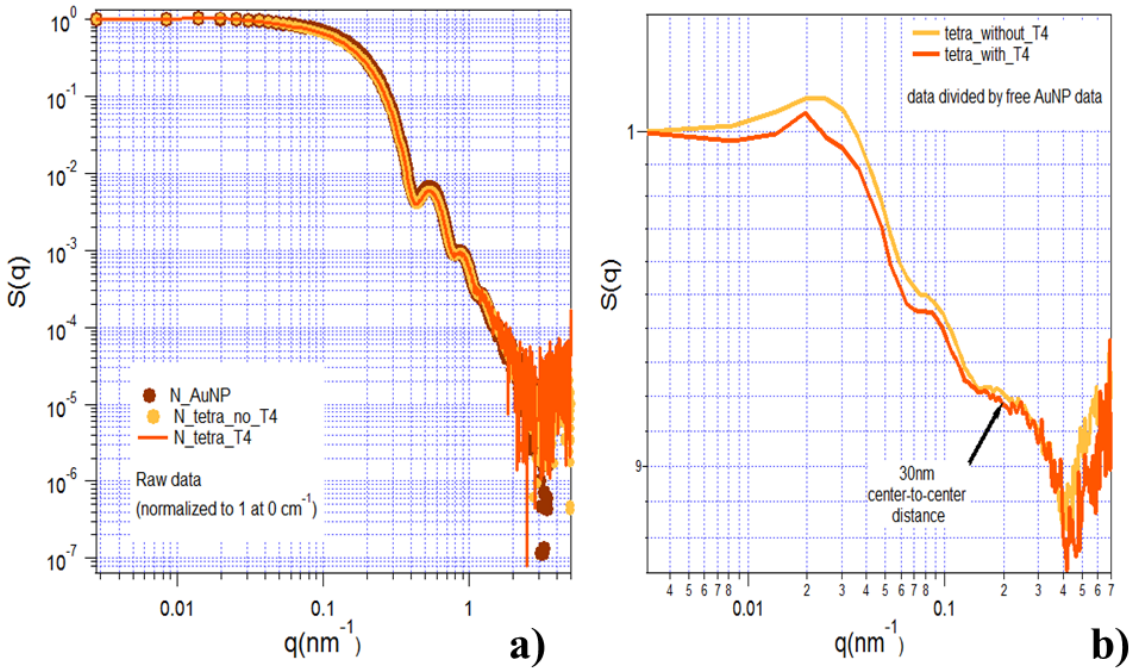

Figure 4.21 SAXS data analysis. **a)** Plot of raw saxs data normalized to 1 at 0 cm^{-1} of DNA origami tetrahedron 3ss with two AuNPs measured in solution before and after the target addition; **b)** plot of the data in a) divided by free AuNP data to remove their contribution and to highlight the differences between the two samples.

Subtracting the data obtained for tetrahedron 3ss to tetrahedron 3ss with target, we focused with more precision on the interparticle distance differences. In particular we noted a peak maximum fixed at 30 nm which represents the AuNP gap of the tetrahedron 3ss, and a maximum valley at 25 nm for DNA origami tetrahedron 3ss after the addition of c120 (Figure 4.22).

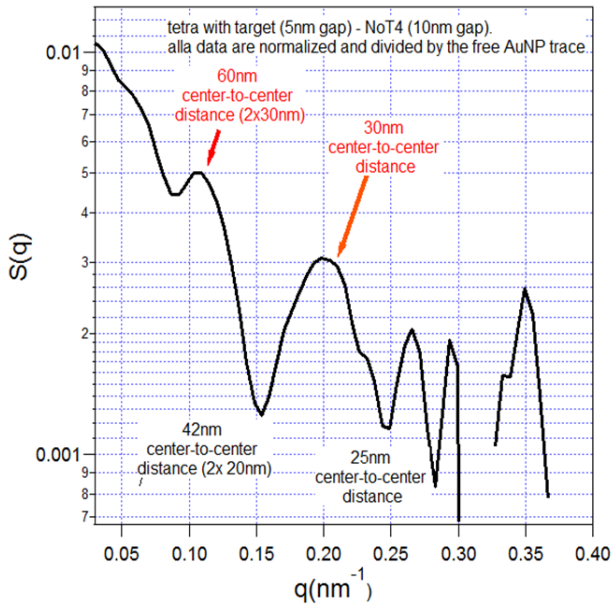

Figure 4.22 SAXS data representing the subtraction of tetrahedron 3ss-gold NP after the addition of the target c120 to the tetrahedron 3ss with AuNP. A peak corresponding to the interparticle distance before the actuation is fixed at 30 nm (center-to-center) and the max valley representing the interparticle distance in the tetrahedron after the target addition is highlighted at 25 nm (center-to-center).

The differences observed in the tetrahedron 3ss are not found in the tetrahedron 0ss, confirming LSPR measurements for both samples. Thanks to these two techniques, we demonstrated that AuNP-DNA origami tetrahedron (0ss and 3ss) behavior is not influenced by liquid or gel environment. Moreover, we confirmed that only tetrahedron 3ss is sufficiently flexible for being actuated by target c120.

LSPR measurements have been performed on the 3ss tetrahedron, previously analyzed with SAXS, to evaluate its actuation before and after the incubation with target c120 and with target 1 (Figure 4.23). Since SAXS results have indicated a distance reduction only after the addition of target c120, we wanted to confirm these results performing LSPR analysis on the previously irradiated samples after their purification through electrophoresis. The results shown in figure 4.23 demonstrate again no effect of the target 1 and a significant reduction in the actuation efficiency operated by the target c120; the shift value of ~ 2 nm does not match with the ~7 nm red-shift observed in the previous experiments. However, the detection of a small shift is a relevant result to prove not only the sensibility offered by our LSPR set-up with respect to SAXS, but also the stability of the structure even after X-ray irradiation.

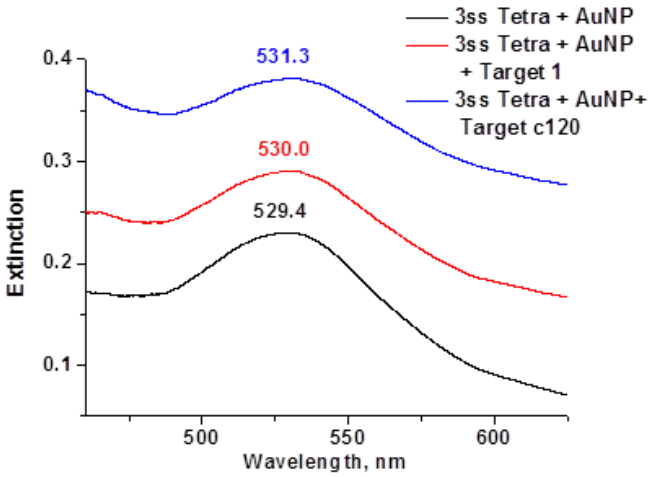

Figure 4.23 LSPR plot of 3ss tetrahedron with and without targets 1 and c120, displaying a restrained red-shift only after the target c120-probe hybridization; target 1 does not considerably affect the AuNP distance.

To reproduce the results obtained without tetrahedral structure, we designed a pool of AuNP aggregates with fixed interparticle distance, linking the particles through a given ssDNA sequence.

For this purpose we functionalized 20 nm gold NP with thiolated single strand oligonucleotides and their complementary strand. The selected DNA filaments are composed by 16-mer, 21-mer, 27-mer and 54-mer. Considering thiol modification at 3′ of approximately 0.7 nm, the final length of these oligos is 6.15 nm, 7.84 nm, 9.88 nm, 19.06 nm respectively. Each functionalized AuNP has been then mixed with the AuNP functionalized with the complementary oligo, producing a disordered aggregation, in which, however the interparticle distance is fixed. SAXS analysis is able to determine the average interparticle distance at nanometer scale. The calibration system offered by interconnected AuNP could be exploited for the selection of an appropriate fit of the AuNP-DNA origami structures. The complexity of SAXS analysis requires a great effort in finding the right fit to better elaborate the information acquired. For this reason we are now working on this purpose.

4.8 Cryo-EM characterization of the AuNP decorated-DNA origami structures

Cryo-EM provides a characterization of the samples in physiological conditions, in solution and without the need of depositing onto a surface, which may lead to structural changes driven by the interaction with the substrate. The synthesis of the tetrahedron has been performed in the structural biology lab using all the reagents delivered from our lab.

The synthesis and the functionalization with two gold nanoparticles have been firstly checked through agarose gel electrophoresis, using the same protocols previously described in this chapter. The gel bend intensity and position were consistent with the ones of the well-folded tetrahedrons (Figure 4.24a,b).

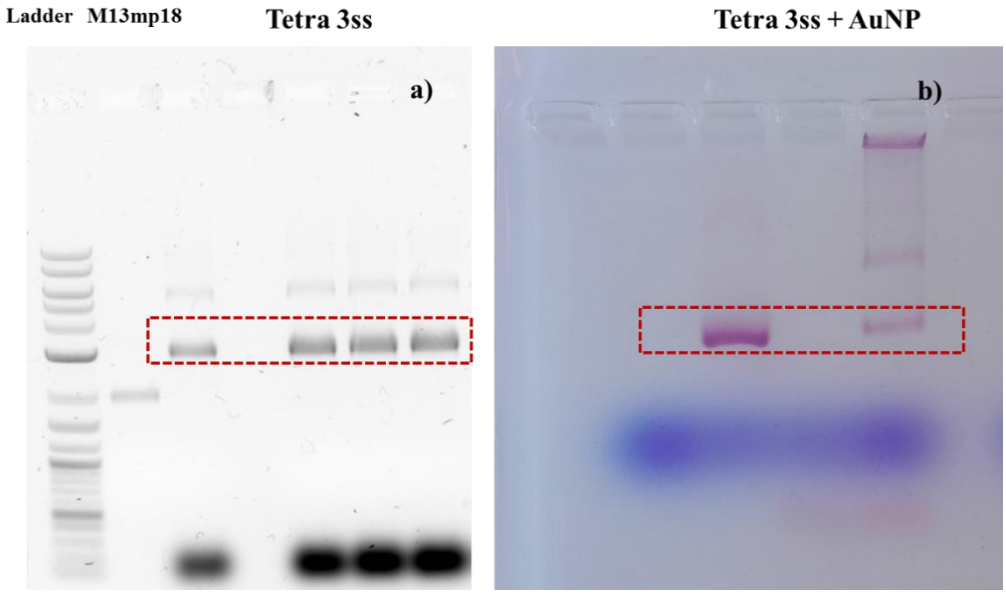

Figure 4.24 Agarose gel images representing the synthesis performed in Berkeley lab: **a)** UV light images in which the red box highlight the tetrahedron 3ss, **b)** agarose gel imaged with Vis light showing the AuNP functionalization of two synthesis of the tetrahedral DNA origami.

The cryo-EM sample preparation and maintenance are critical passages which have been performed following the protocol optimized by Gary Ren's group **[102]**. The images, performed on tetrahedral DNA origami decorated with AuNP, showed a distribution of the structures in close proximity of the holey carbon of the grid as if they were electrostatically attracted. All the structures analyzed, displayed a triangular shape and in many cases the NP position is in the center of the tetrahedral facet (Figure 4.25a,b). We tried also to measure the interparticle distance of the dimers which was comparable with the desired one but the aggregation and the overlapping of the structures didn't allow a precise analysis.

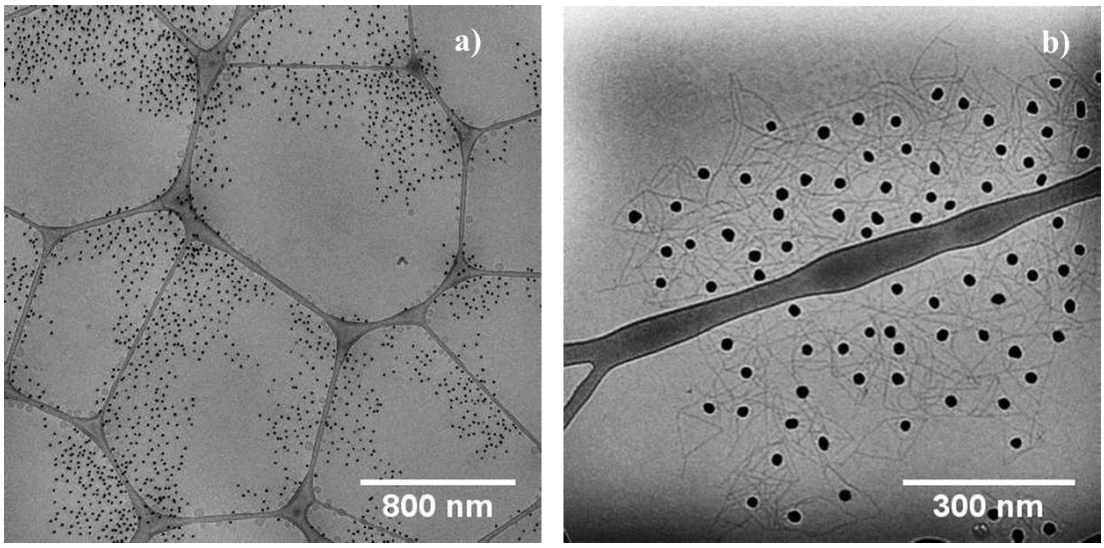

Figure 4.25 Cryo-EM images of tetrahedron 3ss functionalized with AuNP: **a)** most of the structures are arranged in close proximity of the holey carbon grid; **b)** zoomed picture showing the aggregation of the 3ss tetrahedron DNA origami with AuNP, the AuNP is however positioned in the center of a tetrahedral facet.

We found out few single tetrahedral structures (Figure 4.26a,b) and in one of them we performed also the tomography (Figure 4.26c), acquiring a set of electron micrographs (tilt series) at different angular orientations of the sample.

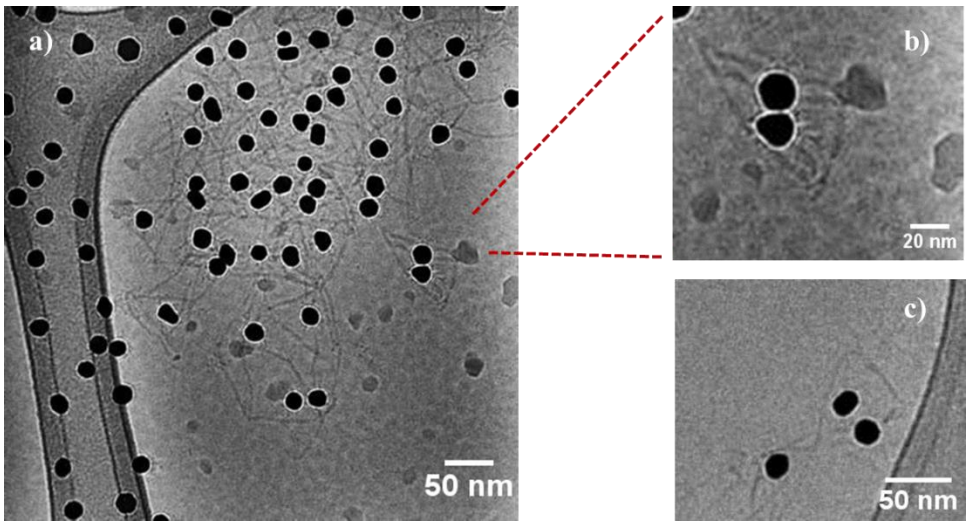

Figure 4.26 Cryo-EM images of 3ss tetrahedron with AuNP: **a)** aggregated structures and one single particle zoomed in figure **b)**. **c)** Dimer of AuNP positioned over a DNA triangular facet used to perform the tomography.

The tomography of the structures has been produced but it is difficult to appreciate the 3-dimensionality of the structure.

There are few possible explanation for the tetrahedral aggregation shown by cryo-EM image: the structure were not sufficiently stabilized by salt charges and so they formed big

aggregates or the oligonucleotides and functionalized gold nanoparticles were degraded from delivery. Another possibility is that the TEM grids were strongly treated by glow-discharge protocol attracting all DNA architectures.

5 DNA origami biomineralization

5.1 Metal Organic Frameworks

DNA preservation is fundamental in genomic research being crucial for bio-banking design, drug delivery, forensic and data storage. Even if DNA is considered a stable molecule over the time, if embedded in water, it is subject to chemical degradation through hydrolysis, oxidation and alkylation and biological fragmentation through nuclease attack. The possibility to encapsulate biopolymers, microorganisms and living cells in crystals lead to the biomimetic mineralization, which is able to preserve the biological activity even after treatments with solvent, heat or toxic reagents. Metal Organic Frameworks (MOF) can be grown around biomolecules to encapsulate and protect from the environment. MOF is a class of porous materials composed by metal nodes and organic linkers forming a versatile hybrid compound. MOF possesses tailored physical and chemical features due to the wide-range of applicable building blocks. The most competitive advantages offered by MOF over other existing coordination networks are the manipulation in shape, size and physiochemical conditions suitable with the hybrid material involved, and the porous structure which allows efficient cargo loading. The biodegradability and the biocompatibility of the MOF and the ease of surface functionalization prone to the molecular recognition are required qualities for the use of MOF in medical application. A well-studied member of the MOF family is the Zeolitic Imidazole Framework (ZIF) which is stable in water, low-cost, form rapidly around biomolecules and can be selectively degraded. ZIF are topologically isomorphic with zeolites and are composed by a tetrahedrally-coordinated transition metal ions (e.g. Fe, Co, Cu, Zn) connected by imidazolate linkers. ZIF-8 represent a class of ZIF in which zinc ions coordinated by four imidazolate rings in the same way as Si and Al atoms are covalently joined by bridging oxygens in zeolites. In one recent work, Liu and coworkers firstly demonstrated the one-pot synthesis of cytochrome C–embedded MOFs by co-precipitating metal ions and organic linkers. TEM images revealed the growth of the particles from rods to rhombic dodecahedron crystals **[103]**. ZIF can be grown around bovine serum albumin (BSA) at room temperature by adding an aqueous solution of zinc acetate to an aqueous solution containing BSA and 2-methylimidalole ligand in water. 90% of the macromolecule have been encapsulated, their coverage was determined through FTIR and confocal microscope tagging the BSA with a fluorophore **[104]**. Later, other biological molecules have been

biomineralized in ZIF-8 structures as ovalbumin, HRP, trypsin and single strand DNA resulting in a wide range of morphologies: nanoleaves, nanostars, and rhombic dodecahedron crystal respectively **[104]**.

There are many studies which demonstrate DNA origami stability over the time and in different medium. DNA origami structures survival was tested in cell lysate, after injection in mouse and also varying chemo-physical parameters as the pH, the temperature and the chemical content of the solution. However after prolonged time, it can be degrade as well as nucleic acids strands. The DNA origami biomeralization prolongs its survival over the time and in an environment- independent manner. Any kind of harsh chemical or physical treatments as irradiation with high energetic photon, such x-rays or UVs, treatments in corrosive media, or exposure to high temperature would not affect with the structural integrity. The defined shape of DNA origami could play a crucial role in the crystal growth, influencing also the final ZIF morphology. ZIF-8 can be dissolved by EDTA solutions in few second. Previous experiments demonstrated that this treatment doesn't influence the biomolecule previously encapsulated. For example, DNA strands released from ZIF-8 coatings were immediately amplified with polymerase chain reaction without further purification .

In this work we biomineralized DNA origami structures encapsulating them in ZIF-8 crystals. The crystals, grown around DNA origami rectangles, have been prepared through the successive addition of 2-methylimidazole and zinc acetate (precursor). The structural morphology and the chemical composition of DNA origami-ZIF covered, prepared using different precursor concentrations, have been analyzed. This project has been performed in collaboration with Joseph J. Richardson from the University of Melbourne, Victoria, Australia.

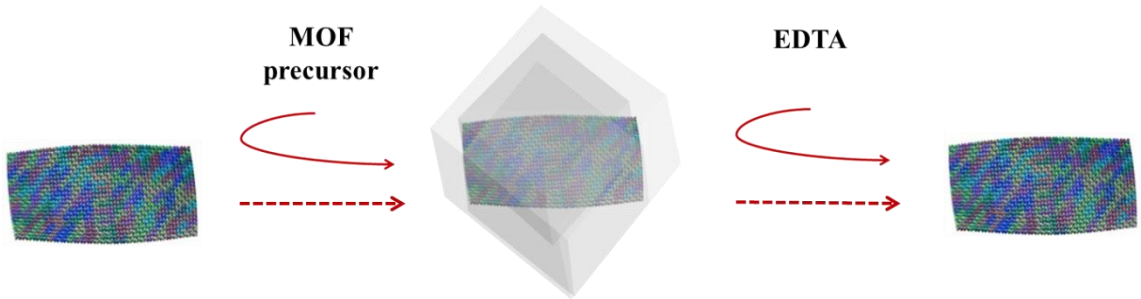

Figure 5.1 Controlled encapsulation in a MOF crystal of DNA origami rectangular after precursor addition and release operated by EDTA addition

5.2 DNA origami-ZIF encapsulation

DNA origami rectangle has been synthetized and purified from excess of staple strands as described in paragraph 3.1. The buffer used for the purification does not contain EDTA, which would interfere with MOF encapsulation. ZIF precursor solutions is prepared separately dissolving in MilliQ water powder of: zinc acetate ($Zn(OAc)_2$) 40 mM and methylimidazole (MeIm) 160 mM (SIGMA Aldrich). Depending on the amount water-soluble biomolecule to encapsulate (mg), the same volume of MeIm and $Zn(OAc)_2$ were sequentially added to the DNA origami solution. Cui and coworkers claimed that the Zn^{2+} concentration and organic ligands are determinant for crystal morphology **[105]**. Adjusting the concentrations of Zn^{2+} ions while keeping the high concentration of 2-methylimidazole, it is possible to directly control the ZIF shape. For this reason, we examined different precursor ratios with respect to DNA origami solution. In particular, we mixed a 8 nM DNA origami rectangle solution in Tris-Acetate buffer 2× with ZIF precursors in a volumetric ratio of 5:1, 5:5, 5:20, 1:20 and 5:1 (10× precursor concentration). The precursor volume is composed of MeIm (160 mM) and $Zn(OAc)_2$ (40 mM) in a 1:1 volume ratio, while for the sample with 10× precursor concentration MeIm and $Zn(OAc)_2$ are 10 times more concentrated. The concentration of DNA origami and ZIF precursor for each volume ratio is presented in Table 5.1.

Volume Ratio DNA origami / ZIF-8 precursor	DNA origami Final Conc (nM)	MeIm Final Conc (mM)	$Zn(OAc)_2$ Final Conc (mM)
5:1	6.7	13.3	3.3
5:5	4	40	10
5:1 (10 × precursor concentration)	6.7	133.3	33.3
5:20	1.6	64	16
1:20	0.38	76.1	19

Table 5.1 Correlation between the final concentration of DNA origami and the ZIF-8 precursor (MeIm and $Zn(OAc)_2$) used for the crystal synthesis.

After the addition of the precursors, the DNA origami solution shortly turned turbid; after a 1-hour incubation, which is sufficient to stabilize the MOF crystals, we removed the

supernatant pelleting the crystals at 10000 × g for 10 min and resuspending them in MilliQ water.

5.3 Crystallized DNA origami characterization

DNA origami-ZIF encapsulated were analyzed through different techniques which revealed structural and chemical properties of the crystals formed.

Small and Wide Angle X-ray Scattering define with high resolution the crystallinity level of the ZIF-8 produced. All the sample previously mentioned and the naked DNA origami have been analyzed in SAXS/WAXS beamline of the Australian Synchrotron (Figure 5.2). The peaks observed in the SAXS and WAXS graphs are separated to facilitate the comprehension. In both measurements, increasing concentration of precursor with respect to DNA origami induces the comparison of peaks which represent an enhancement in the crystallinity of the structures. The peaks positions and pattern correspond to the crystal structure of the ZIF-8 phase of Zn(2-methylimidazole)$_2$ MOFs. The evidence that DNA origami is effectively included in the metal organic framework and is involved in their formation is that when the precursor concentration is too high (1:20) respect to the DNA origami, the crystallinity is strongly reduced respect to 5:5 and 5:20 ratios. This is reasonable because MOF formation process is fairly sensitive to the presence of charged molecule like the DNA phosphate backbone. Moreover, SAXS and WAXS analysis also implies that the origami does not interfere with the crystalline structure of the MOF.

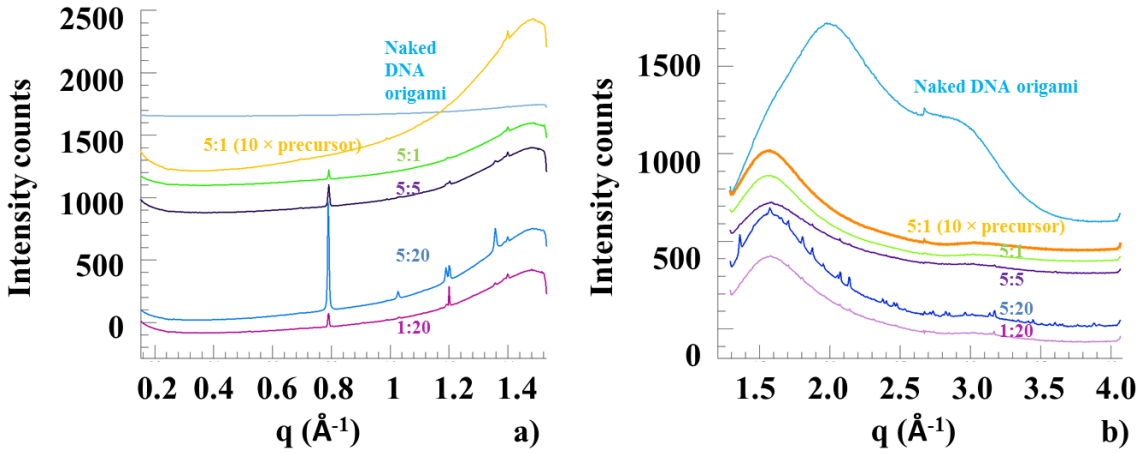

Figure 5.2 a) SAXS and **b)** WAXS graph of DNA origami-MOF and naked DNA origami in light blue. The ratio written in the graphs represents the proportion between DNA origami and MOF precursor concentration.

SEM analysis highlighted that precursor concentration influences the shape and morphology of the crystal formed. The images of 5:5 and 5:20 samples show interesting shapes of crystal similar to ZIF-8 growth confirming the results of SAXS/WAXS measurements which highlighted their orderly arrangements.

All the samples analyzed present fused crystal. A possible explanation to this phenomenon is that they can be produced by DNA origami. The latter creates a bridge between two crystals during the crystallization process, which starts from DNA origami negative backbone thereby causing them to grow together. Some of the images show also the mini MOFs presence or square bumps on the crystals (Figure 5.3, 5:5 image), that might correspond to single DNA origami having MOFs grown around it. That sort of process may occur when the fusing process is stopped because the precursors run out.

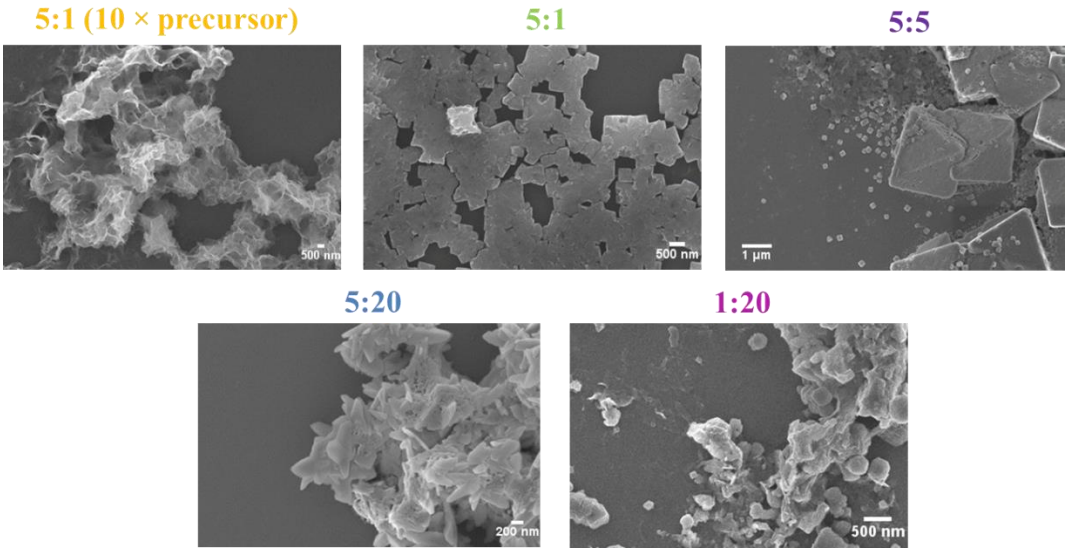

Figure 5.3 SEM images of DNA origami ZIF of samples prepared with different ratio between DNA origami and MOF precursor volume. 5:5 and 5:20 sample present higher crystallinity organization than the other samples; SEM image 5:5 shows mini MOF growth.

The sample with extreme values of the ratio between the DNA and the MOF precursor (1:20 and 5:1) didn't display crystal morphology: when the DNA is in excess the precursor concentration is too low for the crystal growth, while with extremely high concentration of precursor, the Zinc content can aggregate DNA origami structure interfering with crystal formation. The morphology study has been combined with an elemental analysis to determine the element content percentage and distribution detected through the energy-dispersive X-ray spectroscopy (EDX) of the SEM samples. EDX is an analytical technique used for the elemental analysis of a sample. It relies on an interaction of high-energy

electron beam X-ray excitation focused on the sample studied. Its characterization capabilities are due in large part to the fundamental principle that each element has a unique atomic structure allowing a unique set of peaks on its electromagnetic emission spectrum. The output of this analysis is the distribution map of chemical element on SEM image (N, Zn, O, C, Si) and the layered image which merged all the single element maps acquired showing the layers composition. Moreover it provide for an elemental graph where all the element percentage concentration are shown. Maps acquired in all the SEM images of MOF-DNA origami displayed an homogeneously distribution of Zinc ions throughout the crystals.

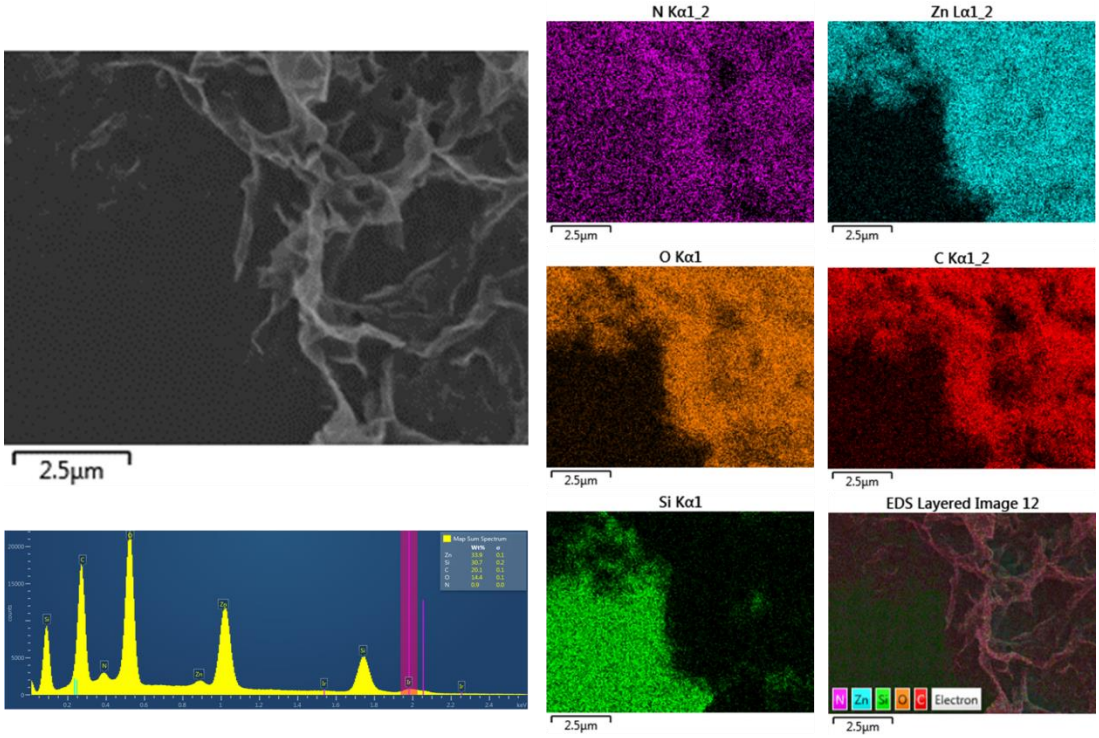

Figure 5.4 EDX **5:1 (10x precursor)**

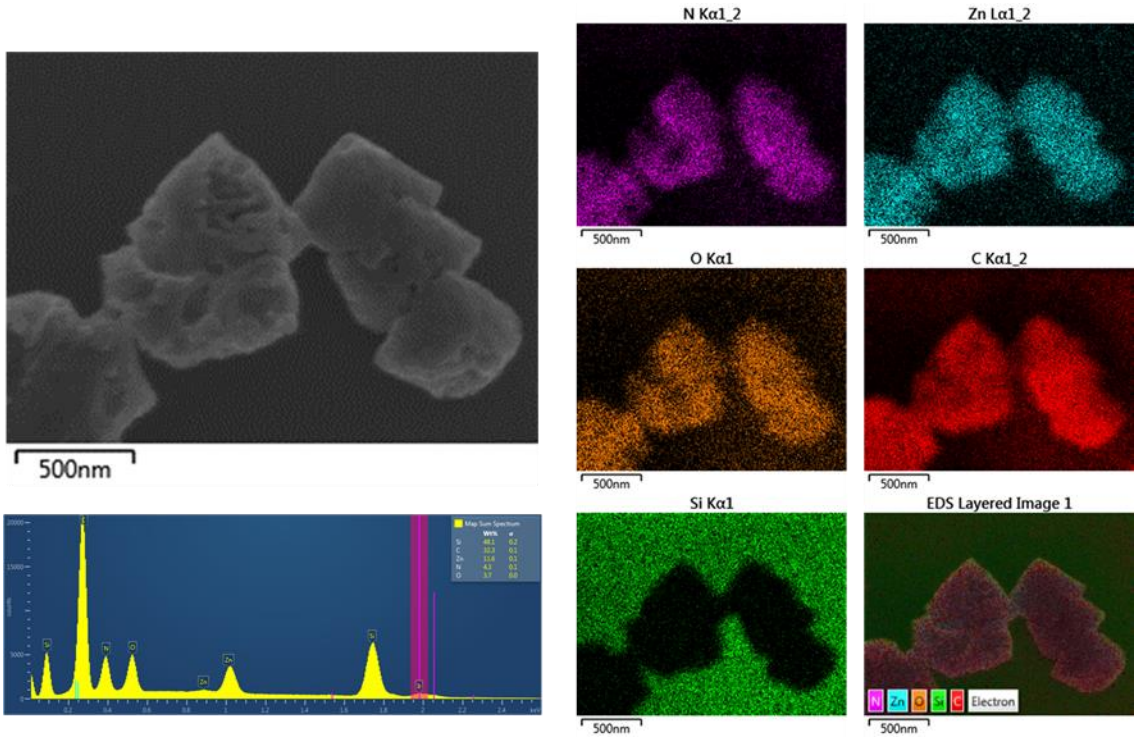

Figure 5.5 EDX 5:1

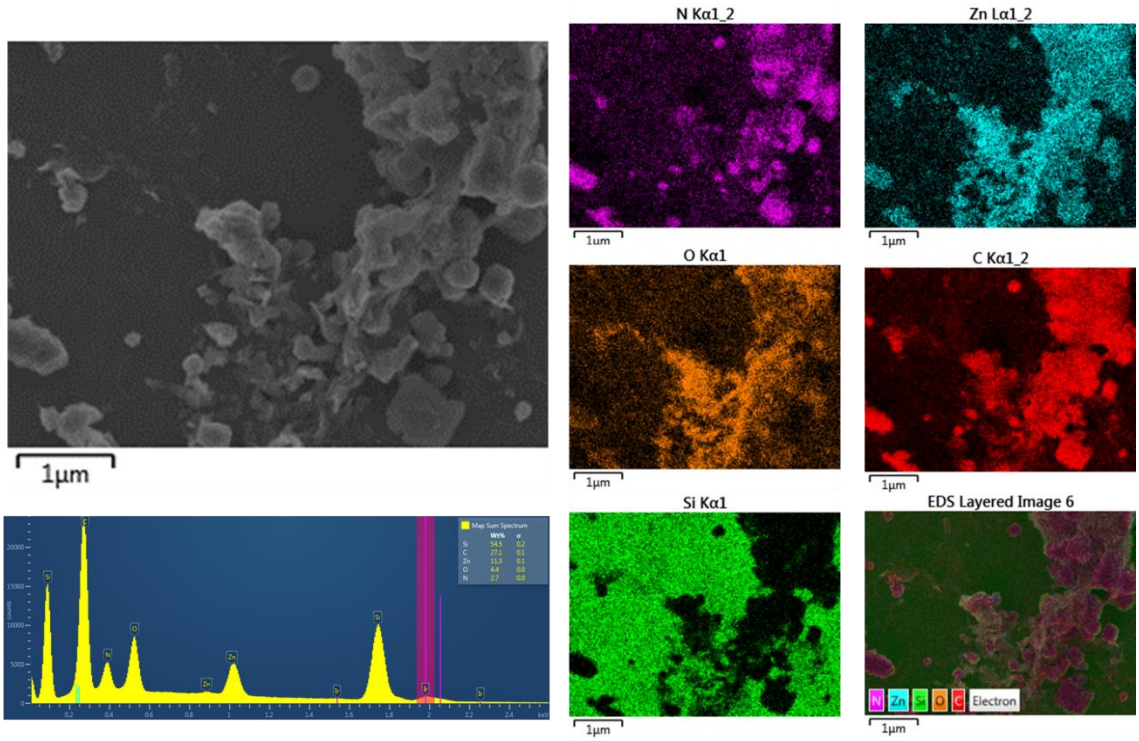

Figure 5.6 EDX 1:20

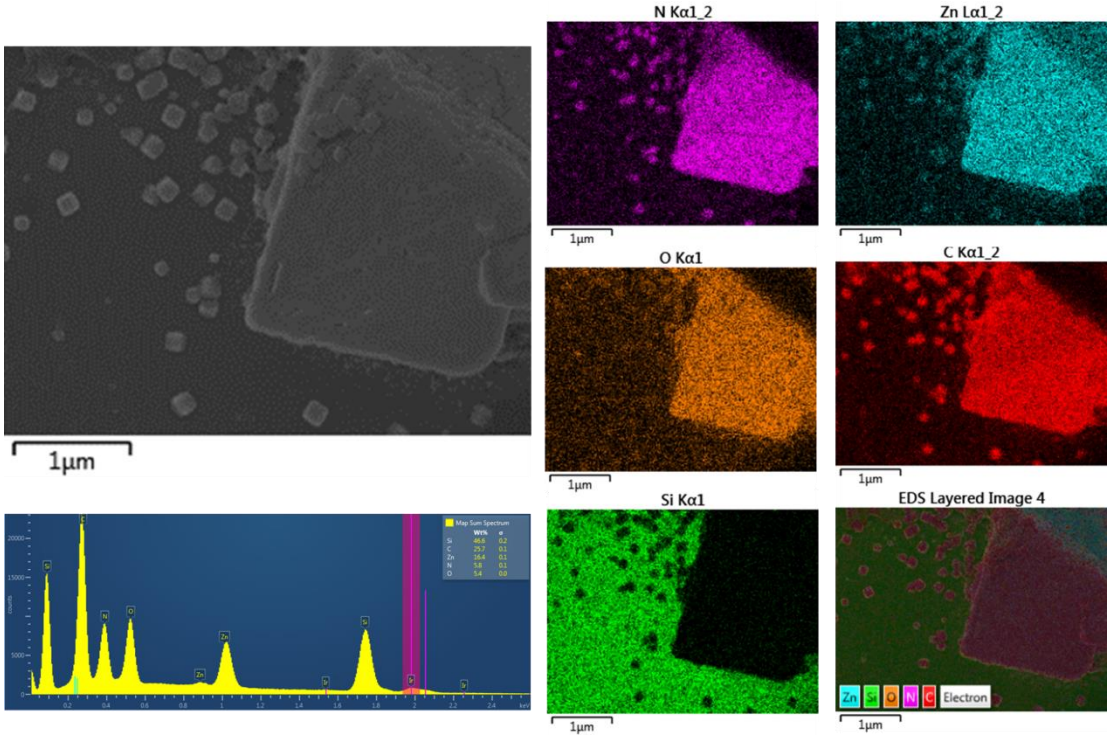

Figure 5.7 EDX **5:5**

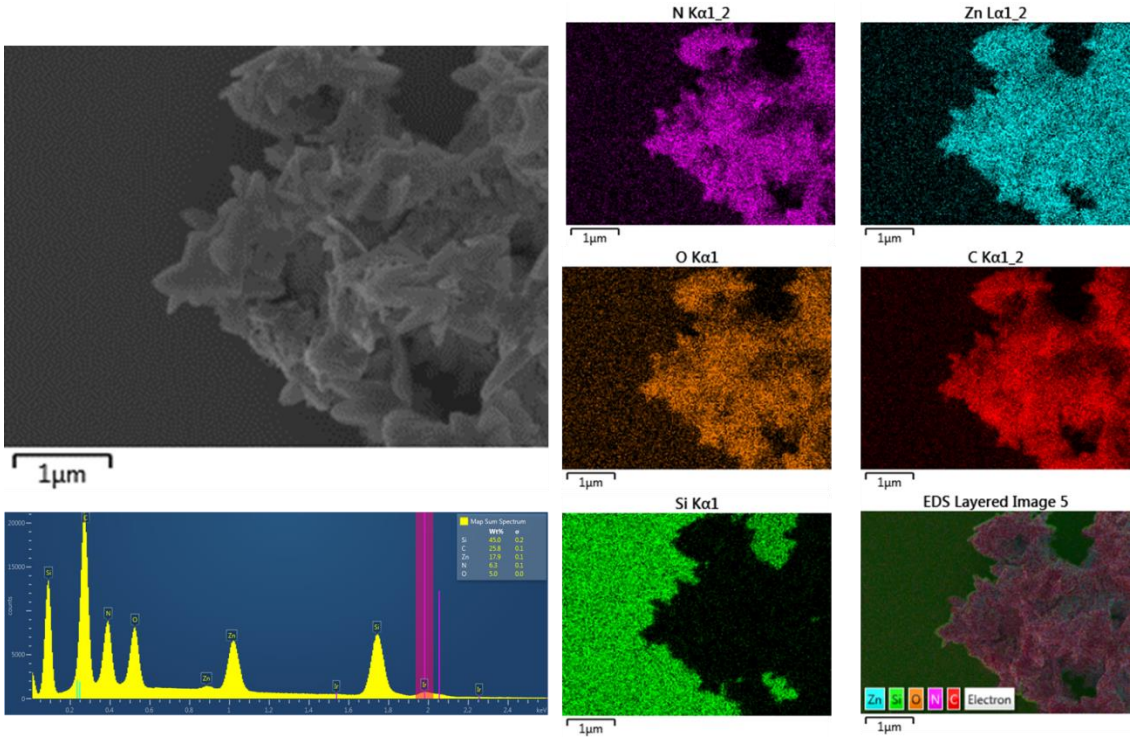

Figure 5.8 EDX **5:20**

The element concentration of all the DNA origami-MOF samples have been summarized in two histograms where the relative contents of each element in each samples have been normalized with respect to C concentration.

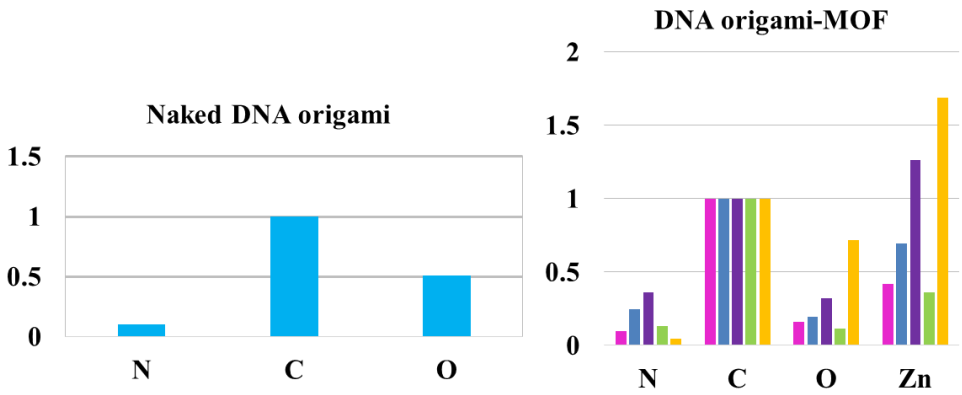

Figure 5.9 Normalized histograms representing the element contents in naked DNA origami and in the DNA origami-MOF samples, considering C concentration = 1 of **naked origami**, **5:1 (10x precursor)**, **5:1**, **1:20**, **5:5**, **5:20**.

The concentration considered in the histograms are averaged over the all EDX maps (Figure 5.9). The results obtained with this last morphological and elemental analysis demonstrate that the MOF formation in the DNA origami solution has been performed correctly, matching with ZIF-8 crystal characterization found in literature **[106]**.

The phosphor detection has been also performed in the 5:5 and 5:20 samples but the signal intensity is comparable with the background noise and so it cannot be considered to evaluate the DNA origami presence. To prove the encapsulation of DNA origami structure inside the formed crystal, I have detected the fluorescence signal of the MOF-DNA origami stained with a commercial DNA intercalant (Gel Red, Biotium) compared with a non-stained sample. I have incubated 10 µL of DNA origami with 0.3 µL of the intercalant following the same protocol adopted by B. Ding's group to load doxorubicine inside a triangular DNA origami **[107]**. After an overnight incubation, the DNA origami has been centrifuged at 10000 × g for 10 min to remove the excess of dye. The ZIF-8 synthesis has been performed using a ratio of 5:20 between DNA origami and ZIF-8 precursor because this ratio has given the best results for crystal formation, and then the sample has been washed as described in the previous paragraph. Fluorescence micrographs have been acquired for both samples with and without DNA staining using two different filters: a filter assembled on purpose for the Gel Red analysis, with an excitation window in the UV and an emission window in the red, and a standard FITC filter with an excitation window in the blue and an emission window in the green, used to check he intensity of the ZIF-8 broadband autofluorescence.

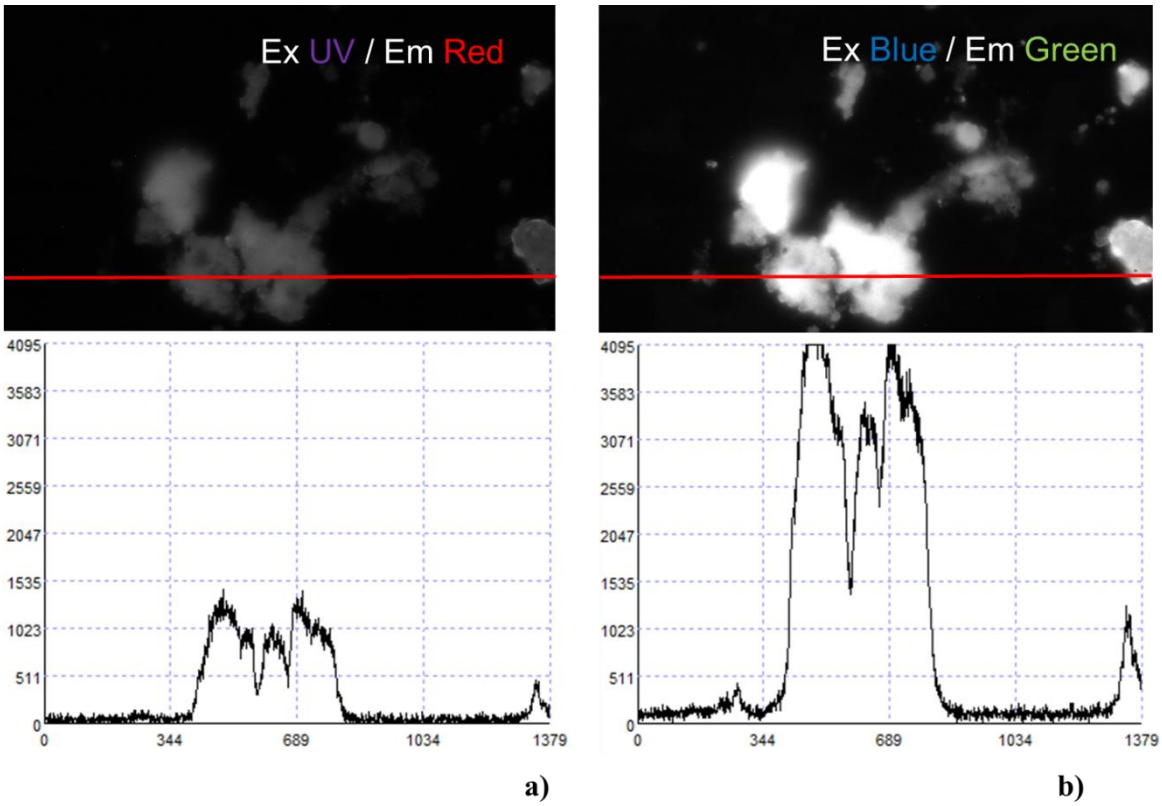

Figure 5.10 Fluorescence images of ZIF-8 encapsulating stained DNA origami observed with **a)** the specific filter for intercalant dye (ex UV/ em Red) and **b)** non-specific filter (ex Blue / em Green). The red line represents the region in which the underlying plots has been measured.

The detection has been performed with both filters to highlight the emission of fluorescence not related with the dye staining in the non-stained sample.

The images in 5.10 represent the fluorescence observed with the specific (a) and non-specific (b) filter of MOF-DNA origami stained with intercalant dye. The red line indicates the region along which the intensity profiles shown in the underlying plots have been extracted. The autofluorescence signal saturates the camera, while the fluorescence emitted in the proper conditions is three times lower.

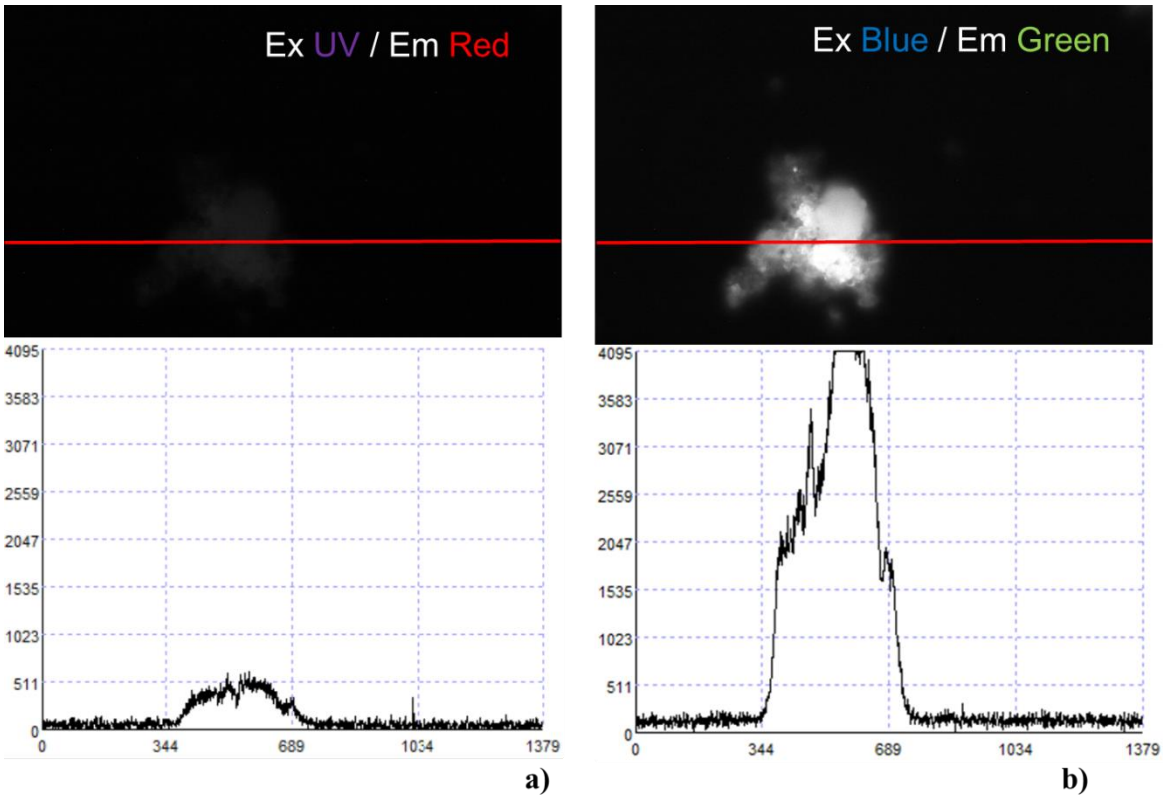

Figure 5.11 Fluorescence images of ZIF-8 encapsulating non-stained DNA origami observed with **a)** the specific filter for intercalant dye (ex UV/ em Red) and **b)** non-specific filter (ex Blue / em Green). The red line represents the line in which the underlying plots has been measured.

The autofluorescence observed with non-specific filter has been confirmed through the measurement of ZIF-8 which encapsulates DNA origami without any staining (Figure 5.11). The signal emitted with the non-specific filter saturate the camera as in the stained sample, while the fluorescence observed with the specific filter is three times less than the one measured in the same condition but with the labeled DNA. The presence of non-specific fluorescence emission using the specific filter can be due to the overlapping of the transmission window of the filter with the end of the spectral region where the autofluorescence is emitted. The comparative analysis of these two samples suggests a significant increase of the fluorescence signal in the sample containing the intercalant dye with respect to the non-labeled one: this results strengthen the idea that the DNA origami is effectively encapsulated inside the crystal.

Further confirmation of the effective encapsulation of the DNA origami inside the ZIF-8 crystal should be provided by AFM and SEM analysis of the samples after EDTA addition, which is expected to dissolve the MOF crystals and free the DNA origami. However, a specific purification step to allow a precise identification of the origami structure is

required and so far its development has been unsuccessful. This represents the future work to be performed in the immediate future.

Conclusions and future perspectives

I have planned a DNA origami-based plasmonic device in which a molecular stimulus produces a structural reconfiguration. To define all the conditions for the design, the synthesis, the decoration with AuNP and the purification from particles in excess, I have first set up a test-bench structure: DNA origami rectangle. It represents a robust platform to define all the preferable working conditions to be used in more challenging structures. In particular, employing a new purification protocol, based on a density gradient ultrafast separation I have been able to separate free NP from AuNP-decorated rectangular shape DNA origami avoiding architectural alterations. DNA origami-AuNP conjugates can be analyzed also at single particle level measuring the optical response for SERS, Raman and dark-field analysis, in the perspective of its use in the location-specific molecular detection.

The shape chosen for the final DNA origami device is the tetrahedron with rigid struts connected by flexible joints (0ss), allowing a wide range of structural motions. To tune the mechanical properties of the tetrahedron, I have designed another structure introducing three 4-nucleotides gaps in the two struts connected by the actuator strand (3ss). The designed detection system was based on two AuNP strategically positioned in two opposite facets of the tetrahedron. In this way, any relevant structural change, which may results in a nanometric shift of the interparticle distance, can be effectively monitored through extinction measurements. The actuation, triggered by the hybridization with a molecular target, induces a clearly detectable red-shift of the peak position of the LSPR spectrum of AuNP proportional to the interparticle distance reduction, thus creating a plasmon meter. The optical extinction measurements performed on actuated and not-actuated structures confirmed the presence of an LSPR shift in the actuated 3ss samples only, confirmed by in-depth analysis of conformational changes performed using high resolution detection. SAXS analysis performed in liquid samples, in fact, confirmed the results obtained with LSPR measurements in gel, highlighting the gap reduction between AuNP after the target binding in the 3ss tetrahedron structures only. SEM imaging on the 3ss DNA origami further confirmed the reduction of the interparticle distance in the presence of the target strand. From this analysis I understood that after the deposition on a substrate the flexibility of the tetrahedron allows two main conformations at the equilibrium, in which AuNP are separated by a bimodal distribution of the interparticle distance centered at 26 nm and 33 nm; after the target addition the configuration is stabilized at 24-25 nm. These

results are in line with the results obtained both with LSPR and SAXS analysis, demonstrating its robustness also if dried. An important issue still open regards the large scale production and purification: I tested several different purification protocols, but all have introduced damages, dirt and conformational changes on the starting DNA origami design. Nonetheless, in all the conditions (dried, wet and in gel) the results are comparable, thus demonstrating the ability to preserve the desired behavior independently from the analysis environment.

A further DNA origami characterization through cryo-EM has been attempted at the Molecular Foundry, Berkeley CA. Frozen samples can be imaged in their physiological conditions, providing for an accurate study of the thermodynamic configurations of the tetrahedron DNA origami before and after its actuation without any modification induced by sample pretreatment. The analyzed samples displayed DNA origami aggregation, making the identification of well-folded structures difficult; only in some cases I have found isolated structures with AuNP dimers and, with one of them, I have been able to perform tomographic analysis. Tetrahedron shaped DNA origami has demonstrated the environment independence feature for which it has been originally designed, paving the way to its application in the field of molecular recognition in different conditions. Moreover, its biocompatibility due to both its shape and its material allows to use it in *in vivo* analysis, for example as an injectable biosensor or as a contrast medium for biomarker detection.

These perspective applications are limited by the difficulties in purifying the structure, hindering its use in the clinical field. By pursuing the same approach and aims applied to the tetrahedron, I will design a different structure: the new shape will be a triangle designed to avoid weak points inside the structure during the folding and where the helix bundles are connected by more robust joints. The choice of the triangular shape is supported by many works already reported in literature, which confirm its stability and biocompatibility in *in vitro* and *in vivo* studies.

Finally, I tried to explore a strategy to prolong the DNA origami half-life, encapsulating it on metal-organic frameworks (MOFs). ZIF-8 crystals with the inclusion of DNA origami were successfully produced, demonstrating that the addition of the origami doesn’t interfere with the crystal formation. We also noted that the DNA origami didn’t affect the shape of the crystals, while its dimension can induce a fusion among crystals. We are now working on the release of the DNA origami through the addition of EDTA, but further investigations are required to monitor the DNA origami presence inside the grown MOFs.

The demonstration of the successful inclusion of the DNA origami inside a zeolitic imidazole framework can help in the preservation and long-term storage of the structures. Moreover, by exploring the combination of DNA origami with different MOFs, these hybrid structures could also be used as improved drug delivery systems.

Appendix 1

NAME	START	END	Sequence 5' ----->3'	Length
ST1	23[3]	21[215]	AAATCAAATTTAATTGACGGTGTCTGGAAGTT	32
ST2	4[298]	5[298]	ATAGCCGAACAGAGATGGTTTA	22
ST3	3[168]	1[183]	GTAAAGCACAAGTTTTCCAACGTCAAAGGGCG	32
ST4	22[119]	20[104]	ACCACATTGATAGCGTCTAATGCAGAACGCGC	32
ST5	15[232]	13[247]	TGCCTGCAACAACATAGGCGCCAGGGTGGTTT	32
ST6	1[216]	3[231]	CGTATTAATTCCGAAAGACGGGGAAAGCCGGC	32
ST7	2[151]	0[136]	ACCACCGGATCAAAATGAACAAGATGATATTC	32
ST8	16[135]	18[128]	CTAAATCGTTTTGCGGCTCAGAGC	24
ST9	6[215]	4[200]	AAGGGAACTAAAACGACTTATTACGCAGTATG	32
ST10	13[248]	15[263]	TTCTTTTCTGGGTTATCTAGAGGATCCCCGGG	32
ST11	0[39]	0[21]	AGTGTACTGGTAATAAGTT	19
ST12	9[216]	11[231]	GAATTGAGAGCCGTTTACAGCCATATTATTTA	32
ST13	12[39]	14[32]	AAATTCTTCAATAGGATTCCGGCA	24
ST14	8[135]	10[120]	CTTGCTTCAATCAATAATTTCAATTACCTGAG	32
ST15	17[280]	19[287]	CTCATTTTGTCAATAAAAACAAGA	24
ST16	9[56]	11[71]	GGCAATTCTAAGACGCGTAGATTTTCAGGTTT	32
ST17	12[103]	14[88]	ATAAGAATAAATGTGAGCATCTGCCAGTTTGA	32
ST18	21[144]	23[159]	TATTACAGCTGAATATGTAATTCTGAATCCCC	32
ST19	14[183]	12[168]	TAACTCACCGCCAGGGAAATATATTTTAGTTA	32
ST20	0[135]	2[120]	ACAAACAAGTCAGACGCCCTCAGAGCCGCCAC	32
ST21	4[39]	6[21]	GTAAATATAAATGAATCGCCCACGCATAACCGATA	35
ST22	2[279]	0[264]	CACTAACAACAGTTGACAGCAAGCGGTCCACG	32
ST23	13[88]	15[103]	TCAACATTAAACACCGTGTTGGGAAGGGCGAT	32
ST24	7[72]	5[87]	TCACCCTCGCTTGATAACAGTTTCAGCGGAGT	32
ST25	12[167]	14[152]	ATTTCATCAGTCGGGACGTTGCGCTCACTGCC	32
ST26	12[231]	14[216]	GCTGATGCGCGTATTGCGAGCCGGAAGCATAA	32
ST27	1[56]	3[71]	ATTTGGGAATACATGGCAAGTTTGCCTTTAGC	32
ST28	1[248]	3[263]	TTTAAAAGCCCCAGCAGAAGGGAAGTCAGTTG	32
ST29	2[215]	0[200]	CTTTACAATAGAGCTTTCGGCAAAATCCCTTA	32
ST30	21[120]	23[127]	TAAAACGAATGTTCAGCCAATACT	24
ST31	9[248]	11[263]	AACAATGAAAACCAAGAAACGATTTTTTGTTT	32
ST32	23[104]	21[119]	TTAGACTGCAACTAATGAAAAATCTACGTTAA	32
ST33	20[199]	22[184]	GCCAGTAAACTAAAGTCTCCTTTTGATAAGAG	32
ST34	8[111]	10[88]	TAATTAATTTTCCCTTTGAATTACAACAAACATCAAGAAA	40
ST35	9[120]	11[135]	AGTACATATGTAAATCAATAACGGATTCGCCT	32
ST36	0[199]	2[184]	TAAATCAATCTATCAGCACTACGTGAACCATC	32
ST37	14[87]	12[72]	GGGGACGATGCGCAACGAATCATAATTACTAG	32
ST38	16[231]	18[216]	CAATTCTATAAATTGTTAATCAGAAAAGCCCC	32
ST39	11[200]	9[215]	GCCAGTTAGAGCAAGATAAATATAACCCACAA	32
ST40	3[136]	1[151]	TTTTCATAAACCGCCTATTGGCCTGTCCACTA	32
ST41	4[135]	6[120]	GGAATAAGTTTTTTCAGGAGCCTTTAATTGTA	32
ST42	16[175]	18[152]	GAATTAGCAAAATTAAGATAAAAAGCCGGAGAACCGCCAC	40

ST43	8[71]	10[56]	GCTTAGATATCAATATGTTTGGATTATACTTC	32
ST44	22[215]	20[200]	AGAGTACCAATCAGGTGCAGAGGCATTTTCGA	32
ST45	7[40]	5[55]	GCAGGGAGACAACCATTTTCTGTATGGGATTT	32
ST46	4[103]	6[88]	AATTCATAAAAGGAACCTTTCGAGGTGAATTT	32
ST47	2[183]	0[176]	ACCCAAATCTAAATCGCCCGAGAT	24
ST48	7[200]	5[215]	CACCAACCCGAACTGATTACCCAAATCAACGT	32
ST49	23[32]	21[55]	CGACGATAAAAACCAAACCCTCGTTCATTGTGAATTACCT	40
ST50	8[199]	10[184]	AATCATTATGAAGCCTTTAGTTGCTATTTTGC	32
ST51	18[151]	16[136]	CCTCAGAATACCGCCAGCCTCAGAGCATAAAG	32
ST52	5[184]	7[199]	AAGAACCGCGTAGAAAAATGCCACTACGAAGG	32
ST53	1[88]	3[103]	CACCAGAGCAGTCTCTTTTTCATCGGCATTTT	32
ST54	17[56]	19[71]	GCCCGTATATAGTTAGTGCTCAGTACCAGGCG	32
ST55	17[80]	19[103]	CTGCCTATCCATGTACACAACGCCAGGGTTGATATAAGTA	40
ST56	21[280]	23[287]	CATTTCGCTATAAAGCGAAAGACT	24
ST57	6[159]	4[136]	GCGCATAGAAAAAAGGTTTTTCATAACGCAAAGACACCAC	40
ST58	10[119]	8[112]	CAAAAGAAGGAGAAACGTCGCTAT	24
ST59	7[232]	5[247]	CACTAAAAAACGAGGCCAGTGAATAAGGCTTG	32
ST60	20[231]	22[216]	CCAACATGTATAACAGAACAGGTCAGGATTAG	32
ST61	16[39]	18[32]	TTTGTCGTGGGGTCAGCCTCAAGA	24
ST62	23[233]	21[247]	TAGTCAGCAAACTCCTTGATTCCCAATTCTG	31
ST63	11[232]	9[247]	TCCCAATCAAGTCAGAAATAATAAGAGCAAGA	32
ST64	16[71]	18[56]	CAGCCCTCAAACAGTTCTGAAACATGAAAGTA	32
ST65	11[136]	9[151]	GATTGCTTAATTATTCTATGTGAGCTAAGAAC	32
ST66	15[72]	13[87]	ATTCAGGCCGACAGTACTGTAGCCAGCTTTCA	32
ST67	12[263]	14[248]	GCTTAGGTACCAGTGAATTGTTATCCGCTCAC	32
ST68	15[136]	13[151]	GCGAAAGGGGATAGGTACAAACGGCGGATTGA	32
ST69	8[298]	9[298]	CAATAATCGGCTAAGAAAAGTA	22
ST70	10[247]	8[232]	CCTGAACACAAATAAGTACCGCACTCATCGAG	32
ST71	3[72]	1[87]	GTCAGACTGCCAAATCCAGCAACCAGAACCAC	32
ST72	20[71]	22[56]	GAAAAATATTTAAGAACATAGTAAGAGCAACA	32
ST73	5[120]	7[135]	AATAATAATTTATTTTACAGAGGCTTTGAGGA	32
ST74	9[88]	11[103]	ATTTCATTAGAATCCTACAGTAACAGTACCTT	32
ST75	1[120]	3[135]	TGAGGCAGATAAATCCATTAGCGTTTGCCATC	32
ST76	16[263]	18[248]	TTCATTTGCGCATTAAACTAGCATGTCAATCA	32
ST77	20[143]	22[120]	GACGACAATAAACAACACTAACGGGTTGAGATTTAGGAAT	40
ST78	10[215]	8[200]	ATATCAGACAAAATAATTATTTTCATCGTAGG	32
ST79	5[21]	4[21]	CAGACGTTAGTTGACGGAAATT	22
ST80	14[247]	12[232]	AATTCCACGGTCGACTATAACTATATGTAAAT	32
ST81	9[184]	11[199]	GGAGGTTTCCGCGCCCTTCCAGAGCCTAATTT	32
ST82	11[72]	9[87]	AACGTCAGAATTGATTAATCCTACATTTAACA	32
ST83	17[155]	19[167]	GCAAGGCAATAAACCCTCAGACAGTCAAA	29
ST84	19[200]	17[215]	TGATAAATGAAAGTAAGCCTGGATTGTATAAG	32
ST85	2[298]	2[280]	TCTAAAATATCTTTAGGAG	19
ST86	18[215]	16[200]	AAAAACAGTAATGCCGAGTAGCATTAACATCC	32
ST87	10[151]	8[136]	CAGAGGCGTGAATACCCCGGTATTTGAATAAC	32

ST88	11[40]	9[55]	GAAATAAAGGAAGGGTCTGATTATCAGATGAT	32
ST89	11[104]	9[119]	TTACATCGGATGATGACTTTTTTAATGGAAAC	32
ST90	0[231]	2[216]	GATGGTGGATCCTTTGATTTAGAAGTATTAGA	32
ST91	6[298]	6[280]	GTATCATCGCCTGATAAAT	19
ST92	5[248]	7[263]	CCCTGACGAATAACGGTTTGACCCCCAGCGAT	32
ST93	19[264]	17[279]	CCTGAGAGATCGTAAAATTTTTGTTAAATCAG	32
ST94	13[216]	15[231]	GGCGGTTTAAATCCAACAGTGCCAAGCTTGCA	32
ST95	4[71]	6[56]	AGGGCGACAACTTTCACCGATAGTTGCGCCGA	32
ST96	9[280]	11[298]	GCCCTTTTTGTCTTTCATAGCAGCCTTTACAGAGA	35
ST97	21[176]	23[199]	ATGTTTTAAATATGCATAAGAGAAAAACGAGAATGACCAT	40
ST98	2[247]	0[232]	GATAATACCGAGAAAGGGCGAAAATCCTGTTT	32
ST99	20[167]	22[160]	AAGGTAAAAATGCTGTGCTTAGAG	24
ST100	5[144]	7[167]	ATCTCCAAGCTGGCTGATAAAAGAGAGGAAGTTTCCATTA	40
ST101	0[71]	2[56]	TAAGCGTCATTAGAGCACCAGTAGCACCATTA	32
ST102	19[32]	17[55]	GAAGGATTAGGATTAGCTGAGACTTGCCTTGAGTAACAGT	40
ST103	4[231]	6[216]	GGCATGATTGCTCATTGCAGACGGTCAATCAT	32
ST104	0[263]	2[248]	CTGGTTTGTTTGAGTAATTAGAGCCGTCAATA	32
ST105	8[231]	10[216]	AACAAGCATTAAGCCCGGGTAATTGAGCGCTA	32
ST106	0[175]	2[152]	AGGGTTGAGTGTTGTTCGTGGACTTTGGGGTCCCAGAGCC	40
ST107	17[248]	19[263]	TTAAAATTGGGCGCGAGGCTATCAGGTCATTG	32
ST108	10[55]	8[40]	TGAATAATGAAATTGCTGAGAAGAGTCAATAG	32
ST109	16[199]	18[184]	AATAAATCAATGCAATTGTGTAGGTAAAGATT	32
ST110	18[55]	16[40]	TTAAGAGGCGGGGTTTCGTAACGATCTAAAGT	32
ST111	20[39]	22[32]	TGTAGAAAAACTTTAATTACCAGA	24
ST112	22[287]	20[264]	TCAAATATCGCGTTTTGGAAGCCCCAACGCTCAACAGTAG	40
ST113	3[104]	1[119]	CGGTCATACCGCCACCAGCATTGACAGGAGGT	32
ST114	11[168]	9[183]	ACGCTAACACAATTTTAACCTCCCGACTTGCG	32
ST115	7[168]	5[183]	AACGGGTAACGGTGTACAAGAGTAATCTTGAC	32
ST116	13[176]	15[191]	GTGCCAGCTGCATTAAACTTTTTCTTTTCCCA	32
ST117	18[287]	16[264]	GAATCGATGAACGGTATCTGGAGCCCTGTTTAGCTATATT	40
ST118	22[159]	20[144]	CTTAATTGGTAGAAAGTATTCATTGTCCAGAC	32
ST119	8[263]	10[248]	CGGGTATTAATAGCAAAGAATTAACTGAACAC	32
ST120	9[21]	8[21]	CGGAATTATCATCAAAATCATA	22
ST121	11[21]	11[39]	ATTATTTGCACGTAAAACA	19
ST122	3[21]	3[39]	ATCGATAGCAGCACCGTAA	19
ST123	19[232]	17[247]	TTGAGAGACCGGTTGAAAACGTTAATATTTTG	32
ST124	6[55]	4[40]	CAATGACATTAAAGGCGATTGAGGGAGGGAAG	32
ST125	17[184]	19[199]	ATATTTTAATACAGGCATTCAACCGTTCTAGC	32
ST126	11[264]	9[279]	AACGTCAATAGACGGGTAGCTATCTTACCGAA	32
ST127	21[88]	23[103]	GTCAGGACCAACAATAGGTAATAGTAAAATGT	32
ST128	7[136]	5[143]	CTAAAGACCTCCAAAACGTTGAAA	24
ST129	4[263]	6[248]	AACGCAATAGAAACACACCTGCTCCATGTTAC	32
ST130	8[39]	10[21]	TGAATTTATCATATTCTAGAACCTACCATATCAAA	35
ST131	17[216]	19[231]	CAAATATTCTAATAGTGAGAGGGTAGCTATTT	32
ST132	7[104]	5[119]	GAGGGTAGTCAGCTTGAACTAAAGGAATTGCG	32

ST133	13[152]	15[167]	CGCTTTCCTTCTGACCCTGCAAGGCGATTAAG	32
ST134	12[135]	14[120]	AAATACCGCCGTGGGACACGTTGGTGTAGATG	32
ST135	4[167]	6[160]	GGCAACATACCTTCATCAGACCAG	24
ST136	3[40]	1[55]	TCAGTAGCAAGGCCGGGTCACCGACTTGAGCC	32
ST137	15[104]	13[119]	CGGTGCGGGTAACCGTGCGAGTAACAACCCGT	32
ST138	21[248]	23[263]	CGAACGAGTGAGAATCCGGATTGCATCAAAAA	32
ST139	6[279]	4[264]	TGTGTCGAGCGCGAAAAGAAGGAAACCGAGGA	32
ST140	3[200]	1[215]	CCCCGATTACATGGCCGGCGAATTCGACAACT	32
ST141	7[264]	5[279]	TATACCAAAATCCGCGCAGAACGAGTAGTAAA	32
ST142	6[87]	4[72]	CTTAAACAAGCAGCGACAGCGCCAAAGACAAA	32
ST143	19[72]	17[79]	GATAAGTGCTATTATTAATGCCCC	24
ST144	1[152]	3[167]	TTAAAGAACCAGTTTGCACCGGAAGAGGTGCC	32
ST145	0[103]	2[88]	GGAAAGCGCCGCCGCCCTCAGAGCCACCACCC	32
ST146	2[119]	0[104]	CCTCAGAAGCCCCCTTTCATTAAAGCCAGAAT	32
ST147	1[280]	3[298]	GAACAAAGGAGAGTTGAAGGAATTGAGGAAGGTTA	35
ST148	19[168]	17[183]	TCACCATCTGAGAAAGTTTTTAGAACCCTCAT	32
ST149	13[120]	15[135]	CGGATTCTACCGTGTGGCTATTACGCCAGCTG	32
ST150	5[216]	7[231]	AACAAAGCTAAGACTCAAGAGGCAAAAGAATA	32
ST151	0[298]	1[298]	CCTGGCCCTGAAAACCACCAGA	22
ST152	21[216]	23[232]	TCATTCCATAATTTAGCTTTACCCTGACTATTA	33
ST153	1[184]	3[199]	AAAAACCGAAGAATAGGAACCCTAAAGGGAGC	32
ST154	13[56]	15[71]	TTCGCGTCTGTTTAGTCAAAGCGCCATTCGCC	32
ST155	10[279]	8[264]	AAGCGCATAAATGAAACTTATCATTCCAAGAA	32
ST156	12[71]	14[56]	AAAAAGCCTGGCCTTCTCGGCCTCAGGAAGAT	32
ST157	15[32]	13[55]	CCGCTTCTGGTGCCGGAGCCAGCTACGCCATCAAAAATAA	40
ST158	2[87]	0[72]	TCAGAGCCGTAGCGCGGAATTTACCGTTCCAG	32
ST159	16[103]	18[96]	TACAAACTCGTAACACCAAGCCCA	24
ST160	20[263]	22[248]	GGCTTAATTAGATTTACTTCAAAGCGAACCAG	32
ST161	5[56]	7[71]	TGCTAAACATTCAACCCGCTTTTGCGGGATCG	32
ST162	23[264]	21[279]	GATTAAGAAATTCGAGGTTTGACCATTAGATA	32
ST163	3[232]	1[247]	GAACGTGGATTTGAGGCCCGAACGTTATTAAT	32
ST164	21[56]	23[71]	TATGCGATATATCCCAGAGGCTTTTGCAAAAG	32
ST165	5[280]	7[298]	TTGGGCTTAAGTTACCCAAAGTACAACGGAGATTT	35
ST166	13[280]	15[287]	TTGCCCTTGAGAGACTGTAATCAT	24
ST167	9[152]	11[167]	GCGAGGCGAGGCTTATAAGTTACATCTTACCA	32
ST168	18[247]	16[232]	TATGTACCTCTACAAAGCTGAAAAGGTGGCAT	32
ST169	23[72]	21[87]	AAGTTTTGTTACGAGGCTGGCTCATTATACCA	32
ST170	10[298]	10[280]	GAATAACATAAAAACAGGG	19
ST171	22[87]	20[72]	AAAAGGAACCAGAGGGGATAAGTCCTGAACAA	32
ST172	22[247]	20[232]	ACCGGAAGAAGCAAAGGCCATATTTAACAACG	32
ST173	20[103]	22[88]	CTGTTTATGTTGGGAAGCAGATACATAACGCC	32
ST174	14[55]	12[40]	CGCACTCCAAACCAGGATCATATGCGTTATAC	32
ST175	6[247]	4[232]	TTAGCCGGCACTCATCAATACCCAAAAGAACT	32
ST176	6[119]	4[104]	TCGGTTTACAACGGCTGTCACAATCAATAGAA	32
ST177	14[119]	12[104]	GGCGCATCGCCTCTTCATAAATAAGGCGTTAA	32

ST178	14[287]	12[264]	GGTCATAGCTGTTTCCTCGAATTCACCTTTTTAACCTCCG	40
ST179	18[95]	16[72]	ATAGGAACTTCGGAACCCGTCGAGTGTAGCATTCCACAGA	40
ST180	2[55]	0[40]	CCATTAGCGACAGAATCTTTTGATGATACAGG	32
ST181	23[128]	21[143]	GCGGAATCGTCATAAAATTCATCAAACAACAT	32
ST182	7[21]	7[39]	TATTCGGTCGCTGAGGCTT	19
ST183	10[87]	8[72]	ACAAAATTATGAATATTGAAAACATAGCGATA	32
ST184	15[264]	13[279]	TACCGAGCTGTGTGAAGACGGGCAACAGCTGA	32
ST185	5[88]	7[103]	GAGAATAGTGGTTTACAAGACAGCATCGGAAC	32
ST186	22[55]	20[40]	CTATCATAAATAGCGATCCTAATTTACGAGCA	32
ST187	3[264]	1[279]	GCAAATCAACTAATAGACATTATCATTTTGCG	32
ST188	1[21]	2[21]	TTAAAGGTGAATTATCACCAAACGTCACCAATGAAACC	38
ST189	4[199]	6[184]	TTAGCAAAGATATTCACCAACTTTGAAAGAGG	32
ST190	8[167]	10[152]	GATATAGATTTTAGCGATCCTGAAAAATCGCG	32
1NP1	10[183]	27[118]	ACCCAGCTGAGCGTCTAATAGCAAGCAAATCAGTACTTCCTTAAA CGACGCAGGCTTATCCTTCACGATTGCCACTTTCCAC	83
1NP2	14[151]	29[140]	CCGTAATGGGGATGTGTAAATTTAATGGTTTGGTACTTCCTTAAA CGACGCCTTCACGATTGCCACTTTCCAC	73
2NP1	18[183]	33[190]	CAAAAGGGAATATGATAAGGCAAAGTACTTCCTTAAACGACGCC TTCACGATTGCCACTTTCCAC	65
2NP2	23[160]	24[171]	CTCAAATGCTTTAAACTGCGGATGAGCTCAACGTACTTCCTTAAA CGACGCCTTCACGATTGCCACTTTCCAC	73
1NP3	22[183]	31[124]	GTCATTTTAGTTCAGATATAAAGTACCGACAAGTACTTCCTTAAAC GACGCACTTCACGATTGCCACTTTCCAC	74
2NP3	6[183]	25[110]	ACAGATGAAAATACGTATACATACATAAAGGTGTACTTCCTTAAA CGACGCAGGCTTATCCTTCACGATTGCCACTTTCCAC	83
CATCHERS ACTUATOR 1	15[168]	26[246]	TTGGGTAAATTAATTGAACCTGTCCTGCGAGCCCGGGAAGCT	42
CATCHER ACTUATOR 2	28[159]	17[154]	GGGAGGAAGGTCGGATCGTTTATTTCAAC	29
ACTUATOR	probe		CGATCCGACCTTCCTCCCTCCTCCTCTTCCCTTGGGTCGAACATTG CTCGTCGTCACTGGGTCCTGCTCATATTGGGTTTACAGCTCACATA GGTAGACTTTAGCTTCCCGGGCTCGCAG	120
			GGGCGGGGCGGGGGCGCGAAAGTCTACCTATGTGAGCTGTAAA CCCAATATGAGCAGGACCCAGTGACGACGAGCAATGTTCGACCC AAGGGAAGAGGAGGACGCGCCCCCGCCCCGCCC	120
SET OF STAPLES FOR 1SS TETRAHEDRON				
1ss1	13[192]	14[184]	TGAATCGGTGCCTAATGAGTGAGC	24
1ss2	19[104]	17[127]	TAGCCCGGAGGGATAGTGAGTTTCTATGACCCTGTAATAC	40
1ss3	16[123]	17[143]	TACCTATCACCGTACTCAGGAGGTTTAGCCGCCACCGAGAAGCC	44
1ss4	18[127]	16[104]	CACCACCCTCATTTTCAATAGGTGAAAAACATGTCACCAG	40
1ss5	14[215]	12[196]	AGTGTAAAACGACGGCTCGCAAGACAAAGAACGCGA	36
1ss6	15[192]	13[215]	GTCACGACGTTGTAAAGCCTGGGGCCAACGCGCGGGGAGA	40
SET OF STAPLES FOR 0SS TETRAHEDRON				
1ss1	13[192]	14[184]	TGAATCGGTGCCTAATGAGTGAGC	24
1ss2	19[104]	17[127]	TAGCCCGGAGGGATAGTGAGTTTCTATGACCCTGTAATAC	40
0ss3	16[127]	17[143]	GTTGTACCTATCACCGTACTCAGGAGGTTTAGCCGCCACCGAGAA	48

			GCC	
1ss4	18[127]	16[104]	CACCACCCTCATTTTCAATAGGTGAAAAACATGTCACCAG	40
0ss5	14[215]	12[192]	AGTGTAAAACGACGGCTCGCAAGACAAAGAACGCGAGAAA	40
1ss6	15[192]	13[215]	GTCACGACGTTGTAAAGCCTGGGGCCAACGCGCGGGGAGA	40
SET OF STAPLES FOR 3SS TETRAHEDRON				
3ss1	13[196]	14[184]	TCGGTGCCTAATGAGTGAGC	20
3ss2	19[104]	17[123]	TAGCCCGGAGGGATAGTGAGTTTCTATGACCCTGTA	36
3ss3	16[123]	17[143]	TACCTATCACCGTACTCAGGAGGTTTAGCCGCCACCGAGAAGCC	44
3ss4	18[123]	16[104]	ACCCTCATTTTCAATAGGTGAAAAACATGTCACCAG	36
3ss5	14[215]	12[196]	AGTGTAAAACGACGGCTCGCAAGACAAAGAACGCGA	36
3ss6	15[196]	13[215]	CGACGTTGTAAAGCCTGGGGCCAACGCGCGGGGAGA	36

Table The table contains the nucleotides sequences used for the synthesis of the DNA origami tetrahedron structures (ST). The catchers strand for the anchoring of AuNP positioned in the facet 1 and 2 are named 1NP and 2NP: the black sequence is complementary with the structure sequence, the green sequences represents the region complementary to the AuNP sequence and the red part in the linker. The catchers for the actuator strand and the actuator strand. Three different sets of staples strand have been used for the synthesis of the DNA origami tetrahedron 0ss, 1ss and 3ss.

Appendix 2

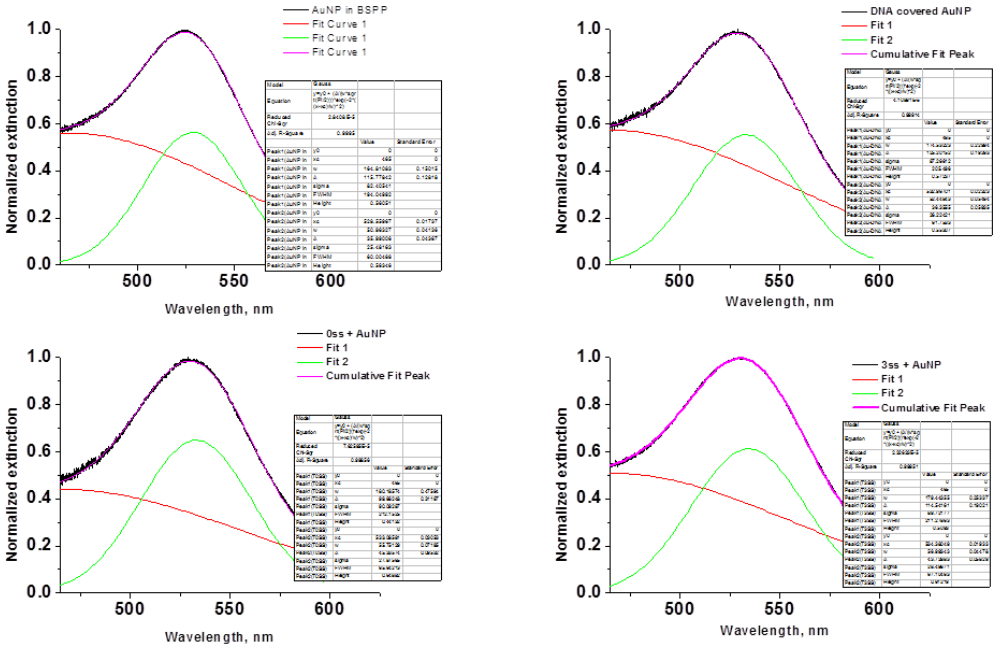

A 0-1 Fit of the graph shown in figure 4.15

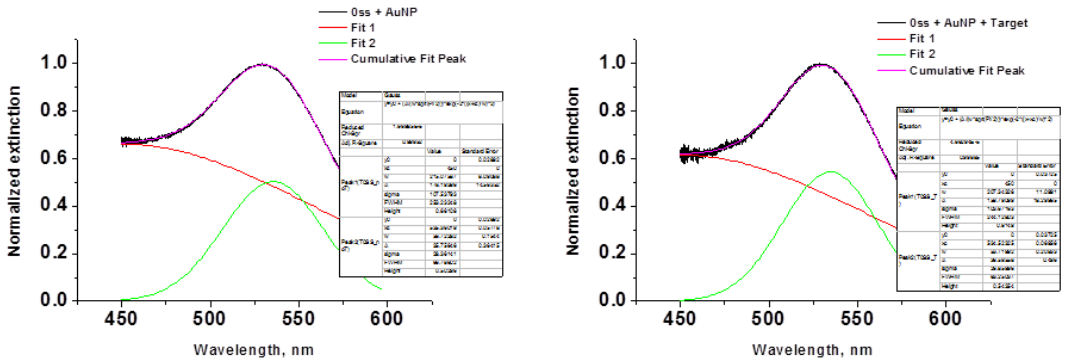

A 0-2 Fit of the graph shown in figure 4.17 a

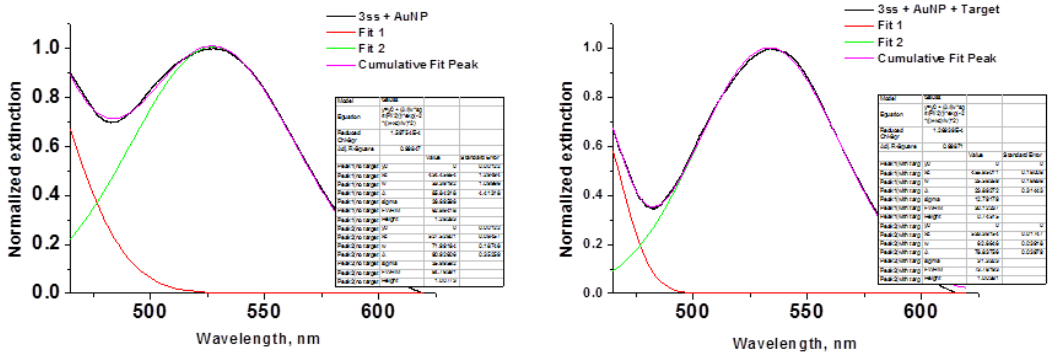

A0-3 Fit of the graph shown in figure 4.17 b

References

1. Watson JD, Crick FH (1953) The structure of DNA. Cold Spring Harbor symposia on quantitative biology 18:123-131
2. Seeman NC (1982) Nucleic acid junctions and lattices. Journal of Theoretical Biology 99 (2):237-247. doi:https://doi.org/10.1016/0022-5193(82)90002-9
3. Zhang X, Yan H, Shen Z, Seeman NC (2002) Paranemic Cohesion of Topologically-Closed DNA Molecules. Journal of the American Chemical Society 124 (44):12940-12941. doi:10.1021/ja026973b
4. Seeman NC (2001) DNA Nicks and Nodes and Nanotechnology. Nano letters 1 (1):22-26. doi:10.1021/nl000182v
5. Seeman NC, Mao C, LaBean TH, Reif JH (2000). Nature 407 (6803):493-496. doi:10.1038/35035038
6. Chen J, Seeman NC (1991) Synthesis from DNA of a molecule with the connectivity of a cube. Nature 350 (6319):631-633. doi:10.1038/350631a0
7. Zhang Y, Seeman NC (1994) Construction of a DNA-Truncated Octahedron. Journal of the American Chemical Society 116 (5):1661-1669. doi:10.1021/ja00084a006
8. Mao C, Sun W, Seeman NC (1997) Assembly of Borromean rings from DNA. Nature 386 (6621):137-138. doi:10.1038/386137b0
9. Seeman NC, Wang H, Yang X, Liu F, Mao C, Sun W, Wenzler L, Shen Z, Sha R, Yan H, Wong MH, Sa-Ardyen P, Liu B, Qiu H, Li X, Qi J, Du SM, Zhang Y, Mueller JE, Fu T-J, Wang Y, Chen J (1998) New motifs in DNA nanotechnology. Nanotechnology 9 (3):257-273. doi:10.1088/0957-4484/9/3/018
10. Winfree E, Liu F, Wenzler LA, Seeman NC (1998). Nature 394 (6693):539-544. doi:10.1038/28998
11. Shin JS, Pierce NA (2004) A synthetic DNA walker for molecular transport. Journal of the American Chemical Society 126 (35):10834-10835. doi:10.1021/ja047543j
12. Idili A, Vallee-Belisle A, Ricci F (2014) Programmable pH-triggered DNA nanoswitches. Journal of the American Chemical Society 136 (16):5836-5839. doi:10.1021/ja500619w
13. Rothemund PWK (2006) Folding DNA to create nanoscale shapes and patterns. Nature 440 (7082):297-302. doi:10.1038/nature04586
14. Shih W. http://cadnano.org/.
15. Bathe M DAEDALUS. http://daedalus-dna-origami.org/.
16. Andersen ES. http://cdna.au.dk/software.
17. Bathe M CanDo. https://cando-dna-origami.org/.
18. Castro CE, Kilchherr F, Kim DN, Shiao EL, Wauer T, Wortmann P, Bathe M, Dietz H (2011) A primer to scaffolded DNA origami. Nature methods 8 (3):221-229. doi:10.1038/nmeth.1570
19. Ke Y, Douglas SM, Liu M, Sharma J, Cheng A, Leung A, Liu Y, Shih WM, Yan H (2009) Multilayer DNA origami packed on a square lattice. Journal of the American Chemical Society 131 (43):15903-15908. doi:10.1021/ja906381y
20. Dietz H, Douglas SM, Shih WM (2009) Folding DNA into Twisted and Curved Nanoscale Shapes. Science 325 (5941):725-730. doi:10.1126/science.1174251
21. Han D, Pal S, Nangreave J, Deng Z, Liu Y, Yan H (2011) DNA origami with complex curvatures in three-dimensional space. Science 332 (6027):342-346. doi:10.1126/science.1202998
22. Han D, Pal S, Yang Y, Jiang S, Nangreave J, Liu Y, Yan H (2013) DNA gridiron nanostructures based on four-arm junctions. Science 339 (6126):1412-1415. doi:10.1126/science.1232252
23. Zhang F, Jiang S, Wu S, Li Y, Mao C, Liu Y, Yan H (2015) Complex wireframe DNA origami nanostructures with multi-arm junction vertices. Nature nanotechnology 10 (9):779-784. doi:10.1038/nnano.2015.162
24. Iinuma R, Ke Y, Jungmann R, Schlichthaerle T, Woehrstein JB, Yin P (2014) Polyhedra self-assembled from DNA tripods and characterized with 3D DNA-PAINT. Science 344 (6179):65-69. doi:10.1126/science.1250944

25. Smith DM, Schuller V, Forthmann C, Schreiber R, Tinnefeld P, Liedl T (2011) A structurally variable hinged tetrahedron framework from DNA origami. Journal of nucleic acids 2011:360954. doi:10.4061/2011/360954
26. Veneziano R, Ratanalert S, Zhang K, Zhang F, Yan H, Chiu W, Bathe M (2016) Designer nanoscale DNA assemblies programmed from the top down. Science 352 (6293):1534. doi:10.1126/science.aaf4388
27. Mei Q, Wei X, Su F, Liu Y, Youngbull C, Johnson R, Lindsay S, Yan H, Meldrum D (2011) Stability of DNA Origami Nanoarrays in Cell Lysate. Nano letters 11 (4):1477-1482. doi:10.1021/nl1040836
28. Hahn J, Wickham SFJ, Shih WM, Perrault SD (2014) Addressing the Instability of DNA Nanostructures in Tissue Culture. ACS nano 8 (9):8765-8775. doi:10.1021/nn503513p
29. Jiang Z, Zhang S, Yang C, Kjems J, Huang Y, Besenbacher F, Dong M (2015) Serum-induced degradation of 3D DNA box origami observed with high-speed atomic force microscopy. Nano Research 8 (7):2170-2178. doi:10.1007/s12274-015-0724-z
30. Ramakrishnan S, Krainer G, Grundmeier G, Schlierf M, Keller A (2016) Structural stability of DNA origami nanostructures in the presence of chaotropic agents. Nanoscale 8 (19):10398-10405. doi:10.1039/c6nr00835f
31. Wang D, Da Z, Zhang B, Isbell MA, Dong Y, Zhou X, Liu H, Heng JYY, Yang Z (2015) Stability study of tubular DNA origami in the presence of protein crystallisation buffer. RSC Adv 5 (72):58734-58737. doi:10.1039/c5ra12159k
32. Jiang Q, Song C, Nangreave J, Liu X, Lin L, Qiu D, Wang Z-G, Zou G, Liang X, Yan H, Ding B (2012) DNA Origami as a Carrier for Circumvention of Drug Resistance. Journal of the American Chemical Society 134 (32):13396-13403. doi:10.1021/ja304263n
33. Jiang Q, Shi Y, Zhang Q, Li N, Zhan P, Song L, Dai L, Tian J, Du Y, Cheng Z, Ding B (2015) A Self-Assembled DNA Origami-Gold Nanorod Complex for Cancer Theranostics. Small 11 (38):5134-5141. doi:10.1002/smll.201501266
34. Zhuang X, Ma X, Xue X, Jiang Q, Song L, Dai L, Zhang C, Jin S, Yang K, Ding B, Wang PC, Liang X-J (2016) A Photosensitizer-Loaded DNA Origami Nanosystem for Photodynamic Therapy. ACS nano 10 (3):3486-3495. doi:10.1021/acsnano.5b07671
35. Schüller VJ, Heidegger S, Sandholzer N, Nickels PC, Suhartha NA, Endres S, Bourquin C, Liedl T (2011) Cellular Immunostimulation by CpG-Sequence-Coated DNA Origami Structures. ACS nano 5 (12):9696-9702. doi:10.1021/nn203161y
36. Douglas SM, Bachelet I, Church GM (2012) A Logic-Gated Nanorobot for Targeted Transport of Molecular Payloads. Science 335 (6070):831-834. doi:10.1126/science.1214081
37. Perrault SD, Shih WM (2014) Virus-Inspired Membrane Encapsulation of DNA Nanostructures To Achieve In Vivo Stability. ACS nano 8 (5):5132-5140. doi:10.1021/nn5011914
38. Mikkilä J, Eskelinen A-P, Niemelä EH, Linko V, Frilander MJ, Törmä P, Kostiainen MA (2014) Virus-Encapsulated DNA Origami Nanostructures for Cellular Delivery. Nano letters 14 (4):2196-2200. doi:10.1021/nl500677j
39. Subramanian HKK, Chakraborty B, Sha R, Seeman NC (2011) The Label-Free Unambiguous Detection and Symbolic Display of Single Nucleotide Polymorphisms on DNA Origami. Nano letters 11 (2):910-913. doi:10.1021/nl104555t
40. Johnson-Buck A, Nangreave J, Jiang S, Yan H, Walter NG (2013) Multifactorial Modulation of Binding and Dissociation Kinetics on Two-Dimensional DNA Nanostructures. Nano letters 13 (6):2754-2759. doi:10.1021/nl400976s
41. Nickels PC, Wünsch B, Holzmeister P, Bae W, Kneer LM, Grohmann D, Tinnefeld P, Liedl T (2016) Molecular force spectroscopy with a DNA origami–based nanoscopic force clamp. Science 354 (6310):305-307. doi:10.1126/science.aah5974
42. Kilchherr F, Wachauf C, Pelz B, Rief M, Zacharias M, Dietz H (2016) Single-molecule dissection of stacking forces in DNA. Science 353 (6304):aaf5508-aaf5508. doi:10.1126/science.aaf5508
43. Ding B, Deng Z, Yan H, Cabrini S, Zuckermann RN, Bokor J (2010) Gold Nanoparticle Self-Similar Chain Structure Organized by DNA Origami. Journal of the American Chemical Society 132 (10):3248-3249. doi:10.1021/ja9101198

44. Pal S, Deng Z, Ding B, Yan H, Liu Y (2010) DNA-Origami-Directed Self-Assembly of Discrete Silver-Nanoparticle Architectures. Angewandte Chemie International Edition 49 (15):2700-2704. doi:10.1002/anie.201000330
45. Acuna GP, Bucher M, Stein IH, Steinhauer C, Kuzyk A, Holzmeister P, Schreiber R, Moroz A, Stefani FD, Liedl T, Simmel FC, Tinnefeld P (2012) Distance Dependence of Single-Fluorophore Quenching by Gold Nanoparticles Studied on DNA Origami. ACS nano 6 (4):3189-3195. doi:10.1021/nn2050483
46. Schreiber R, Do J, Roller EM, Zhang T, Schuller VJ, Nickels PC, Feldmann J, Liedl T (2014) Hierarchical assembly of metal nanoparticles, quantum dots and organic dyes using DNA origami scaffolds. Nature nanotechnology 9 (1):74-78. doi:10.1038/nnano.2013.253
47. Liu W, Tagawa M, Xin HL, Wang T, Emamy H, Li H, Yager KG, Starr FW, Tkachenko AV, Gang O (2016) Diamond family of nanoparticle superlattices. Science 351 (6273):582-586. doi:10.1126/science.aad2080
48. Tian Y, Zhang Y, Wang T, Xin HL, Li H, Gang O (2016) Lattice engineering through nanoparticle–DNA frameworks. Nature materials 15 (6):654-661. doi:10.1038/nmat4571
49. Mie G (1908) Beiträge zur Optik trüber Medien, speziell kolloidaler Metallösungen. Annalen der Physik 330 (3):377-445. doi:10.1002/andp.19083300302
50. Prodan E (2003) A Hybridization Model for the Plasmon Response of Complex Nanostructures. Science 302 (5644):419-422. doi:10.1126/science.1089171
51. Pal S, Deng Z, Wang H, Zou S, Liu Y, Yan H (2011) DNA directed self-assembly of anisotropic plasmonic nanostructures. Journal of the American Chemical Society 133 (44):17606-17609. doi:10.1021/ja207898r
52. Klein WP, Schmidt CN, Rapp B, Takabayashi S, Knowlton WB, Lee J, Yurke B, Hughes WL, Graugnard E, Kuang W (2013) Multiscaffold DNA origami nanoparticle waveguides. Nano letters 13 (8):3850-3856. doi:10.1021/nl401879r
53. Kuzyk A, Schreiber R, Fan Z, Pardatscher G, Roller EM, Hogele A, Simmel FC, Govorov AO, Liedl T (2012) DNA-based self-assembly of chiral plasmonic nanostructures with tailored optical response. Nature 483 (7389):311-314. doi:10.1038/nature10889
54. Shen X, Song C, Wang J, Shi D, Wang Z, Liu N, Ding B (2012) Rolling up gold nanoparticle-dressed DNA origami into three-dimensional plasmonic chiral nanostructures. Journal of the American Chemical Society 134 (1):146-149. doi:10.1021/ja209861x
55. Kuzyk A, Schreiber R, Zhang H, Govorov AO, Liedl T, Liu N (2014) Reconfigurable 3D plasmonic metamolecules. Nature materials 13 (9):862-866. doi:10.1038/nmat4031
56. Acuna GP, Moller FM, Holzmeister P, Beater S, Lalkens B, Tinnefeld P (2012) Fluorescence Enhancement at Docking Sites of DNA-Directed Self-Assembled Nanoantennas. Science 338 (6106):506-510. doi:10.1126/science.1228638
57. Prinz J, Heck C, Ellerik L, Merk V, Bald I (2016) DNA origami based Au–Ag-core–shell nanoparticle dimers with single-molecule SERS sensitivity. Nanoscale 8 (10):5612-5620. doi:10.1039/c5nr08674d
58. Taminiau TH, Stefani FD, Segerink FB, van Hulst NF (2008) Optical antennas direct single-molecule emission. Nature Photonics 2 (4):234-237. doi:10.1038/nphoton.2008.32
59. Curto AG, Volpe G, Taminiau TH, Kreuzer MP, Quidant R, van Hulst NF (2010) Unidirectional Emission of a Quantum Dot Coupled to a Nanoantenna. Science 329 (5994):930-933. doi:10.1126/science.1191922
60. Prinz J, Schreiber B, Olejko L, Oertel J, Rackwitz J, Keller A, Bald I (2013) DNA Origami Substrates for Highly Sensitive Surface-Enhanced Raman Scattering. The Journal of Physical Chemistry Letters 4 (23):4140-4145. doi:10.1021/jz402076b
61. Andersen ES, Dong M, Nielsen MM, Jahn K, Subramani R, Mamdouh W, Golas MM, Sander B, Stark H, Oliveira CLP, Pedersen JS, Birkedal V, Besenbacher F, Gothelf KV, Kjems J (2009) Self-assembly of a nanoscale DNA box with a controllable lid. Nature 459 (7243):73-76. doi:10.1038/nature07971

62. Marini M, Piantanida L, Musetti R, Bek A, Dong M, Besenbacher F, Lazzarino M, Firrao G (2011) A Revertible, Autonomous, Self-Assembled DNA-Origami Nanoactuator. Nano letters 11 (12):5449-5454. doi:10.1021/nl203217m
63. Piantanida L, Naumenko D, Torelli E, Marini M, Bauer DM, Fruk L, Firrao G, Lazzarino M (2015) Plasmon resonance tuning using DNA origami actuation. Chemical communications 51 (23):4789-4792. doi:10.1039/C5CC00778J
64. Piantanida L, Naumenko D, Torelli E, Marini M, Bauer DM, Fruk L, Firrao G, Lazzarino M (2015) Plasmon resonance tuning using DNA origami actuation. Chem Commun 51 (23):4789-4792. doi:10.1039/c5cc00778j
65. Marras AE, Zhou L, Su H-J, Castro CE (2015) Programmable motion of DNA origami mechanisms. Proceedings of the National Academy of Sciences 112 (3):713-718. doi:10.1073/pnas.1408869112
66. Gerling T, Wagenbauer KF, Neuner AM, Dietz H (2015) Dynamic DNA devices and assemblies formed by shape-complementary, non-base pairing 3D components. Science 347 (6229):1446-1452. doi:10.1126/science.aaa5372
67. Ke Y, Meyer T, Shih WM, Bellot G (2016) Regulation at a distance of biomolecular interactions using a DNA origami nanoactuator. Nature Communications 7:10935. doi:10.1038/ncomms10935
68. Surwade SP, Zhao S, Liu H (2011) Molecular Lithography through DNA-Mediated Etching and Masking of SiO2. Journal of the American Chemical Society 133 (31):11868-11871. doi:10.1021/ja2038886
69. Schreiber R, Kempter S, Holler S, Schüller V, Schiffels D, Simmel SS, Nickels PC, Liedl T (2011) DNA Origami-Templated Growth of Arbitrarily Shaped Metal Nanoparticles. Small 7 (13):1795-1799. doi:10.1002/smll.201100465
70. Fu J, Liu M, Liu Y, Woodbury NW, Yan H (2012) Interenzyme Substrate Diffusion for an Enzyme Cascade Organized on Spatially Addressable DNA Nanostructures. Journal of the American Chemical Society 134 (12):5516-5519. doi:10.1021/ja300897h
71. Linko V, Eerikainen M, Kostiainen MA (2015) A modular DNA origami-based enzyme cascade nanoreactor. Chemical communications 51 (25):5351-5354. doi:10.1039/c4cc08472a
72. Helmi S, Ziegler C, Kauert DJ, Seidel R (2014) Shape-Controlled Synthesis of Gold Nanostructures Using DNA Origami Molds. Nano letters 14 (11):6693-6698. doi:10.1021/nl503441v
73. Walsh AS, Yin H, Erben CM, Wood MJA, Turberfield AJ (2011) DNA Cage Delivery to Mammalian Cells. ACS nano 5 (7):5427-5432. doi:10.1021/nn2005574
74. Hemmi H, Takeuchi O, Kawai T, Kaisho T, Sato S, Sanjo H, Matsumoto M, Hoshino K, Wagner H, Takeda K, Akira S (2000) A Toll-like receptor recognizes bacterial DNA. Nature 408 (6813):740-745. doi:10.1038/35047123
75. Lee H, Lytton-Jean AK, Chen Y, Love KT, Park AI, Karagiannis ED, Sehgal A, Querbes W, Zurenko CS, Jayaraman M, Peng CG, Charisse K, Borodovsky A, Manoharan M, Donahoe JS, Truelove J, Nahrendorf M, Langer R, Anderson DG (2012) Molecularly self-assembled nucleic acid nanoparticles for targeted in vivo siRNA delivery. Nature nanotechnology 7 (6):389-393. doi:10.1038/nnano.2012.73
76. Douglas SM, Marblestone AH, Teerapittayanon S, Vazquez A, Church GM, Shih WM (2009) Rapid prototyping of 3D DNA-origami shapes with caDNAno. Nucleic acids research 37 (15):5001-5006. doi:10.1093/nar/gkp436
77. Kim DN, Kilchherr F, Dietz H, Bathe M (2012) Quantitative prediction of 3D solution shape and flexibility of nucleic acid nanostructures. Nucleic acids research 40 (7):2862-2868. doi:10.1093/nar/gkr1173
78. Douglas SM, Dietz H, Liedl T, Hogberg B, Graf F, Shih WM (2009) Self-assembly of DNA into nanoscale three-dimensional shapes. Nature 459 (7245):414-418. doi:http://www.nature.com/nature/journal/v459/n7245/suppinfo/nature08016_S1.html

79. Brewer SH, Glomm WR, Johnson MC, Knag MK, Franzen S (2005) Probing BSA binding to citrate-coated gold nanoparticles and surfaces. Langmuir : the ACS journal of surfaces and colloids 21 (20):9303-9307. doi:10.1021/la050588t
80. Reinhard BM, Siu M, Agarwal H, Alivisatos AP, Liphardt J (2005) Calibration of dynamic molecular rulers based on plasmon coupling between gold nanoparticles. Nano letters 5 (11):2246-2252. doi:10.1021/nl051592s
81. Zanchet D, Micheel CM, Parak WJ, Gerion D, Alivisatos AP (2001) Electrophoretic Isolation of Discrete Au Nanocrystal/DNA Conjugates. Nano letters 1 (1):32-35. doi:10.1021/nl005508e
82. Thompson DG, Stokes RJ, Martin RW, Lundahl PJ, Faulds K, Graham D (2008) Synthesis of unique nanostructures with novel optical properties using oligonucleotide mixed-metal nanoparticle conjugates. Small 4 (8):1054-1057. doi:10.1002/smll.200700938
83. Piantanida L, Naumenko D, Lazzarino M (2014) Highly efficient gold nanoparticle dimer formation via DNA hybridization. RSC Advances 4 (29):15281-15287. doi:10.1039/C3RA47478J
84. Ko SH, Vargas-Lara F, Patrone PN, Stavis SM, Starr FW, Douglas JF, Liddle JA (2014) High-speed, high-purity separation of gold nanoparticle-DNA origami constructs using centrifugation. Soft matter 10 (37):7370-7378. doi:10.1039/c4sm01071j
85. Chen G, Wang Y, Tan LH, Yang M, Tan LS, Chen Y, Chen H (2009) High-purity separation of gold nanoparticle dimers and trimers. Journal of the American Chemical Society 131 (12):4218-4219. doi:10.1021/ja900809z
86. Liu D, Li C, Zhou F, Zhang T, Zhang H, Li X, Duan G, Cai W, Li Y (2015) Rapid synthesis of monodisperse Au nanospheres through a laser irradiation-induced shape conversion, self-assembly and their electromagnetic coupling SERS enhancement. Scientific reports 5:7686. doi:10.1038/srep07686
87. Halas NJ, Lal S, Chang WS, Link S, Nordlander P (2011) Plasmons in strongly coupled metallic nanostructures. Chemical reviews 111 (6):3913-3961. doi:10.1021/cr200061k
88. Ju JW, Chen T-M (1994) Micromechanics and Effective Elastoplastic Behavior of Two-Phase Metal Matrix Composites. Journal of Engineering Materials and Technology 116 (3):310. doi:10.1115/1.2904293
89. Dubochet J, Adrian M, Chang JJ, Homo JC, Lepault J, McDowall AW, Schultz P (1988) Cryo-electron microscopy of vitrified specimens. Quarterly reviews of biophysics 21 (2):129-228
90. Glaeser RM (2008) Retrospective: radiation damage and its associated "information limitations". Journal of structural biology 163 (3):271-276. doi:10.1016/j.jsb.2008.06.001
91. Amenitsch H, Rappolt M, Kriechbaum M, Mio H, Laggner P, Bernstorff S (1998) First performance assessment of the small-angle X-ray scattering beamline at ELETTRA. Journal of synchrotron radiation 5 (Pt 3):506-508. doi:10.1107/S090904959800137X
92. Bernstorff S, Amenitsch H, Laggner P (1998) High-throughput asymmetric double-crystal monochromator of the SAXS beamline at ELETTRA. Journal of synchrotron radiation 5 (Pt 4):1215-1221. doi:10.1107/S0909049597019110
93. Moglianetti M, De Luca E, Pedone D, Marotta R, Catelani T, Sartori B, Amenitsch H, Retta SF, Pompa PP (2016) Platinum nanozymes recover cellular ROS homeostasis in an oxidative stress-mediated disease model. Nanoscale 8 (6):3739-3752. doi:10.1039/c5nr08358c
94. Menon SVG, Manohar C, Rao KS (1991) A new interpretation of the sticky hard sphere model. The Journal of Chemical Physics 95 (12):9186-9190. doi:10.1063/1.461199
95. Kuzuya A, Kimura M, Numajiri K, Koshi N, Ohnishi T, Okada F, Komiyama M (2009) Precisely programmed and robust 2D streptavidin nanoarrays by using periodical nanometer-scale wells embedded in DNA origami assembly. Chembiochem : a European journal of chemical biology 10 (11):1811-1815. doi:10.1002/cbic.200900229
96. Kopielski A, Csaki A, Fritzsche W (2015) Surface Mobility and Ordered Rearrangement of Immobilized DNA Origami. Langmuir : the ACS journal of surfaces and colloids 31 (44):12106-12110. doi:10.1021/acs.langmuir.5b03137
97. Kim H, Carney RP, Reguera J, Ong QK, Liu X, Stellacci F (2012) Synthesis and characterization of Janus gold nanoparticles. Advanced materials 24 (28):3857-3863. doi:10.1002/adma.201200926

98. Xue Y, Li X, Li H, Zhang W (2014) Quantifying thiol-gold interactions towards the efficient strength control. Nat Commun 5:4348. doi:10.1038/ncomms5348
99. Bidault S, Polman A (2012) Water-Based Assembly and Purification of Plasmon-Coupled Gold Nanoparticle Dimers and Trimers. International Journal of Optics 2012:1-5. doi:10.1155/2012/387274
100. Ko SH, Vargas-Lara F, Patrone PN, Stavis SM, Starr FW, Douglas JF, Liddle JA (2014) High-speed, high-purity separation of gold nanoparticle–DNA origami constructs using centrifugation. Soft matter 10 (37):7370. doi:10.1039/c4sm01071j
101. Severin N, Dorn M, Kalachev A, Rabe JP (2011) Replication of Single Macromolecules with Graphene. Nano letters 11 (6):2436-2439. doi:10.1021/nl200846f
102. Yu Y, Kuang Y-L, Lei D, Zhai X, Zhang M, Krauss RM, Ren G (2016) Polyhedral 3D structure of human plasma very low density lipoproteins by individual particle cryo-electron tomography1. Journal of Lipid Research 57 (10):1879-1888. doi:10.1194/jlr.M070375
103. Liu C, Liu Q, Huang A (2016) A superhydrophobic zeolitic imidazolate framework (ZIF-90) with high steam stability for efficient recovery of bioalcohols. Chemical communications 52 (16):3400-3402. doi:10.1039/c5cc10171a
104. Liang K, Ricco R, Doherty CM, Styles MJ, Bell S, Kirby N, Mudie S, Haylock D, Hill AJ, Doonan CJ, Falcaro P (2015) Biomimetic mineralization of metal-organic frameworks as protective coatings for biomacromolecules. Nat Commun 6:7240. doi:10.1038/ncomms8240
105. Cui J, Feng Y, Lin T, Tan Z, Zhong C, Jia S (2017) Mesoporous Metal-Organic Framework with Well-Defined Cruciate Flower-Like Morphology for Enzyme Immobilization. ACS applied materials & interfaces 9 (12):10587-10594. doi:10.1021/acsami.7b00512
106. Lei Y, Sun Y, Zhang H, Liao L, Lee ST, Wong WY (2016) Constructing luminescent particle/MOF composites by employing polyvinylpyrrolidone-modified organic crystals as seeds. Chemical communications 52 (83):12318-12321. doi:10.1039/c6cc06456f
107. Song L, Jiang Q, Liu J, Li N, Liu Q, Dai L, Gao Y, Liu W, Liu D, Ding B (2017) DNA origami/gold nanorod hybrid nanostructures for the circumvention of drug resistance. Nanoscale 9 (23):7750-7754. doi:10.1039/c7nr02222k